Two Color Photodiodes Mounted on the Micromachined Carrier

Žarko Lazić, Milče M. Smiljanić, Dušan Nešić, Ljubiša Zeković

Abstract— **In this paper, two color detector based on silicon photodiodes is studied and fabricated. Standard IHTM photodiode's design is modified to allow mounting one photodiode above another using special micromachined carrier. The carrier is fabricated using wet silicon etching in 25% TMAH water solution and anodic bonding of etched silicon and Pyrex glass. The fabricated carrier also allows easy wire thermocompression bonding from the photodiode's pads to TO-5 housing. Output currents of the photodiodes were measured by applying light of 900 nm and 1060 nm. Obtained results verify applicability of the new packaging for two color detector.**

Index Terms—**Two color detector, photodiodes, micromachined packaging, silicon, Pyrex glass**

I. INTRODUCTION

IN the Institute of Chemistry, Technology and Metallurgy (IHTM) various types of silicon photodiodes were explored and developed for decades [1]. In this work, we will study a modified IHTM silicon photodiodes as two color detectors [2-4]. Two color detectors represent a sandwich structure that contains two photodiodes arranged along the same optical axis and they measure different ranges of wavelengths. Commercially available detectors [3-4] are using two photodiodes based on silicon or silicon and InGaAs. These detectors are mostly utilized for remote temperature measurements and for wide wavelength ranges of detection. The temperature is measured using ratio of radiation intensities at two wavelengths or wavelengths ranges and comparing it with the standard black body radiation [3]. Special advantages of these optical remote temperature measurements are solving problems of physical obstacles on target's optical axes. Two color detectors are used in applications for flame temperature sensing, spectrophotometer, dual-wavelength detection and IR thermometers [3].

In this paper, we will explore design of the silicon-silicon photodiodes sandwich, in which the top silicon photodiode is placed above the other bottom photodiode, as shown in Fig.1. The idea of design is that the photons of shorter wavelengths

Žarko Lazić, Milče M. Smiljanić and Dušan Nešić are with University of Belgrade-Institute of Chemistry, Technology and Metallurgy, National Institute of the Republic of Serbia ICTM, Department of Microelectronic Technologies Njegoševa 12, Belgrade, Serbia, (email: zlazic@nanosys.ihtm.bg.ac.rs; smilce@nanosys.ihtm.bg.ac.rs; nesicad@nanosys.ihtm.bg.ac.rs)

Ljubiša Zeković is with University of Belgrade-Faculty of Physics, Studentski trg 12-16, Belgrade, Serbia, (e-mail: zekovic@ff.bg.ac.rs)

must be absorbed in the top photodiode and the photons of longer wavelengths are absorbed in the bottom photodiode. The sandwich design is obtained using special carrier for photodiodes. Carrier is fabricated using processes of micromachining of silicon in 25% wt. TMAH water solution and anodic bonding of etched silicon and Pyrex glass. In order to provide electrical connections, design and fabrication of the photodiodes are modified. After mounting of sandwich carrier on the TO-5 housing, measurements were performed to confirm detection of two different wavelengths.

II. FABRICATION

In the research and development of two color detector we modified photodiodes using know-how of our previous commercial silicon photodiodes. Problem of thermocompression bonding of golden wires to aluminum electrical connection is solved with design of the lateral photodiodes. The IHTM standard photodiodes have electrical connections on the both sides-the top and the bottom. In two color detection the top photodiode must allow transmission of wavelengths to be absorbed by the bottom photodiode. For this reason, the bottom side of the top photodiode must be designed without any metallization and reflective layer.
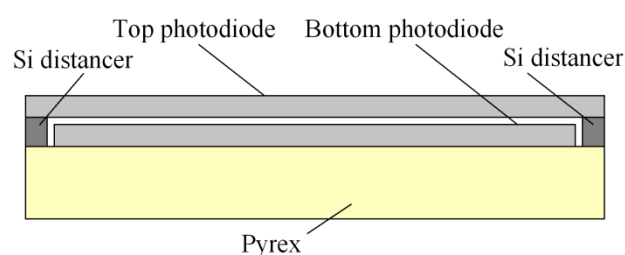

Fig. 1. Cross section of two photodiodes mounted on the micromachined carrier.

In order to simplify fabrication processes, the top and the bottom photodiodes are produced using the identical design, as shown in Fig.1-2. The photodiodes are in the shape of silicon rectangles with surface dimensions of 4000 μm x 3345 μm, as shown in Fig.1-2. The rectangular shape resolves the problem of thermocompression bonding of gold wires to both mounted photodiodes on fabricated carrier and TO-5 housing since both are rotated for 90° relative to each other, as shown
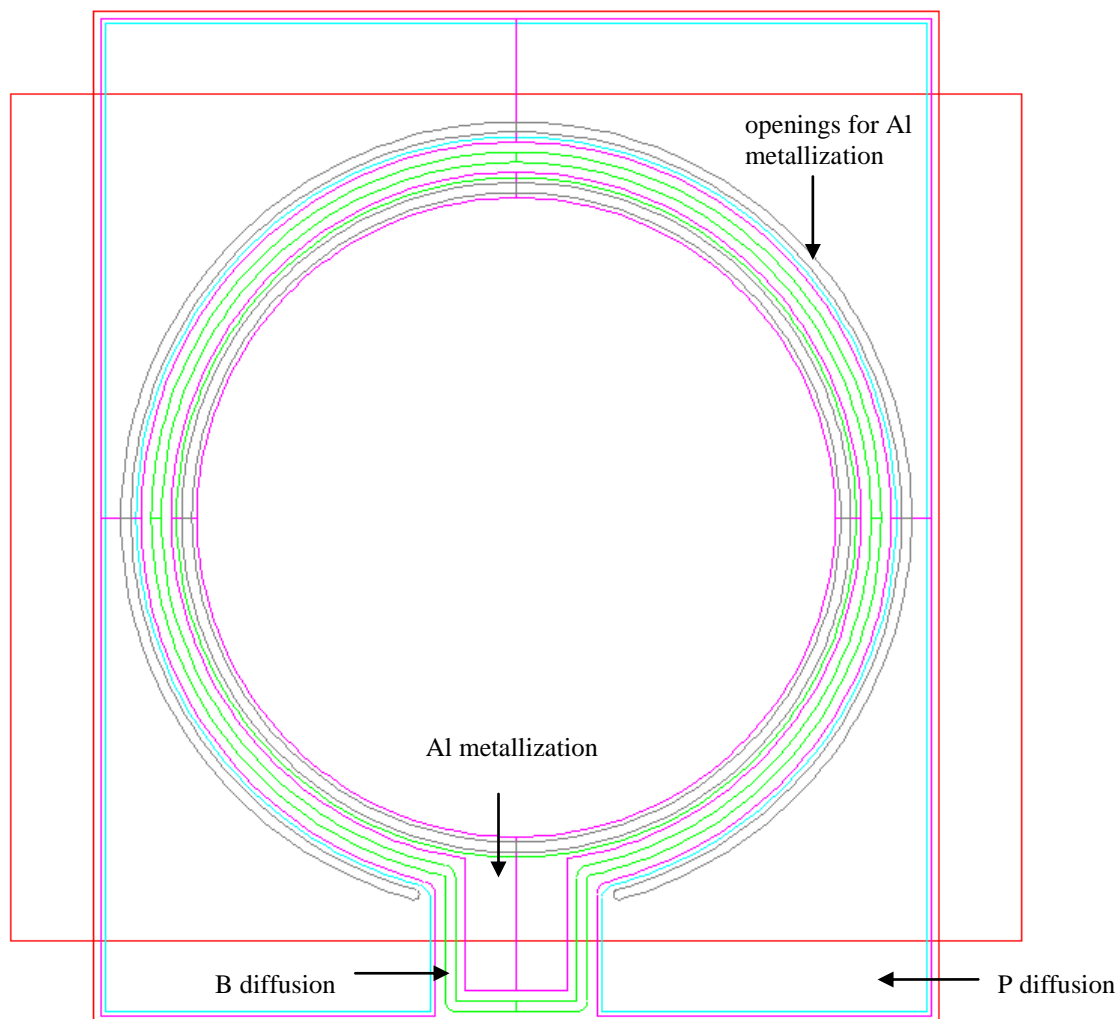
Fig. 2. Two color photodiodes design. Green color-I photolithographic process for boron diffusion. Blue color-II photolithographic process for phosphorus diffusion. Grey color-III photolithographic process for openings for Al metallization in SiO2. Pink color-IV photolithographic process for Al metallization. Red color-rectangular borders of sawed photodiode.

in Fig.2. We used two types of the silicon substrates in fabrication. For the top photodiodes, the silicon wafers of n type, resistivity of 2000 Ωcm and thickness of 180 μm are used. For the bottom photodiodes, we used silicon wafers of n type, resistivity of 500-1000 Ωcm and thickness of 300 μm. Prior to predetermined technological processes, the photolithographic processes were performed to define patterns given in Fig.2. The fabricated photodiodes were obtained according to following list of technological processes:

1. I wet thermal oxidation for boron diffusion
   (T=1100 ℃, t=120 min)
2. I photolithographic process for boron diffusion
3. Boron diffusion (T=1025 ℃, t=60 min)
4. II wet thermal oxidation for phosphorus diffusion (T=1100 ℃, t=100 min)
5. II photolithographic process for phosphorus diffusion
6. Phosphorus diffusion (T=950 ℃, t=60 min)

7. SiO_2 thinning on the top side and its removing on the bottom side of wafer
8. III photolithographic process for openings in SiO_2
9. Al sputtering
10. IV photolithographic process for Al metallization.

Finally, Au layer was sputtered only on the bottom side of the bottom photodiode as reflective layer.

Photodiodes' carrier is micromachined using anisotropic wet etching in 25% wt. water solution at the temperature of 80 ℃ [5-7]. We used phosphorus-doped {100}-oriented 3" silicon wafers with double-sided polished surfaces. The resistivity of the wafers is 1-5 Ωcm and its thickness is 400 μm. Prior to etching, we performed wet thermal oxidations to obtain SiO_2 masking layer of 1 μm and 0.5 μm thicknesses and three photolithographic processes to define patterns for double side etching. First, we performed etching to define appropriate cavities on the top side of silicon substrate. Then the thinner silicon dioxide was removed. Next, wafer had been double side etched until membrane of 50 μm was obtained. Etched wafer was anodically bonded to the Pyrex

TABLE I
PHOTODIODES CURRENTS AND RATIOS OF CURRENTS FOR THE WAVELENGTHS OF 900 NM AND 1060 NM.

Two color detector		900 nm			1060 nm		
		Intensity I_1	Intensity I_2	Intensity I_3	Intensity I_1	Intensity I_2	Intensity I_3
1	I_{top}	8 μA	4 μA	850 nA	14.9 μA	2.32 μA	756 nA
	I_{bottom}	0.55 μA	0.265 μA	57.5 nA	5.1 μA	1.1 μA	395 nA
	Ratio	14.5	15.1	14.8	2.9	2.1	1.9
2	I_{top}	9.05 μA	3.4 μA	1.24 μA	12.55 μA	3.22 μA	995 nA
	I_{bottom}	1.15 μA	0.337 μA	0.128 μA	3.16 μA	1.56 μA	555 nA
	Ratio	7.9	10.1	9.7	4	2.1	1.8
3	I_{top}	5 μA	2.61 μA	800 nA	13.7 μA	3.22 μA	681 nA
	I_{bottom}	0.61 μA	0.33 μA	95 nA	6.15 μA	1.96 μA	467 nA
	Ratio	8.2	7.9	8.4	2.2	1.6	1.46

glass wafer, as shown in Fig.3. The thickness of Pyrex glass wafer is 700 μm. Finally, the last etching of the previously obtained membrane determines distancers on glass support, as shown in Fig.1. The distance between vertical etched silicon inner walls is 3345 μm. Finally, the Pyrex glass wafer was sawed into 4000 μm x 4000 μm carriers.
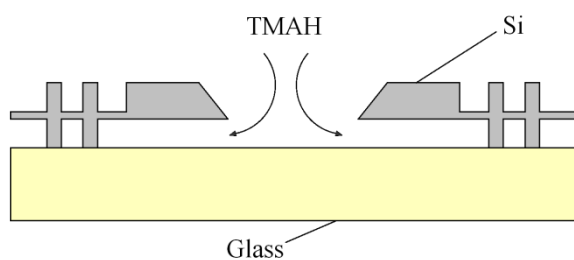

Fig. 3. Schematic picture of partly micromachined silicon wafer anodically bonded to Pyrex glass wafer.
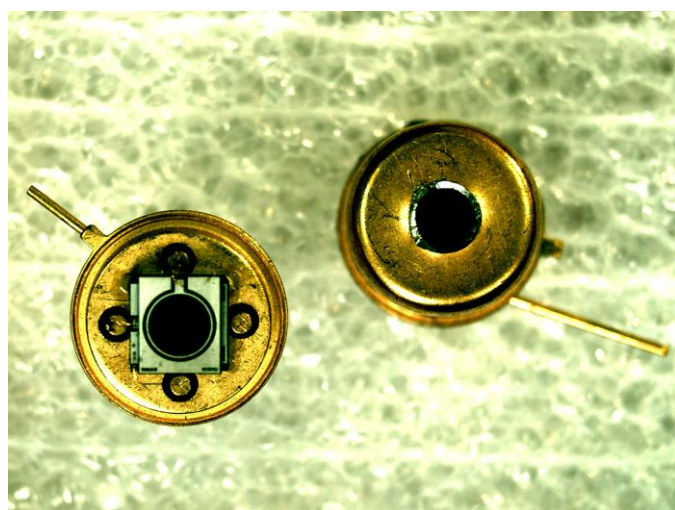

Fig. 4. Two photodiodes mounted on TO-5 housing with and without cap.

III. RESULTS AND DISCUSSION

The photodiodes were measured separately before mounting in order to confirm their quality and compare with IHTM commercial photodiodes. Sensitivities for both photodiodes were 0.65 A/W for 900 nm and 0.2-0.3 A/W for 1060 nm. Breakdown voltages of about 100 V were obtained. These parameters are similar to IHTM commercial photodiodes [1].

The top and bottom photodiodes are mounted on obtained carriers as shown in Fig.1. The carriers are then mounted on TO-5 housing, as shown in Fig.4,5 where the photodiodes are bonded to four pins using 25 μm gold wires. At the end, the cap with aperture was glued to TO-5 housing. Aperture is designed for the optical fiber as shown in Fig.5.
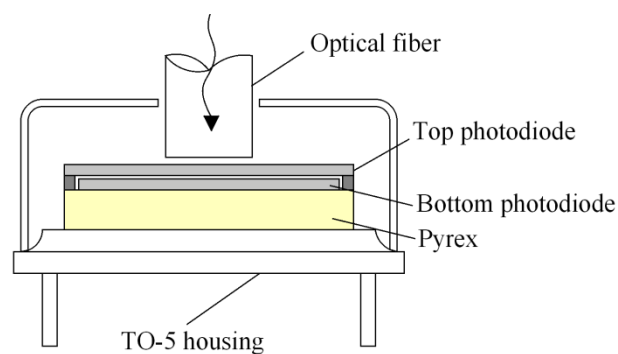.

Fig. 5. Schematic picture of cross section packaging of mounted two photodiodes with optical fiber.

The light is applied through optical fiber in order to measure ratios between the photodiodes' output currents. We used the filters for 900 and 1060 nm when the light is applied. The obtained ratios between the photodiodes' output currents are given in Table 1 for three different detectors. For each two color detector ratios were measured for three different light intensities. From outputs and ratios given in Table 1, we can

conclude that the designed carrier can be used as a part of packaging for two color detector. Our future work will be to improve our modified photodiodes presented in this paper in order to obtain better output characteristics.

IV. CONCLUSION

In this paper, we explored and developed two color detector based on silicon photodiodes. We modified IHTM photodiodes in order to allow mounting of one photodiode above another and easy thermocompression bonding to TO-5 housing. We fabricated special carrier for photodiodes using wet silicon etching in 25% TMAH water solution. Output currents of the produced two color detectors were measured by applying light with the wavelengths of 900 nm and 1060 nm. Performed measurements confirm usability of the new designed carrier for two color detector.

ACKNOWLEDGMENT

REFERENCES

[1] www.ihtm.bg.ac.rs
[2] D.B. Ponomarev, V.A. Zakharenko, "Silicon photodiode as the two-color detector", *Journal of Physics: Conference Series*, Volume 643, 2nd International School and Conference Saint-Petersburg OPEN on Optoelectronics, Photonics, Engineering and Nanostructures (SPbOPEN2015), St Petersburg, Russia, 6–8 April 2015.
[3] www.osioptoelectronics.com
[4] www.hamamatsu.com
[5] M.M. Smiljanić, B. Radjenović, M. Radmilović-Radjenović, Ž. Lazić. V. Jović, "Simulation and experimental study of maskless convex corner compensation in TMAH water solution", *J. Micromech. Microeng.* 24115003, 2014.
[6] M.M. Smiljanić, B. Radjenović, M. Radmilović-Radjenović, Ž. Lazić. V. Jović, "Evolution of Si crystallographic planes-etching of square and circle patterns in 25 wt % TMAH", *Micromachines* 10(2) 102, 2019.
[7] M.M. Smiljanić, Ž. Lazić, V. Jović, B. Radjenović, M. Radmilović-Radjenović, "Etching of Uncompensated Convex Corners with Sides along <n10> and <100> in 25 wt% TMAH at 80 °C", *Micromachines* 11(3), 253, 2020.

Optimization of electrodeposition parameters to improve composite hardness of nickel coatings on brass substrate for varying film thicknesses and applied indentation loads

Ivana Mladenović, Jelena Lamovec, Marko Obradov, Milena Rašljić Rafajilović, Vesna Radojević, Dana Vasiljević Radović, *Member, IEEE* and Nebojša Nikolić

Abstract—In this investigation, nickel coatings were electrodeposited on brass substrate. The effects of electrodeposition process parameters such as, current density and deposition time (coatings thickness), on surface morphology and composite hardness values were studied. The value of the measured composite hardness by Vickers microindentation technique of the selected "hard film on soft substrate" composite system type depends on the applied indentation loads. For this reason, the microindentation loads are also included in the analysis. According to the experiment plan obtained by Design-Expert software, nickel coating has been produced on the brass cathode using galvanostatic regime (DC) with magnetic stirring of the electrolyte. The nickel sulphamate electrolyte with saccharine additive was used for Ni electrodeposition. Then, response surface methodology (RSM) was used to establish an adequate mathematical model. Subsequently, a mathematical model was developed to weight the effects of each input parameters (coating thickness, current density and indentation load) on the output parameter (composite hardness) of electrodeposited nickel coatings on brass substrate. According to the obtained results, the coating thickness and indentation load greatly influenced resulting composite hardness. On the other hand, coating current density primarily influenced microstructure and surface roughness. The topographic modification of the Ni coating surface depending on the post-treatment (mechanical and chemical) after deposition was studied using AFM microscopy.

Index Terms— electrodeposition; composite hardness; RSM; AFM; optimization; nickel coating.

I. INTRODUCTION

THIN metallic coatings are often used for fabrication of different microelectronic and micromechanical devices. Thin coatings and bulk substrates constitute a composite system which mechanical properties depend not only on material characteristics of constituent materials but also on the mechanical interaction between the two such as the adhesion strength, residual stress, toughness and elastic-plastic properties [1-3]. In general, strong adhesion of the coating to the substrate is desired because it results in improved mechanical properties of the composite system. Additionally, reduction of the residual stress is paramount to prevent spontaneous delamination of the coating due to micro-crack growth between the thin coating and the bulk substrate [3].

Nickel (Ni) is one of the most common metals used to synthesize composite electrochemical coatings (CECs). It is characterized by superior corrosion and wear resistance, and enhanced mechanical and tribological properties [4]. Nickel coatings attract a huge attention from both scientific and technological communities owing to their unique properties, such as excellent friction coefficient during the wear testing of LIGA (lithographic) fabrication micro-rotors [5]. Ni alloys such as Co-Ni possess the high aspect ratio (HAR) during electrodeposition process and excellent magnetic and electrochemical properties [6].

Main methods of Ni thin film synthesis include: electrodeposition (ED), electroless plating (EL), physical vapour deposition (PVD), chemical vapour deposition (CVD), thermal spray and RF sputtering [1]. An interesting approach used for growing both pure Ni coatings and Ni alloys is electrochemical deposition technique. Conventional electrodeposition (ED) or new emulsion supercritical ED technique are very suitable ways to obtain nickel of desired characteristics suitable for application in above mentioned purposes [7, 8]. A common problem that exists during electrodeposition of Ni coatings is formation of hydrogen during ED process. The formation of hydrogen may create several pinholes on the coating [8], but the problem is solved by the adding surfactants (organic additives).

The most common electroplating solution for electrodeposition of Ni coatings met in the literature consists of nickel sulfate, nickel chloride, boric acid, saccharine and 1,4-butynediol [8]. In addition to the sulfate electrolyte, sulphamate electrolyte is also used [9]. Deposition parameters affect many properties of the electroplated material both during and after synthesis. By altering the synthesis parameters such as type of electrolyte and substrate, mixing condition, deposition time, applied current regime and density, post-deposition treatment, etc. we can control the grain size and microstructure of Ni coatings resulting in strengthened and hardened films with little or no loss in coating ductility.

Indentation testing is a reliable method for evaluation of material mechanical properties [3]. However, it cannot be

Ivana Mladenović, Marko Obradov, Milena Rašljić Rafajilović, Dana Vasiljević Radović and Nebojša Nikolić are with the Institute of Chemistry, Technology and Metallurgy, University of Belgrade, Njegoševa 12, 11 000 Belgrade, Serbia (e-mail: ivana@nanosys.ihtm.bg.ac.rs, marko.obradov@nanosys.ihtm.bg.ac.rs, milena@nanosys.ihtm.bg.ac.rs, dana@nanosys.ihtm.bg.ac.rs, nnikolic@ihtm.bg.ac.rs).

Jelena Lamovec is with the University of Criminal Investigation and Police Studies, Cara Dušana Street 196, Zemun, Belgrade, Serbia (e-mail: jelena.lamovec@kpu.edu.rs).

Vesna Radojević is with the Faculty of Technology and Metallurgy, University of Belgrade, Karnegijeva 4, 11 000 Belgtrade, Serbia (e-mail: vesnar@tmf.bg.ac.rs).

applied directly for characterization of thin films due to plastic deformation of the sample during the indentation process [9, 10]. For this reason, indentation method is applied to measure composite hardness (thin film on bulk substrate). Various mathematical models have been developed to calculate thin film microhardness based on the directly measured composite hardness of the film [11-14].

The Response Surface Methodology (RSM) is the most insightful method of evaluating a factorial experiment performance [15, 16]. The aim of this paper, in addition to synthesis of excellent quality Ni coatings on brass by the ED method and microindentation characterization of the material, is also to design an optimal experiment (DoE) according to RSM (Response Surface Methodology) [15-20]. Modification of the coating structure after deposition is another contribution of this paper.

II. EXPERIMENTAL

For electrodeposition of fine-grained nickel coatings we chose brass foil (260 1/2 hard, ASTM B36, K&S Engineering, 250 μm thick; composition: 66 % Cu, 34 % Zn) as a substrate (cathode). The surface area of the brass cathode was (2.0×1.0) cm^2. The pure Ni anode (rectangular in shape; positioned along the wall of the glass cell) and 500 ml of electrolyte were used. The nickel depositing apparatus is shown in Fig. 1. Prior to deposition, the cathode was mechanically polished and activated in a solution of sulfuric acid.
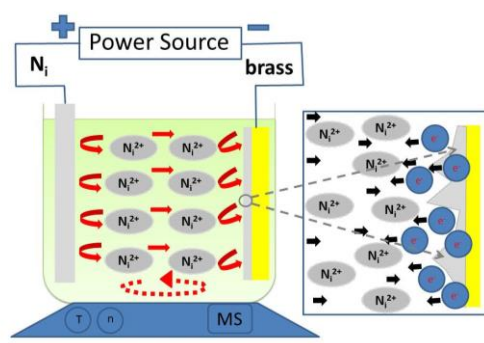

Fig. 1. Schematic presentation of nickel coating electrodeposition on brass substrate from sulphamate electrolyte in DC regime with magnetic stirrer (DC/MS).

Electrodeposition was performed in an open cell type using the direct current galvanostatic regime (DC) from a lab-made sulphamate electrolyte consisting of: 300 g/l Ni (NH$_2$SO$_3$)$_2$·4H$_2$O, 30 g/l NiCl$_2$·6H$_2$O, 30 g/l H$_3$BO$_3$ and 1 g/l saccharine as the wetting agent, with pH-value and the temperature of the process maintained at 4.20 and 50°C, respectively. The electrolytes were stirred by an application of magnetic stirrer (MS) (300 rpm, Heidolph Instruments GmbH & Co. KG, Schwabach, Germany). The DC/MS electrodeposited regime will be used below in the text.

The current density values were maintained at 10 mA cm^{-2} and 50 mA cm^{-2}. The deposition time was determined according to projected thickness of the coating. Five different coating thicknesses were formed: 2, 5, 10, 20 and 50 μm for each applied current density. Cathodic efficiency of 100% was taken to calculate the deposition time. The thickness was

checked across the cross-section using an optical microscope.

The cross-section preparation for characterization was done in a fallowing manner: samples were embedded in a self-curing methyl methacrylate-polymer (Palavit G, Heraeus, Germany) and mechanically polished with different SiC papers (#800 and #1200) and finished with emulsion of alumina powder with different grain size (1-0.3 μm) [21]. Then, rinsing in sodium-carbonate solution and dried in nitrogen flow. The cross-section was prepared in order to validate the thickness of the coating, to observe the adhesion at the coating-substrate interface and to assess the hardness of the coating at the cross-section, see Fig. 2.

The mechanical properties of the composite system and substrate on top side and cross-section were characterized utilizing a Vickers microhardness tester ″Leitz, Kleinharteprufer DURIMET I″ using up to 15 loads ranging from 500 gf (4.9 N) down to 5 gf (0.049 N), see Figs. 2, 3 and 4. Five different loads were selected for optimization (10, 50, 100, 150 and 300 gf). Three indentations were made and the average value of the diagonal was determined by measuring six indentation diagonals, for each load. With the average value of the diagonals, the mean value of the hardness was calculated [9].

The topographic analysis of coatings surface after post-treatment was investigated using an atomic force microscope in the non-contact mode (AFM-Auto Probe CP Research; TM Microscopes-Veeco Instruments, Santa Barbara, CA, USA). The scan area was (20×20) μm^2. A histogram analysis of the coatings and bearing rate curve [22, 23] were done by an application of WSxM AFM software [24]. The analysis was performed in order to assess the resistance of the coating and the change in roughness during mechanical treatment and exposure to aggressive reagents such as hydrochloric acid (Fig. 5).

III. RESULTS AND DISCUSSION

A. Indentation on different locations

The microhardness of Ni coating and influence of the substrate hardness during penetration of indenter is shown to depend on the indentation site. The hardness measured on the cross-section of brass (Fig. 2a) corresponds to the absolute bulk substrate hardness that is used in proportional specimen resistance (*PSR)* model (H_s = 1.41 GPa) [25].

If the indentation is performed on the coating surface, the structural-morphological properties of the coating affect the measurement, and the contribution of the substrate must be taken into account. The measured value of hardness is called composite hardness, H_c. In the case of cross-sectional indentation (Fig. 2b), the measured hardness, H_{c-s} is constant and equal to the hardness of the bulk material without effects of substrate hardness and morphology of coating surface. Comparative values are shown in Table I. The diagonal size measured on the cross-section of the coating (d_{c-s}) is smaller than on the surface of composite (d), for the same applied load. For the "hard film on soft substrate" composite system type, the cross-sectional hardness value is higher than the composite hardness.

The interfacial indentation [3] hardness test (Figs. 2c and 2d) is a quick way to assess interlayer adhesion strength of the coating to the substrate and indentation toughness

properties. The interfacial hardness and diagonal interfacial size (d_i) measurement is complex. The problem with this method of measurement is a possible difference in the height of nickel and brass due to the different wear rate of the material when preparing the cross-section. The delamination of the Ni coating did not occur, so the adhesion of the Ni coating for brass substrate is good. For very thin coatings (2, 5, 10 μm), it is not possible to measure hardness on the cross-section, because the Vickers indent size is larger than the projected thickness of the coating.
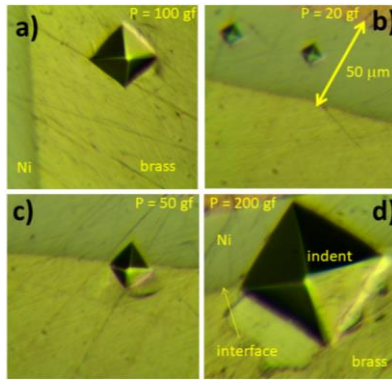

Fig. 2. Indentation on different location of cross-section with variation applied load on Ni/brass composite system: a) indentation on brass substrate, $P = 100$ gf, b) indentation on Ni coating, $P = 20$ gf, c) interfacial indentation, $P = 50$ gf and d) interfacial indentation, $P = 200$ gf. Nickel coating was obtained in DC/MS electrodeposition regime at 50 mA cm^{-2} current density.

TABLE I
CHANGE IN THE HARDNESS OF THE NICKEL COATING DEPENDING ON THE MEASURING LOCATION

P / gf	d / μm	$d_{c\text{-}s}$ / μm	H_c / GPa	$H_{c\text{-}s}$ / GPa
20	11.08	10.50	2.945	3.278
50	18.88	15.40	2.535	3.810
100	24.90	22.00	2.914	3.734
200	36.50	34.05	2.713	3.117

B. Indentation on the top surface of the Ni coatings on brass substrate

Different load-indentation depth curves can be obtained by changing the coating thickness of Ni coatings and current densities (Fig. 3). It can be seen that the coating thickness is the dominant parameter in the loading indentation process, while current density has very little effect, especially for small coating thicknesses.

The dependencies of the composite hardness (H_c) on the relative indentation depth (RID) for the given Ni coatings are shown in Figure 4. The RID is defined as a ratio between an indentation depth, h and a coating thickness, δ ($RID = h/\delta$), where an indentation depth depends on a diagonal size as $h = d/7$ [9, 11-14, 21]. The contribution of substrate to composite hardness increases with the increasing RID value and applied load P, suggesting that the composite hardness matches the substrate hardness at high RID values.

Figure 4 clearly shows three characteristic zones depending on the influence of coating and substrate hardness on the composite hardness: 1) dominant influence of the coatings corresponds to $0.01 < RID < 1$ (for thick 50 μm

coatings), 2) the composite zone corresponds to $0.1 < RID < 1$ for medium-thick films (10 and 20 μm) and 3) the dominant influence of the substrate is characteristic when $RID > 1$; for thin coatings (2 and 5 μm).
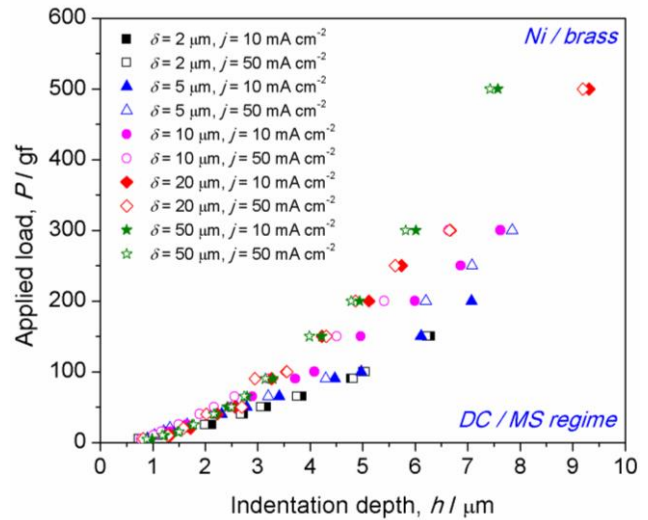

Fig. 3. Load-indentation depth experimental points of different Ni coating thickness electrodeposited on brass substrate in DC/MS regime at two current densities (10 and 50 mA·cm^{-2}).
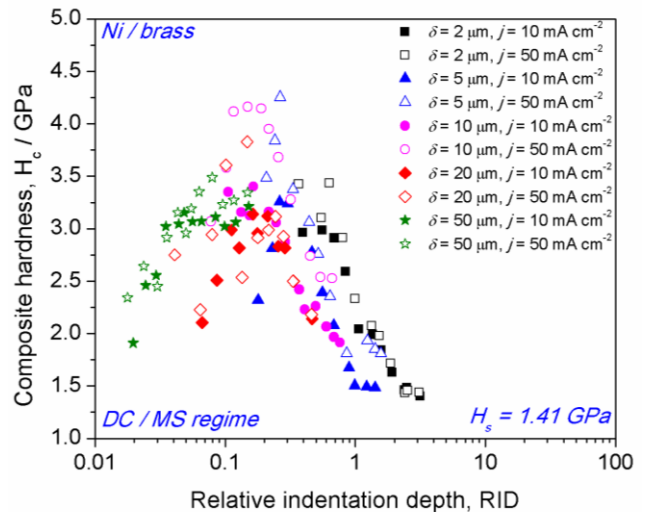

Fig. 4. The dependencies of the composite hardness (H_c) on the RID for the Ni coatings electrodeposited on the brass from the sulphamate electrolyte.

Figure 4 also shows a characteristic turning point, corresponding to a value of RID of 0.14. For the RID values smaller than 0.14, the measured composite hardness corresponds closely to the hardness of the coating. By crossing this critical point, the value of hardness decreases, which indicates the contribution of the softer substrate below. The Ni coatings obtained with a higher current density (50 mA·cm^{-2}) appeared harder than those deposited with 10 mA·cm^{-2}. For hard coating on soft substrate composite systems, with increasing the relative indentation depth ($0.1 \leq RID \leq 1$), the composite hardness H_c decreases until the hardness of the substrate is reached as shown on Fig.4 ($H_s = 1.41$ GPa).

C. Modification of Ni surface after deposition by mechanical and chemical treatments

Stochastically roughened of metallic thin coatings can be obtained with various methods including dry etching, wet chemical etching or mechanical treatment (abrasion). Depending on the applied method, different surface profiles are obtained with microstructural modifications of surface coatings. The goals of this work were to explore the correlations between the AFM-based and treatment method for samples with different roughness and therefore different areas. For example, the difference in mechanical properties on the cross-section and the surface of the coating is one of the consequences of the treatment (mechanical). The roughness of each of the samples was determined using AFM topographic measurements. Figures 5 present the 3D AFM images of Ni / brass systems obtained at 50 mA·cm^2 (left) and histograms (right) with different treatment: mechanical (Figs. 5 a, b), chemical (Figs. 5 c, d) and no-treatment (Figs. 5 e, f).

Comparing the topography of nickel coatings, mechanical treated (Fig. 5a) and chemical treated coating (Fig. 5c) have similar roughness and stochastically nodular topography. Ni coating with mechanical treatment (Fig. 5a) can be observed to have a rather irregular surface with distributed nodular surface features. Deep channels as a result of sanding and scratching the surface were observed, too. From the values of the arithmetic average of the absolute roughness parameter (R_a) of the surfaces presented in Fig. 5, it could be observed that the roughness increases for Ni coatings including either chemical or mechanical treatment relative to non-treated coating (R_a = 28.68 nm for no-treated, R_a = 82.43 for chemical and R_a = 78.14 for mechanical treated coatings).
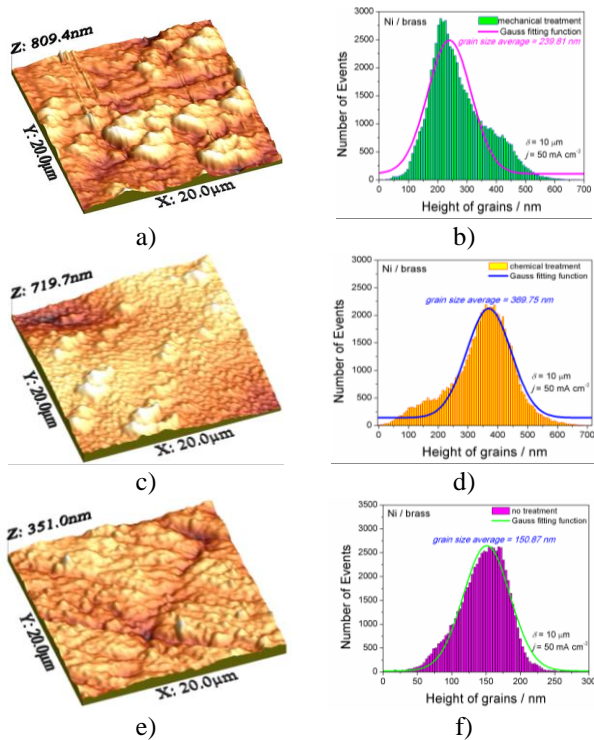

a)

b)

c)

d)

e)

f)

Fig. 5. Examples (20 × 20) µm^2 AFM topographic measurements for a Ni coating (10 µm thick) on brass substrate (left) and corresponding histograms (right) after electrodeposition and roughened surface treatment: a) and b) mechanical; c) and d) chemical; e) and f) no treatment. Ni coatings were obtained by electrodeposition technique in DC/MS regime at a current density of 50 mA cm^{-2} from the sulphamate electrolyte.

Although the topography of the untreated sample and the chemically etched one is very similar, based on the average height of grains obtained via the Gaussian distribution fitting function, it can be seen that the chemically treated sample has higher peaks (369.75 nm). However, mechanical treatment of the surface leads to the suppression of high peaks (Fig. 5b), which results in a reduction of total roughness (239.81 nm), i.e. smoothing of the surface.

Figures 6 show the relationship of bearing ratio (in %) with the grain height (Firestone–Abbott bearing curve, standards DIN4776; STN ISO 13 565-2). The bearing curve is the cumulative probability density function of the surface profile's height which is calculated by integrating the profile of the AFM trace [22]. As can be seen, if the bearing area rate reached 95 %, the order of the corresponding grain height of these treated Ni coatings are mechanical (800 nm) > chemical (700 nm) > no treatment (350 nm), see Fig. 6a.
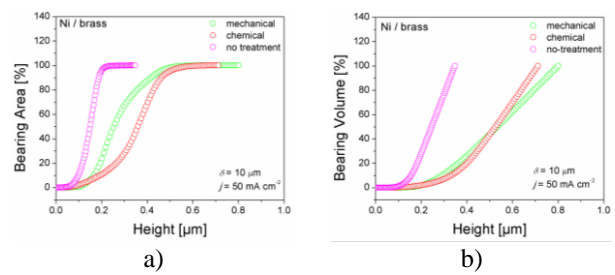

a)

b)

Fig. 6. Bearing ratio curves of Ni coatings on brass substrate with a variation of treatment: a) bearing area and b) bearing volume curve.

With application of post-treatment, the distribution range of nodule sizes shifts to the direction of larger values, see Fig. 6a. It indicated that the Ni coating without any treatment has the finest granule size, comparatively. It suggested that the Ni benefits smooth and fine-grained structure. Bearing flooded volume or bearing area curve indicated that the critical dimension point is 500 nm for peak height (Figs. 6a and 6b) for treated surface.

D. Optimization of composite hardness of Ni/brass systems

Design-Expert 12 (Stat-Ease, US) software and Optimal Design was used for the response methodology to examine correlation between the input variables (coating thickness, current density and applied indentation load) and output parameter (composite hardness). The factors (3 numerical) and factor levels (numerical) are shown in Table II.

TABLE II

INFLUENCE FACTORS ON NI COATING COMPOSITE HARDNESS

Mark	Parameters	Value limit Lower / Upper		unit
P	Applied indentation loads	10	300	gf
δ	Thickness of the Ni coatings	2	20	µm
j	Current densities	10	50	mA cm^{-2}

Using data given in Table II, a regression mathematical model was developed to describe the function between the input parameters and measured response values. The relationship enabling a prediction of the composite hardness (H_c) values of the Ni/brass systems in a function of applied variables (indentation load (P), thickness of the coating (δ) and current density (j) is given by Eq. 1:

$$H_c^{-1}=0.3833+0.0534A-0.11191B-0.024C-0.835AB-0.0391AC-0.033BC-0.0433A^2+0.01374B^2+0.0318C^2 \quad (1)$$

where A, B and C represent numerical factors from Table II corresponding to the input variables, i.e. applied load, coating thickness and current density. Figure 7 shows the dependence of H_c values predicted by the RSM based on the regression model generated by coded Eq. 1 for every combination of two input parameters: applied load, coating thickness and current density (Fig. 7a load and thickness; Fig.7c current density and load; Fig. 7e current density and thickness). Each combination has a positive and statistically significant effect on composite hardness as also revealed by the contour lines presented in Figs. 7b, 7d and 7f. The red color corresponds to high values of composite hardness i.e. dominant influence of the coatings ($H_c \rightarrow 3.4$ GPa), yellow and green correspond to the composite zone and the blue indicates the dominant influence of the substrate i.e. composite hardness approaches to the hardness of the substrate ($H_c \rightarrow H_s$).

a)   b)

c)   d)
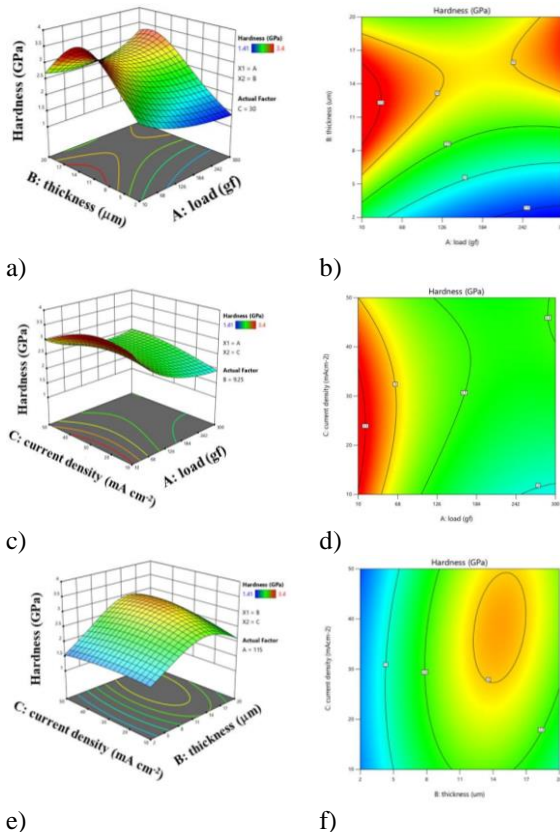
e)   f)

Fig. 7. 3D response surface (left) and contour plot (right) of Ni/brass composite hardness for different coded values: a) and b) of A (indentation load) and B (thickness), c) and d) of A (indentation load) and C (current density), e) and f) for B (thickness) and C (current density).

An increase in current density also indicates an increase in composite hardness value, but for indentation loads corresponding to the "film zone" (up to 50 gf), see Fig. 7d. It can be seen from Fig. 7 that the coating thickness and applied loads have a significant impact on the Ni/brass composite hardness systems. The current density is the least dominant factor in composite hardness change (Figs. 7f).

IV. CONCLUSION

The parameters suitable for fabrication of hard, compact and uniform Ni coatings on brass substrate were obtained in the direct current regime with magnetic stirring (DC/MS) from lab-made sulphamate electrolyte. Nickel coatings of various thickness were obtained utilizing different current densities. The maximal composite hardness of Ni/brass composite system was achieved for a current density of 50 mA·cm^{-2}, 15 μm coating thickness and with applied indentation load of 50 gf (0.49 N).

Two ways of measuring micro hardness are presented: on the cross-section and the top of surface coating. The measured hardness at the cross-section of depth Ni is higher than composite hardness on top surface. Based on the interfacial indentation test, good adhesion between the coating and the substrate was determined, and no delamination occurred.

Stochastically roughened of electrodeposited Ni thin coatings can be obtained with various methods including mechanical and chemical treatment after electrodeposition process. Based on topographic analysis, it has been shown that each additional treatment after electrochemical deposition introduces an increase in stochastic roughness. That means, after deposition, it is not necessary to treat the surface of the coating before micro indentation.

The RSM optimization of operating parameters for the synthesis of the Ni/brass composite system was applied. Analysis of variance confirmed that the proposed regression model is in good agreement with the experimental data, providing a high determination and adjusted determination coefficients. The results suggested that the used adequate micro indentation loads, as well as the synthesis parameters, can directly affect the material mechanical properties such as composite hardness.

REFERENCES

[1] D. T. Read, A. A. Volinsky, "Thin Films for Microelectronics and Photonics: Physics, Mechanics, Characterization and Reliability, Micro- and Opto-Electronic Materials and Structures, Springer US, 2007, Part I, pp. 135-180.

[2] S. E. Lyshevski, "Nano- and microelectromechanical systems: Fundamentals of nano- and microengineering, CRC Press LLC, New York, NY, 2001, pp. 11-25.

[3] A. A Volinsky, N. R Moody, W. W Gerberich, "Interfacial toughness measurements for thin films on substrates", *Acta Mater.*, vol. *50*, no. *3*, pp. *441-466*, Feb., 2002.

[4] A. Siddaiah, P. Kumar, A. Henderson, M. Misra, P. L. Menezes, "Surface Energy and Tribology of Electrodeposited Ni", *Lubricants*, vol. *7*, no. *10*, p. *87*, Oct., 2019.

[5] J. Goettert, P. Datta, Y. Desta, Y. Jin, Z. Ling, V. Singh, "LiGA Research and Service at CAMD", *J. Phys.: Conf. Ser.*, vol. *34*, no. *912*, "International MEMS conference", Singapore, 9–12 May, 2006.

[6] M. Duch, J. Esteve, E. Gómez, R. Pérez-Castillejos, E. Vallés, "Electrodeposited Co-Ni alloys for MEMS", *Micromech. Microeng.*, vol. *12*, no. *4*, pp. *400-405*, July, 2002.

[7] M. Schlesinger, M. Paunovic, *Modern Electroplating 4*th ed. New York, US, John-Wiley and Sons Inc, 2000.

[8] H. Yoshida, M. Sone, H. Wakabayashi, H. Yan, K. Abe, X. T. Tao, A. Mizushima, S. Ichihara, S. Miyata, "New electroplating method of nickel in emulsion of supercritical carbon dioxide and electroplating solution to enhance uniformity and hardness of plated film", *Thin Solid Films*, vol. *446*, no. *2*, pp. *194-199*, 2004.

[9] J. Lamovec, V. Jović, D. Randjelović, R. Aleksić, V. Radojević, "Analysis of the composite and film hardness of electrodeposited nickel coatings on different substrates", *Thin Solid Films*, vol. *516*, no. *23*, pp. *8646-8654*, June, 2008.

[10] Z. S. Ma, Y. C. Zhou, S. G. Long, C. Lu, "On the intrinsic hardness of a metallic film/substrate system: Indentation size and substrate effects", *Int. J. Plast.*, vol. *34*, no. *1*, pp. *1-11*, July, 2012.

[11] J. Lesage, D. Chicot, A. Pertuz, P. -Y. Jouan, N. Horny, A. Soom, "A model for hardness determination of thin coatings from standard micro-indentation tests", *Surf. Coat. Technol.*, vol. *200*, no.*1–4*, pp. *886–889*, Oct., 2005.

[12] J. L. He, W. Z. Li, H. D. Li, "Hardness measurement of thin films: Separation from composite hardness," *Appl. Phys. Lett.*, vol. *69*, no. *10*, pp. *1402–1404*, Jun., 1996.

[13] E. S. Puchi-Cabrera, "A new model for the computation of the composite hardness of coated systems", *Surf. Coat. Technol.*, vol. *160*, no. *2–3*, pp. *177-186*, Oct., 2002.

[14] J. R Tuck, A. M Korsunsky, R. I Davidson, S. J Bull, D. M Elliott, "Modelling of the hardness of electroplated nickel coatings on copper substrates", *Surf. Coat. Technol.*, vol. *127*, no. *1*, pp. *1-8*, May, 2000.

[15] M. Santhanakrishnan, P. S. Sivasakthivel, R. Sudhakaran, "Modeling of geometrical and machining parameters on temperature rise while machining Al 6351 using response surface methodology and genetic algorithm", *J Braz. Soc. Mech. Sci. Eng.*, vol. *39*, no. *1*, pp. *487–496*, June, 2017.

[16] M. Santhanakrishnan, N. Venkateshwaran, M. Rajkumar, T. Vignesh, "Performance evaluation of Ni/Nano SiC coated tool insert for machining SS316l using Response Surface Methodology (RSM)", *Mater. Today: Proc.*, vol. *47*, no. *14*, pp. *4671-4675*, Oct., 2021.

[17] R. El-Khalfaouy, K. Khallouk, A. Elabed, A. Addaou, A. Laajeb, A. Lahsini, "Modeling and synthesis of carbon-coated LiMnPO4 cathode material: Experimental investigation and optimization using response surface methodology", *J. Electrochem. Sci. Eng.*, vol. *12*, no. *2*, pp. *305-316*, Jan., 2022.

[18] W. Jau-Kai, C. Jir-Ming, "Optimization study on hardness of gold film through supercritical electroplating process by response surface methodology", *Chem. Ind. Chem. Eng. Q.*, vol. *21*, no. *2*, pp. *311-317*, Aug., 2015.

[19] A. F. Almeida, J. I. V. Souto, M. L. Santos, R. A. C. Santana, J. J. N. Alves, A. R. N. Campos, S. Prasad, "Establishing relationships between bath composition and the properties of amorphous Ni–Mo alloys obtained by electrodeposition, *J. Alloys Compd.*, vol. *888*, p. *161595*, Dec., 2021.

[20] S. Esmailzadeh, T. Shahrabi, Y. Yaghoubinezhad, Gh. Barati Darband, "Optimization and characterization of pulse electrodeposited nickel selenide nanostructure as a bifunctional electrocatalyst by response surface methodology", *Int. J. Hydrogen Energy*, vol. *46*, no. *36*, pp. *18898-18912*, May, 2021.

[21] I. Mladenović, Z. Jakšić, M. Obradov, S. Vuković, G. Isić, D. Tanasković, J. Lamovec, "Subwavelength nickel-copper multilayers as an alternative plasmonic material", *Opt. Quant. Electron.*, vol. *50*, no. *5*, p. *203*, Apr., 2018.

[22] D. P. Linklater, F. Haydous, C. Xi, D. Pergolesi, J. Hu, E. P. Ivanova, S. Juodkazis, T. Lippert, J. Juodkazytė,"Black-Si as a Photoelectrode", *Nanomaterials*, vol. *10*, no. *5*, p. *873*, May, 2020.

[23] B. Li, W. Zhang, T. Mei, S. Du, Y. Miao, D. Li, "Synthesis and properties of YSZ and CeO2 dual nanoparticles doped Ni–B matrix nanocomposite coating", *Ceram. Int.*, vol. *46*, no. *6*, pp. *8047-8058*, Apr., 2020.

[24] I. Horcas, R. Fernández, J. M. Gómez-Rodríguez, J. Colchero, J. Gómez-Herrero, A. M. Baro, "WSXM: A software for scanning probe microscopy and a tool for nanotechnology", *Rev. Sci. Instrum.*, vol. *78*, no. *1*, p. *013705*, Jan., 2007.

[25] I. O. Mladenović, N. D. Nikolić, J. S. Lamovec, D. Vasiljević-Radović, V. Radojević, "Application of the Composite Hardness Models in the Analysis of Mechanical Characteristics of Electrolytically Deposited Copper Coatings: The Effect of the Type of Substrate", *Metals*, vol. *11*, no. *1*: p. *111*, Jan., 2021.

PROCEEDINGS, IX INTERNATIONAL CONFERENCE IcETRAN, Novi Pazar, Serbia, 6 - 9. june 2022.

1

Electrically Programmable Analog Device As An Ultraviolet Light Sensor

Stefan D. Ilić, *Student Member, IEEE*, Milija Sarajlić, *Member, IEEE*, Dana Vasiljević-Radović, *Member, IEEE*, Marko S. Andjelković, Alberto Palma, Russell Duane, and Goran S. Ristić

Abstract—**Electrically Programmable Analog Device (EPAD) is a commercial semiconductor device based on a floating gate MOS transistor. It is possible to charge the EPADs floating gate with electrons and thus increase the threshold voltage of the MOS transistor. Decapsulation of the ALD1108E integrated circuit containing four EPADs was performed to expose the semiconductor structure to ultraviolet light. By irradiating with different UV light sources, the threshold voltage of an EPAD with a pre-charged floating gate decreases, indicating a possibility for UV radiation detection. The sensitivity of EPAD to the UV light range of 311 to 400 nm was investigated. The floating gate MOS transistor (EPAD), which has a more charged floating gate with electrons, i.e. higher threshold voltage value, shows higher sensitivity compared to EPAD with a lower charged floating gate, i.e. lower threshold voltage value.**

Index Terms—**Floating gate MOS transistor, Ultraviolet Light, Light Sensor, EPAD, IC decapsulation**

I. INTRODUCTION

MEMORIES that remember content even after a power failure are called Non-Volatile Memories. First came the Mask ROM (Read Only Memory) memory, i.e. mask programmed ROM. A whole array of memory cells is formed on the chip in the form of a matrix. Then, according to the user's request, a mask for the photolithographic procedure is created, which defines the openings for drawing the lines of connection between cells and the power supply. Cells that should contain a logic "1" are connected to the power supply (highly doped polysilicon is applied through the opening on the mask to make contact), while cells that should contain a logic "0" remain unbound to the power supply. The Mask ROM stores data permanently, the process is very expensive, and every change requires a change of the photolithography mask.

S. D. Ilić, M. Sarajlić and D. Vasiljević-Radović are with the Center of Microelectronic Technologies, Institute of Chemistry, Technology and Metallurgy, University of Belgrade, Serbia, S. D. Ilić is also with the Applied Physics Laboratory at Faculty of Electronic Engineering, University of Niš, Serbia, E-mail: stefan.ilic@nanosys.ihtm.bg.ac.rs

M. S. Andjelković is with the System Architectures Department, IHP - Leibniz-Institut für innovative Mikroelektronik, Frankfurt (Oder), Germany, E-mail: andjelkovic@ihp-microelectronics.com

A. Palma is with the Department of Electronics and Computer Technology, University of Granada, Granada, Spain, E-mail: ajpalma@ugr.es

R. Duane is with the Centre for Micro and Nano Systems, Tyndall National Institute, University College Cork, Dyke Parade, Cork, Ireland, E-mail: russell.duane@tyndall.ie

G. S. Ristić is with the Applied Physics Laboratory at Faculty of Electronic Engineering, University of Niš, Serbia, E-mail: goran.ristic@elfak.ni.ac.rs

In order to solve the problem of expensive production, PROM (Programmable ROM) memory is created; here, the data is stored by the user himself with specialized electrical devices. Namely, PROM is produced so that all cells have a logic "1", and they are all connected to the power supply. The interruption of connection lines between individual cells is done by passing a high-density current, which melts the desired line. Once programmed, the PROM cannot be reprogrammed.

The next memory that emerged with technology development is an EPROM (Erasable & Programmable ROM). For the first time, it is possible to delete data, which is done by exposing the memory to UV rays. EPROM is the first memory to have a floating gate (FG) in its structure, and thanks to such a device, it is possible to erase the charge on the pre-charged floating gate and thus change the threshold voltage of the MOS transistor. Decreasing the threshold voltage leads to a change in the logical state of the cell from "0" to "1". The memory is byte-addressable when writing and reading, while the deletion process covers the entire memory. When deleting, the memory chip must be removed from the motherboard and exposed to UV radiation for 20 minutes [1]. The complete deletion process needs to be done even though only one byte needs to be changed.
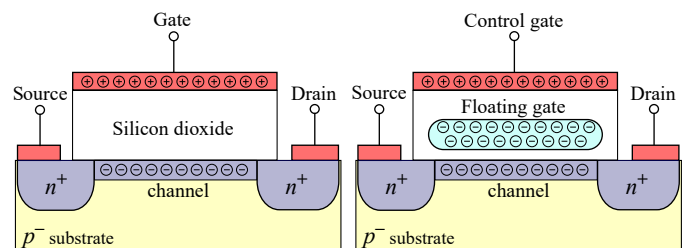
Fig. 1. Left: Cross-section of a MOS transistor. Right: Cross-section of a MOS transistor with a floating gate

Figure 1 shows the structure of a MOS transistor, and the structure of a MOS transistor with a floating gate (FG). During ultraviolet radiation, photons reach the floating gate and generate electron-hole pairs in the vicinity of the floating gate. Due to the electric field that originates from the floating gate, the generated carriers are separated because it is charged with electrons. The holes recombine with the electrons located on the floating gate, and thus the amount of charge is reduced, which leads to a lower threshold voltage value of the MOS transistor.

PROCEEDINGS, IX INTERNATIONAL CONFERENCE IcETRAN, Novi Pazar, Serbia, 6 - 9. june 2022.

2

II. MATERIALS AND EXPERIMENTAL SETUP

The experiment consisted of irradiating the decapsulated IC ALD1108E [2] with three different types of UV sources. Decapsulation of the ALD1108E integrated circuit is a high-tech process that requires the removal of plastic above the chip so that light can reach the semiconductor device, while the bonds connecting the chip to the package must not be damaged. This process was performed at the Tyndall National Institute, Cork, Ireland. Since decapsulated integrated circuits are extremely sensitive to handling and potential mechanical damage and chip contamination if handled in dirty conditions, the experiment was performed in a cleanroom at the Center of Microelectronic Technologies, Institute of Chemistry, Technology and Metallurgy, Serbia. The number of particles in a cleanroom was controlled using a PCE-PCO 1 particle counter. During the experiment, all measured particle sizes were filtered to zero. The measurement of particles was done in 21 seconds, which corresponds to airflow of 1 litre.

In order to protect the decapsulated chip from mechanical damage during the handling and measurements, special housing for UV experiments made of polylactic acid (PLA) material with a quartz window was designed, as shown in Figure 2.
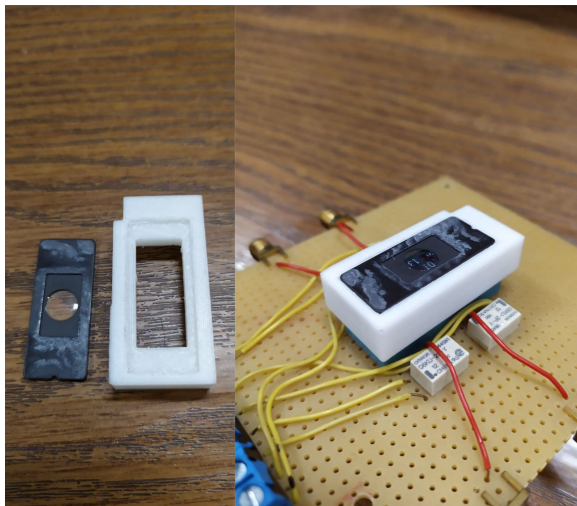

Fig. 2. Left: A quartz window and housing for decapsulated IC made of PLA material. Right: Assembled housing on the IC ALD1108E inserted in the ZIF socket.

The housing was designed in the Solid Edge 2021 Academic version and then fabricated using the Creality Ender 6 Core-XY 3D printer. The decapsulated integrated circuit has a weakened plastic housing and therefore needs to be handled very carefully, especially when inserted into the IC socket. Therefore, an electric circuit for measuring the characteristics of EPAD on the IC ALD1108E with a zero insertion force (ZIF) socket has been designed.

The housing is designed to protect the decapsulated IC from all sides but not to touch the plastic DIP of the integrated circuit due to potential damage to the bonds during handling. Therefore the housing is mounted on the ZIF socket in which the integrated circuit is inserted.

Since it is necessary for UV light to penetrate the housing, a quartz window has been installed to enable this. Old EPROM memories had a quartz window on their package so that UV light could erase the memory, and this gave the idea to the authors to use a quartz window from an old memory from ST Microelectronics.

To ensure that a sufficient amount of UV light passes through the selected quartz window, the transmission of our housing was measured using a UV-Visible Spectrophotometer Evolution 60 from Thermo Scientific, and shown in Figure 3.
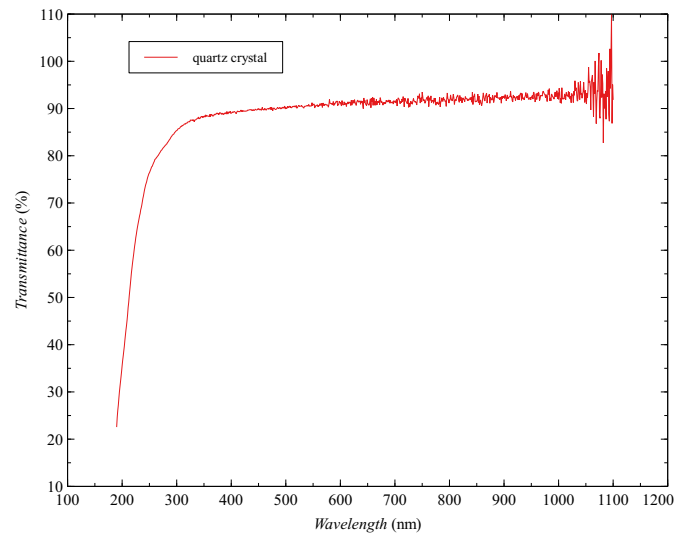
Fig. 3. Transmittance of quartz window mounted in housing made of PLA material.

For a wavelength value of 300 nm, the transmittance is 85% and then increases to 90% for the visible part of the spectrum. The wavelength range for this research is from 300 to 400 nm. The UV light sources used for the purposes of this experiment are: a UV lamp with a 311 nm peak, a UV lamp with a 365 nm peak and a UV LED with a 400 nm peak; their spectrographs are shown in Figures 4 to 6, respectively.

Fig. 4. Spectrogram of UV lamp with 311 nm peak.

PROCEEDINGS, IX INTERNATIONAL CONFERENCE IcETRAN, Novi Pazar, Serbia, 6 - 9. june 2022.

3

Fig. 5. Spectrogram of UV lamp with 365 nm peak.

Fig. 6. Spectrogram of UV LED with 400 nm peak.

A UV lamp that emits light with a peak at 311 nm is used for the phototherapeutic treatment of skin diseases by producing vitamin D. As can be seen in Figure 4, this lamp has two peaks in the ultraviolet part of the spectrum at 311 nm and then at 365 nm. Other emitted light is in the visible part of the spectrum.
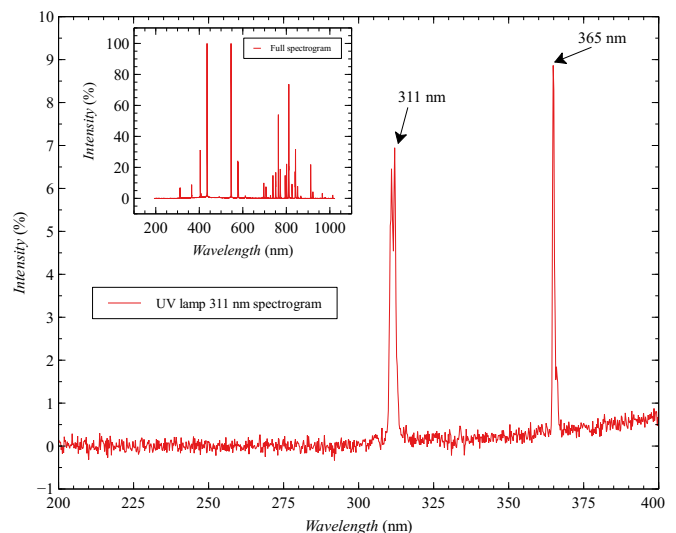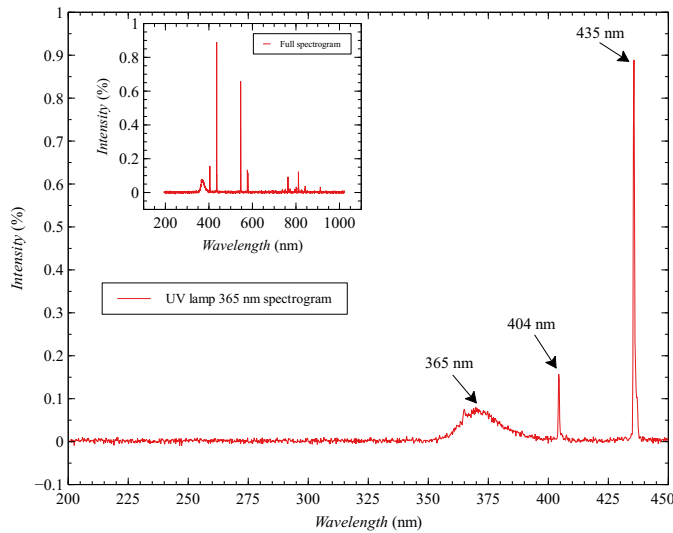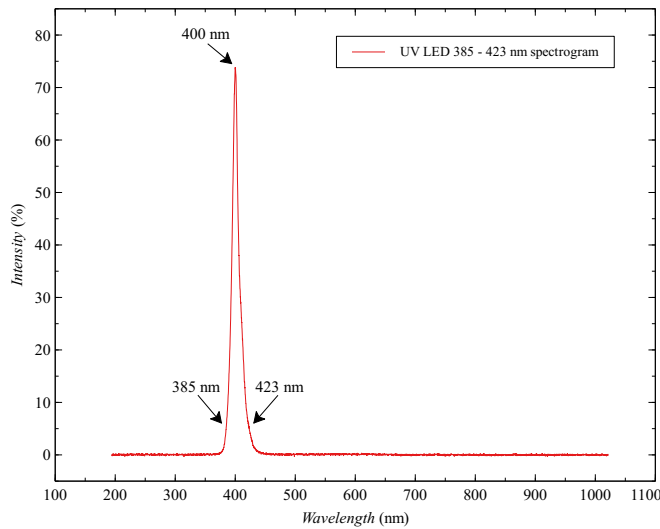
The following UV lamp used in the experiment has an application as a gel nail dryer. This lamp has only one broad peak in the ultraviolet part of the spectrum at 365 nm, while the others are in the visible part of the spectrum, as can be seen in Figure 5.

The third UV source used in this experiment is a matrix of UV LEDs. The spectrum of this source is clear, unlike UV lamps and has only one peak at 400 nm, at the border of UV and visible light.

III. RESULTS

During the irradiation of the ALD1108E chip, the drift of two floating gate MOS transistors (EPADs) was measured using a Keithley 2636A source measure unit connected to a computer. Drift is monitored at one point of the current-voltage characteristic called the zero temperature coefficient (ZTC) point [3]. Monitoring the change in the drift at this point cancels the influence of temperature on the measurements, which is an essential factor.

ZTC voltage drifts before, during and after UV irradiation for two EPADs with the same value of threshold voltage (initial $V_{th} = 4$ V) is shown in Figure 7.
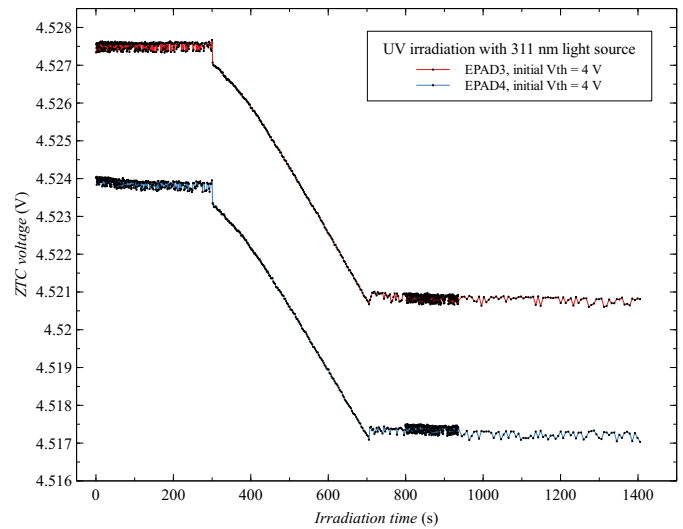
Fig. 7. ZTC voltage drift of EPAD3 and EPAD4 before, during and after UV irradiation of 311 nm light source.

Based on the ZTC point, it is possible to calculate the threshold voltage of the MOS transistor and thus indirectly monitor the threshold voltage but without the influence of temperature because for a fixed temperature (e.g. 25 °), the difference between the threshold voltage value and the ZTC point voltage value is constant. Figure 8 shows the threshold voltage shift during irradiation of two EPADs with a UV lamp of 311 nm peak.

The figure 8 shows EPADs that during the first irradiation had an initial threshold voltage of $V_{th} = 3$ V, and during the second irradiation, under the same conditions, EPADs had a threshold voltage of $V_{th} = 4$ V. It can be noticed that EPADs have higher sensitivity with higher threshold voltage means with a larger amount of electrons on the floating gate, which can be compared as an analogy to gamma radiation [4]. Also, it is possible to recharge the EPADs floating gate without degradation of its dosimetric characteristics [5].

Figure 9 shows the EPAD threshold voltage shift with the initial threshold voltage value $V_{th} = 4$ V.

The weakest response of the EPAD was observed for the UV LED light source, where the threshold voltage shift values are shown in Figure 10.

A linear dependence during irradiation can be observed for all types of UV radiation sources. The same behaviour of this sensor at small threshold voltage shifts was observed

PROCEEDINGS, IX INTERNATIONAL CONFERENCE IcETRAN, Novi Pazar, Serbia, 6 - 9. june 2022.
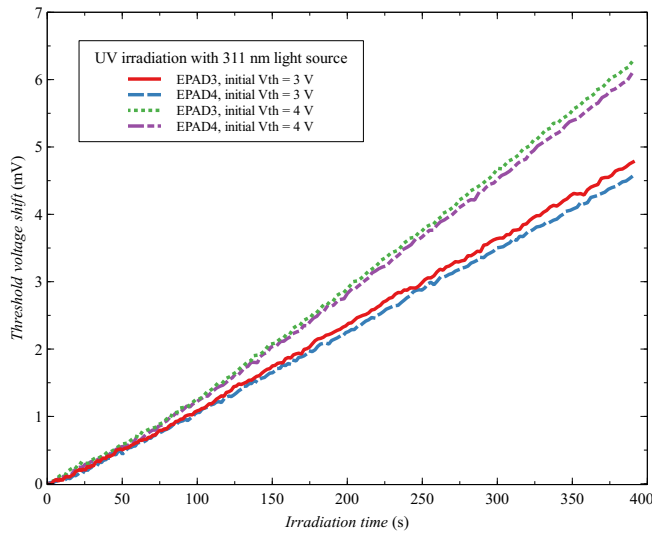
4

Fig. 8. Threshold voltage shift of EPAD3 and EPAD4 during irradiation of 311 nm light source with different charge on the floating gate.
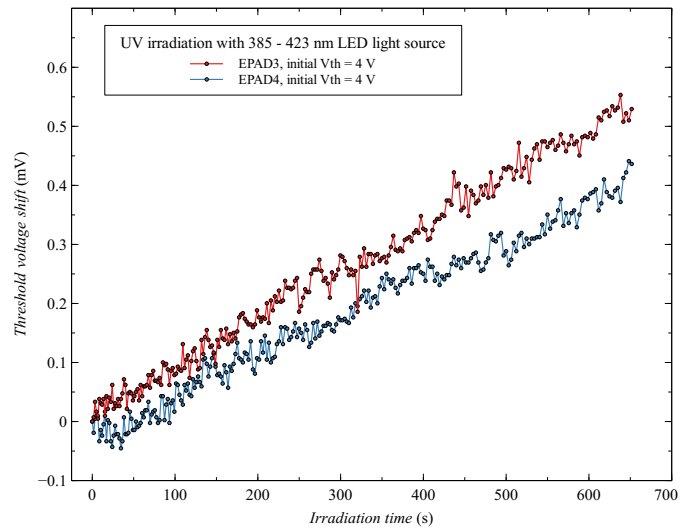

Fig. 10. Threshold voltage shift of EPAD3 and EPAD4 during irradiation of UV LED source.
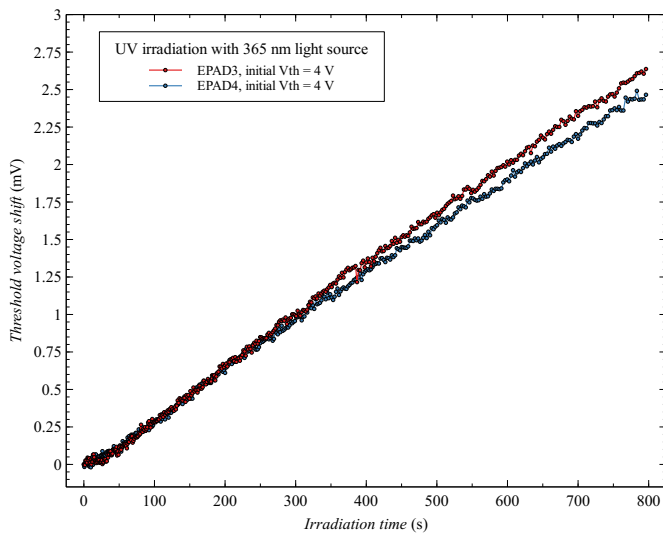

Fig. 9. Threshold voltage shift of EPAD3 and EPAD4 during irradiation of 365 nm light source.

for gamma radiation [4]. These results indicate that it is possible to record UV irradiation with the presented floating gate structure.

IV. DISCUSSION

By analyzing the spectrum of the UV lamp 311 nm in Figure 4 and the spectrum of the UV lamp 365 nm in Figure 5, we can see that both have a peak at 365 nm, which may indicate the possibility that the Vth shift from the first lamp with a peak at 311 nm (presented in Figure 8) originates from the peak at 365 nm. However, the nature of the floating gate device is that the electrons in the floating gate need to receive the minimum energy to surmount the energy barrier (similar to the photoelectric effect), and all photons with minimum or higher energy can decrease the charge on the floating gate and thus reduce the threshold voltage of the transistor

[6]. This means that all photons with a smaller wavelength of 400 nm (higher energy than 3.09 eV) can decrease the threshold voltage. It is necessary to examine the photon energy limit value of this FG dosimeter in the future.

The UV sensor enables the detection of dangerous wavelengths for human health. The floating gate MOS transistor has good properties as an ionizing radiation dosimeter, so it is possible to use the same component for ultraviolet radiation dosimetry. However, it is necessary to provide a special housing with the quartz window in which the integrated circuit is mounted.

V. CONCLUSION

The paper presents the possibility of using a floating gate MOS transistor as an ultraviolet sensor. The EPAD has been shown to respond to an ultraviolet radiation range of 311 to 400 nm. A sensor with a floating gate charged with a larger amount of electrons shows higher sensitivity. This component shows promising possibilities for dosimetry of UV radiation for medical purposes such as monitoring the received dose of patients during phototherapy.

REFERENCES

[1] W. D. Brown, W. D. Brown, and J. Brewer, *Nonvolatile semiconductor memory technology: a comprehensive guide to understanding and using NVSM devices*. Wiley-IEEE Press, 1998, vol. 6.
[2] ALD, "QUAD/DUAL Electrically Programmable Analog Device," 2012. [Online]. Available: http://www.aldinc.com/pdf/ALD1110E.pdf
[3] Z. Prijić, S. Dimitrijev, and N. Stojadinović, "The determination of zero temperature coefficient point in CMOS transistors," *Microelectronics Reliability*, vol. 32, no. 6, pp. 769–773, 1992.
[4] S. Ilić, A. Jevtić, S. Stanković, and G. Ristić, "Floating-Gate MOS Transistor with Dynamic Biasing as a Radiation Sensor," *Sensors*, vol. 20, no. 11, p. 3329, 2020.
[5] S. D. Ilić, M. S. Andjelković, R. Duane, A. J. Palma, M. Sarajlić, S. Stanković, and G. S. Ristić, "Recharging process of commercial floating-gate MOS transistor in dosimetry application," *Microelectronics Reliability*, vol. 126, p. 114322, 2021.
[6] L. Scheick, P. McNulty, and D. Roth, "Dosimetry based on the erasure of floating gates in the natural radiation environments in space," *IEEE Transactions on Nuclear Science*, vol. 45, no. 6, pp. 2681–2688, 1998.

Origin of the Open Circuit Voltage and Important Processes that Affect its Value in Organic Solar Cells

Teodora Pavličević, Jovana P. Gojanović, Nataša A. Ćirović and Sandra Živanović, Member, IEEE

Abstract—In this paper, the origin of an open circuit voltage (V_{oc}) in organic solar cells (OSCs) and processes which have a dominant impact on it were examined. The measured light current-voltage (*I-V*) characteristics of ITO/PEDOT:PSS/P3HT:PCBM/LiF/Al solar cells fabricated and characterized under similar conditions were collected from literature. The gathered V_{oc} data was statistically processed and 75 % of the results belonged to the range $0.52 - 0.64$ V and obeyed Gaussian distribution. However, 12.5 % results had a value around 0.4 V, and another 12.5 % around 0.48 V. Three *I-V* curves with different V_{oc} values belonging to three observed V_{oc} ranges were simulated by the drift-diffusion model (DDM). By changing the photogeneration, transport, recombination, and extraction parameters, but with the same value of a built-in voltage (V_{bi}), which corresponds to a difference between electrodes work functions, the measured *I-V* curves were excellently reproduced. The experimental light *I-V* curves from literature of solar cells with different polymer blends used as an active layer (PTB7:PCBM, or MDMO-PPV:PCBM) but having the same electrodes and transport layers were also successfully simulated in the same way. Based on our review of published experimental results and our theoretical investigations, we confirm that the difference between electrode work functions is the source of the V_{oc}. The difference between acceptor's lowest unoccupied molecular orbital (LUMO) and donor's highest occupied molecular orbital (HOMO) affects the V_{oc} indirectly through photogeneration, transport and recombination parameters, and extraction efficiency.

Index Terms— Organic solar cells; open circuit voltage; drift-diffusion model.

Introduction

Organic solar cells (OSCs) have been getting a great deal of attention due to their potential as low-cost, simply processed and environment-friendly photovoltaic devices [1]. An improvement of OSCs is demonstrated through an increase in their power conversion efficiency (PCE), the most important performance parameter. So far, the PCE has reached value of 18 % for a single-layer OSC, 12 % for organic photovoltaic modules and even 23.6 % for perovskite/organic tandem solar cells [2–4]. Although these results are commendable, a further progress in properties of active layer blends, and an improvement of OSCs' long-term stability are seen as a path to their commercialization [5].

To reach a full potential of OSCs, we need to clarify their basic working principles. Knowledge of OSCs physics would help us to single out the basic prerequisites for an efficient photoconversion and identify loss mechanisms. However,

research so far was not focused much on elucidating physics but rather on increasing OSCs efficiency through new donor and acceptor materials to improve the photoconversion in the active layer, as well as through new transport layer materials to maximize the charge carrier collection [5,6]. The metal-semiconductor-metal (MSM) drift-diffusion model (DDM) [7] has been widely used for modeling the OSCs. This model is successful to a certain extent, but it is not able to reproduce the experimentally observed OSCs behavior to a full extent. Thus, a refinement of the DMM for OSCs has yet to be done by clarifying vague parts of it.

One of the parameters with unclear origin that directly affects the OSC's PCE is an open-circuit voltage (V_{oc}). There are many presumptions about processes that influence the V_{oc} and how they can be correlated [1]. Frequently, the V_{oc} is defined as $e \cdot V_{oc} = (E_g - 0.3)$ eV, where E_g is an active layer energy gap determined as a difference between the highest occupied molecular orbital level (HOMO) of the donor and the lowest molecular orbital level (LUMO) of the acceptor, and e is the elementary charge [8]. Trying to resolve 0.3 V voltage loss in the V_{oc} and other aspects of the V_{oc} behavior, many factors have been found that directly or indirectly have impact on it [1]. These include temperature, light intensity, active layer morphology, microstructure, recombination processes, quality and properties of donor/acceptor (D/A) interface area, density of states (DOS), electrode work functions, existence of charge transfer (CT) states, carrier density, reverse saturation current, defect states, and crystallinity [1]. All these factors are interrelated, and for a complete analysis of the V_{oc} all of them should be considered. The V_{oc} dependence on temperature and light intensity are most often researched and analyzed in the literature [9, 10]. It was found that the V_{oc} decreases as temperature increases, and for a wide temperature range that dependence is nearly linear [9]. On the other hand, the V_{oc} showed a logarithmic dependence on light intensity [10]. The reverse saturation current is one of the important parameters that influences the V_{oc}, and it was found that the V_{oc} is inversely proportional to it [11]. The influence of the charge carrier recombination on the V_{oc} was described through a correlation between the V_{oc} and the recombination rate [12] that differs for different recombination types – monomolecular, bimolecular or their combination. The monomolecular recombination implies a recombination through a recombination center or a trap state, while the bimolecular recombination indicates that holes and

T. Pavičević, J. P. Gojanović and N. A. Ćirović are with the School of Electrical Engineering, University of Belgrade, Belgrade 11120, Serbia (e-mail: pavlicevicteodora@gmail.com; jovana@etf.bg.ac.rs; natasa@etf.bg.ac.rs)

S. Živanović is with Institute for Micromanufacturing, Louisiana Tech University, Ruston, LA 71272 USA (e-mail: sz@latech.edu).

electrons are mutually recombined [12]. Higher recombination rates mean a reduced number of carriers and eventually a smaller V_{oc} [12]. A lower carrier density leads to a decreased V_{oc}. The improvement of the microstructure can minimize recombination rates, improve carrier dynamics, and benefit the V_{oc} [13]. Defect states introduce irregularities into the material structure, and thus energy disorders and a reduced crystallinity. In organic materials, these disorders are usually modelled via the Gaussian or exponential DOS, and it was shown that they degrade the performance of OSCs by degrading the V_{oc} [14]. Losses in the V_{oc} are also related to a non-radiative decay of the CT states on the D/A interface [15]. The impact of the morphology is mostly related to the quality of D/A interface (e.g., whether it is homogenous or not) [15]. In addition, it was shown that a reduction of the D/A interface area can contribute to a higher V_{oc} [16]. One of the most debatable matters is the influence of electrode work functions on the V_{oc}. It was shown that if the Fermi levels are well inside the energy gap of the active layer polymer-fullerene blend, the V_{oc} is strongly affected even by a small variation of each electrode work function [17]. However, if the anode work function is close to the donor's HOMO and the cathode work function is close to the acceptor's LUMO, the V_{oc} value reaches a plateau and is less sensitive to work functions variations [17]. In this case, the device operation is the most effective [17].

To investigate the origin of the V_{oc} and analyze important processes which affect its value, we have collected measured light current-voltage (I-V) characteristics of ITO(indium tin oxide)/PEDOT(poly(3,4-ethylene dioxythiophene):PSS(poly(styrenesulfonate)/ P3HT (poly(3-hexyl-2,5-dimethylthiophene):PCBM([6,6]-phenyl-C_{61}-butyric acid methyl ester)/LiF(lithium fluoride)/Al solar cells fabricated and characterized under nearly same conditions available in the literature [19-40]. We statistically processed the collected V_{oc} data and analyzed the obtained distribution function by determining its mean value and standard deviation. Three I-V curves (each with a representative and significantly different value of V_{oc}) were selected and simulated by the DDM. Viewing the OSC as an MSM structure, the built-in voltage (V_{bi}) was taken to be the difference between the two electrode work functions. The I-V characteristics with different V_{oc} values were successfully simulated by varying the reduction factor of the Langevin bimolecular recombination rate and by changing the effective density of states (N_c, N_v) at boundaries.

To inspect the influence of E_g on V_{oc}, two more solar cells with the same electrode contacts but different active layer polymer-fullerene blends, PTB7 (poly [[4,8-bis[(2-ethylhexyl)oxy]benzo[1,2-b:4,5-b′] dithiophene-2,6-diyl][3-fluoro–2-[(2-ethylhexyl)carbonyl]thieno[3,4-b] thiophenediyl]]):PCBM [41] and IMDMO-PPV (poly[2-methoxy-5-(30,70-dimethyloctyloxy)-1,4-phenylenevinylene]):PCBM [42] were considered. Their measured I-V characteristics obtained from literature were successfully fitted with the DDM by varying active layer transport and recombination parameters together with the N_c, and N_v at the boundaries. Based on the statistically processed experimental V_{oc} data and our DDM I-V curve simulations, we confirm that the V_{oc} originates from the difference of

electrode work functions and that the contact phenomena and the recombination losses have the greatest impact on its value.

OPEN CIRCUIT VOLTAGE IN ITO/PEDOT:PSS/POLYMER-FULLERENE BLEND/LiF/Al ORGANIC SOLAR CELLS

A. Review of Experimental Data

We started the investigation of the V_{oc} in OSCs by choosing one of the most researched device structure ITO/PEDOT:PSS/P3HT:PCBM/LiF/Al. This OSC structure is used as a reference in a large number of experimental research papers aimed at improving the OSC performance. The performance parameters for considered OSCs together with fabrication and characterization conditions are presented in Table 1. The gathered V_{oc} data are statistically processed and graphically presented in Fig. 1. The three distinct V_{oc} ranges are observed (see Fig. 1). The dominant range contains 75 % of collected data. Two smaller ranges each contain 12.5 % of the V_{oc} results. The largest number of collected V_{oc} values belongs to the 0.52–0.64 V range and the data follows the standard Gaussian distribution with the expected value $\mu = 0.58$ V and the standard deviation $\sigma = 0.024$ V. The V_{oc} values in the range of 0.46–0.48 V are mostly obtained for the devices illuminated by 3 sun (see Table 1), where 1 sun corresponds to standard illumination at AM1.5, or 1 kW/m^2. The V_{oc} of about 0.40 V is obtained mainly for the OSCs in which P3HT:PCBM active layer is produced from chloroform solution rather than from chlorobenzene solution (see Table 1).

According to the literature [17, 18], if injection barriers at electrode contacts are significant (i.e., rectifying junctions), the V_{oc} is defined as the difference between electrode work functions, while for optimised devices with Ohmic contacts, the V_{oc} is interpreted as the difference between the LUMO of the acceptor and the HOMO of the donor (i.e., with a mysterious loss of 0.3 V). From Fig. 1, it is clear that even for the OSCs with the same electrodes and the same D/A polymer-fullerene blend, a wide distribution of the V_{oc} values exists. This led us to the conclusion that the active layer photogeneration, transport and recombination parameters, as well as the charge extraction efficiency differ in the considered devices probably due to a different quality of the active layer, hole and electron transport layers and electrode junctions.

Additionally, the OSCs with PTB7:PCBM or MDMO-PPV:PCBM active layers with the same electrodes (ITO, Al) and transport layers (PEDOT:PSS, LiF) were examined. Although $E_g^{MDMO-PPV:PCBM} < E_g^{P3HT:PCBM}$ [35] and $E_g^{PTB7:PCBM} > E_g^{P3HT:PCBM}$[43], the V_{oc} values obtained for these devices ($V_{oc}^{MDMO-PPV:PCBM} = 0.82$ V, and $V_{oc}^{PTB7:PCBM} = 0.75$ V) are larger than any $V_{oc}^{P3HT:PCBM}$ from Table 1. Thus, we proposed that the difference between the acceptor LUMO and the donor HOMO is not crucial for the V_{oc}, but rather the parameters of photogeneration, transport, recombination, and extraction.
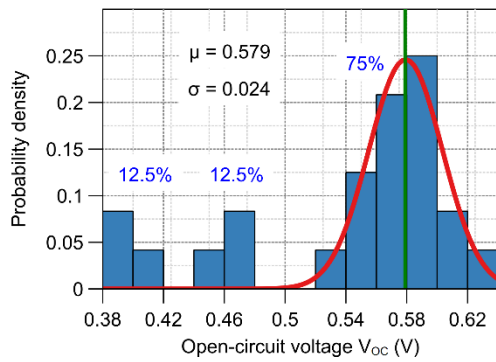
Fig. 1 Probability density obtained by statistical processing of the experimental V_{oc} data from Table 1. Gaussian function is applied to the V_{oc} data in the range 0.52 – 0.64 V (red solid curve).

TABLE I
REVIEW OF PERFORMANCE, FABRICATION AND TESTING PARAMETERS OF ITO/PEDOT:PSS/P3HT:PCBM/LiF/Al SOLAR CELLS REPORTED IN THE LITERATURE

	V_{OC} [V]	J_{SC} $\left[\frac{mA}{cm^2}\right]$	PCE [%]	Light intensity	Anneal.	Blend ratio	Solvent	Ref.
1.	**0.40**	9.50	1.55	1 sun	5 min at 120°C	1:1	Chloroform	[19]
2.	**0.59**	11.00	4.07	1 sun	10 min at 150°C	1:1	Chloroform	[20]
3.	**0.40**	0.70	/	1 sun	15 min at 120°C	1:1	Chlorobenzene	[21]
4.	**0.59**	9.70	2.64	1 sun	10 min at 120°C	1:1	Chlorobenzene	[22]
5.	**0.56**	8.92	3.31	1 sun	10 min at 140°C	3:2	1,2-Dichlorobenzene	[23]
6.	**0.48**	17.06	2.11	3 sun	5 min at 115°C	1:1	Chloroform	[24]
7.	**0.42**	17.06	2.11	3 sun	5 min at 115°C	1:0.8	Chloroform	[25]
8.	**0.57**	3.64	0.62	1 sun	No anneal.	1:1	Chlorobenzene	
9.	**0.55**	7.75	2.42	1 sun	10 min at 110°C	1:1	Chlorobenzene	[26]
10.	**0.62**	13.72	2.76	1 sun	20 min at 100°C	5:3	Chlorobenzene: Chloroform (1:1)	
11.	**0.59**	10.08	3.20	1 sun	10 min at 120°C	1:1	Dichlorobenzene	[27]
12.	**0.59**	14.27	2.61	1 sun	/	1:1	Chlorobenzene	[28]
13.	**0.60**	5.36	2.10	1 sun	15 min at 130°C	1:1	Chlorobenzene	[29]
14.	**0.55**	5.58	1.55	1 sun	10 min at 120°C	1:0.8	Chlorobenzene	[30]
15.	**0.54**	3.83	1.18	1 sun	12 min at 100°C	1:1	1,2-Dichlorobenzene	[31]
16.	**0.58**	4.79	1.10	/	at 120°C	1:0.8	/	[32]
17.	**0.58**	8.06	2.20	1 sun	10 min at 150°C	1:1	Dichlorobenzene	[33]
18.	**0.58**	/	/	/	15 min at 150°C	1:0.75	Ortho-dichlorobenzene	[34]
19.	**0.46**	6.10	1.02	1 sun	No anneal.	1:1	Chlorobenzene	[35]
20.	**0.58**	5.84	/	1 sun	15 min at 140°C	1:1	Chlorobenzene	[36]
21.	**0.64**	8.50	2.80	1 sun	30 min at 150°C	1:0.8	Chlorobenzene	[37]
22.	**0.62**	9.54	2.40	1 sun	10 min at 120°C	1:1	O-chlorobenzene	[38]
23.	**0.48**	17.06	2.11	3 sun	10 min at 120°C	1:1	Chlorobenzene	[39]
24.	**0.60**	9.23	1.79	1 sun	20 min at 130°C	1:1	Chlorobenzene	[40]

B. Drift-Diffusion Modeling

It has been shown that photoconductive polymer-fullerene blend placed between identical electrodes fabricated under the same environment, does not exhibit a rectifying effect and

their V_{oc} is zero [44–46]. This means that the D/A interface in polymer-fullerene blends does not contribute to the built-in voltage. Accordingly, the direct source of the V_{oc} in OSCs is the difference between the electrode work functions. The difference between the acceptor's LUMO and the donor's HOMO level influences the V_{oc} indirectly through the Fermi-level pinning [47], photogeneration, transport and recombination parameters, or extraction efficiency. In this paper, the metal-semiconductor-metal DDM was used for modeling the *I-V* characteristics of several OSCs. The model is based on the Poisson's equation, the hole and electron continuity equations, and the drift-diffusion transport equation for holes and electrons inside the active layer [48]. The photogeneration rate was calculated by using the transfer matrix theory and by assuming that the electric field is independent of the exciton dissociation efficiency [48]. Constant hole and electron mobilities were applied, and a reduced Langevin recombination was proposed. The Dirichlet boundary conditions were used. The solving of the equations system was done based on the finite difference discretization improved by the Scharfetter and Gummel approach and the Newton algorithm [48]. In all our calculations, a built-in voltage V_{bi} of 0.9 V as the difference between the electrode work functions was used along with the dielectric permittivity of 3.4 and the room temperature of 293.9 K.

The light *I-V* characteristic of three ITO/PEDOT:PSS/P3HT:PCBM/LiF/Al devices with $V_{oc} =$ 0.40 V [21], $V_{oc} = 0.48$ V [24], and $V_{oc} = 0.59$ V [27] were simulated and compared with the measured ones in Fig. 2 (a), (b), and (c), respectively. The parameter values used in simulations are listed in the Insets of Fig. 2, where $\mu_{n(p)}$ is the electron (hole) mobility, $N_{c(v)}$ is the effective density of states for electrons (holes), d is the active layer thickness, g is the photoconductive gain [49], and ξ is the reduction factor of the Langevin recombination rate [50]. All three measured *I-V* curves are reproduced very well by the DDM, which means that the difference in the photogeneration (g), transport (μ_n, μ_p), recombination (ξ) and extraction (N_c, N_v) parameter values may explain the observed V_{oc} diversity (see Table 1, Fig. 1). The occurrence of the photoconductive gain may be explained through a volume modulation effect, where the light illumination can increase the conductive area of the cell, thus, the generated photocurrent becomes larger [51]. The N_c and N_v are used as the boundary majority charge carrier concentrations at cathode and anode, respectively, and they are the fitting parameters in the OSCs modeling of Koster et al. [7].

These parameters are representatives of contact physics in OSCs and they have a large impact on the V_{oc}. The reduction of recombination losses in OSCs quantified by ξ leads to an improvement of the V_{oc}. In most OSCs, $\xi \leq 0.2$ [52], and its higher value indicates that CT states are significant in polymer-fullerene blend and that they recombine very rapidly. The existence of CT states and their participation in the charge carrier photogeneration and recombination [7] was not considered in our DDM. Therefore, $\xi > 1$ is possible in our simulations. A higher electron mobility leads to a lower V_{oc} [53], and an increased hole mobility slightly improves the V_{oc}.

ITO/PEDOT:PSS/P3HT:PCBM/LiF/Al

V_{OC} = 0.4 V	
μ_n [cm^2/Vs]	$3 \cdot 10^{-3}$
μ_p [cm^2/Vs]	$3 \cdot 10^{-4}$
$N_c = N_v$ [cm^{-3}]	$1.5 \cdot 10^{19}$
d [nm]	80
g	2.38
ξ	5

(a)

V_{OC} = 0.48 V	
μ_n [cm^2/Vs]	$3 \cdot 10^{-3}$
μ_p [cm^2/Vs]	$3 \cdot 10^{-3}$
$N_c = N_v$ [cm^{-3}]	$8 \cdot 10^{18}$
d [nm]	100
g	1
ξ	0.9

(b)

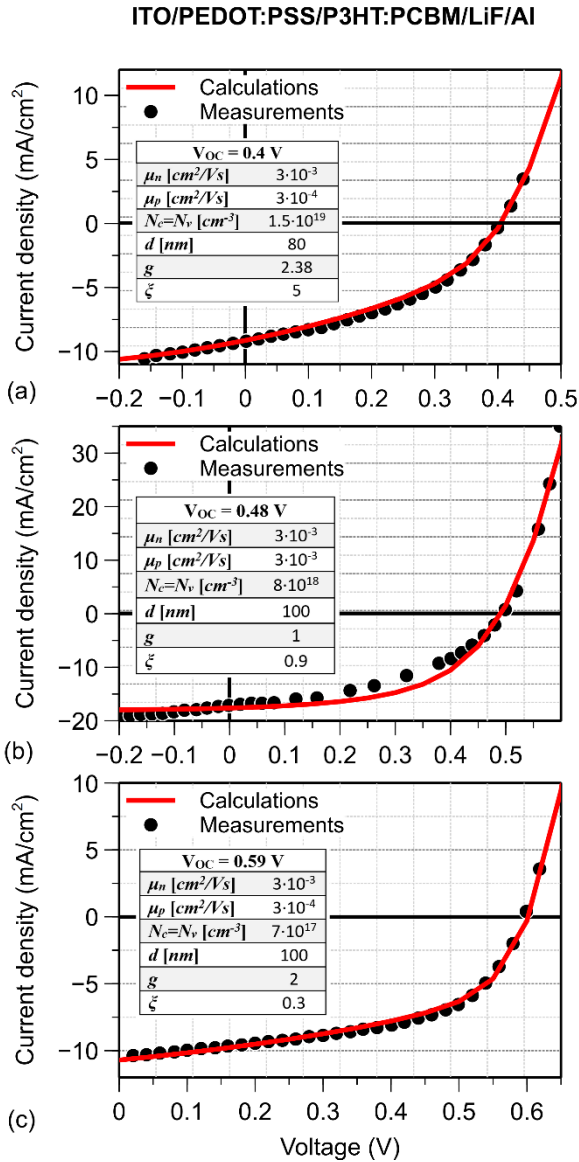| V_{OC} = 0.59 V	
μ_n [cm^2/Vs]	$3 \cdot 10^{-3}$
μ_p [cm^2/Vs]	$3 \cdot 10^{-4}$
$N_c = N_v$ [cm^{-3}]	$7 \cdot 10^{17}$
d [nm]	100
g	2
ξ	0.3

(c)

Fig 2. DDM simulated *I-V* curves compared to experimental ones taken from (a) Ref. [17], (b) Ref. [33], (c) Ref. [25]. The corresponding simulation parameters are given in the Insets.

In Figs. 3, and 4, calculated light *I-V* characteristics for the PTB7:PCBM and MDMO-PPV:PCBM based solar cells are compared with the measured ones. The simulation parameters are given in the Insets of Figs. 3, and 4.
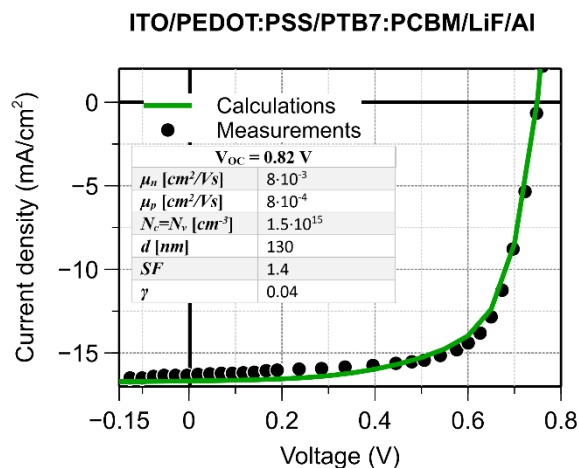
ITO/PEDOT:PSS/PTB7:PCBM/LiF/Al

V_{OC} = 0.82 V	
μ_n [cm^2/Vs]	$8 \cdot 10^{-3}$
μ_p [cm^2/Vs]	$8 \cdot 10^{-4}$
$N_c = N_v$ [cm^{-3}]	$1.5 \cdot 10^{15}$
d [nm]	130
SF	1.4
γ	0.04

Fig. 3 DDM simulated *I-V* curve compared to experimental one taken from

Ref. [39]. The corresponding simulation parameters are given in the Inset.

ITO/PEDOT:PSS/MDMO-PPV:PCBM/LiF/Al

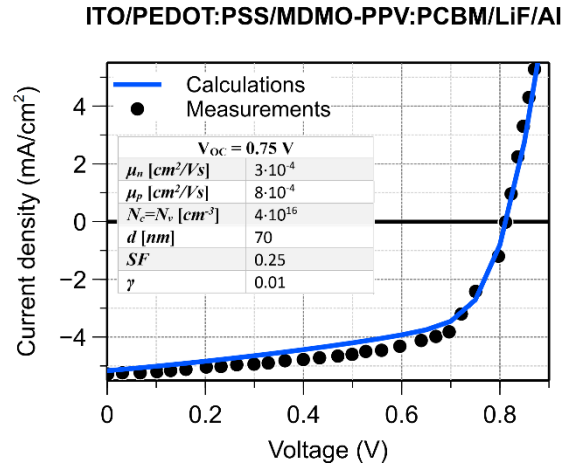| V_{OC} = 0.75 V	
μ_n [cm^2/Vs]	$3 \cdot 10^{-4}$
μ_p [cm^2/Vs]	$8 \cdot 10^{-4}$
$N_c = N_v$ [cm^{-3}]	$4 \cdot 10^{16}$
d [nm]	70
SF	0.25
γ	0.01

Fig.4 DDM simulated *I-V* curve compared to experimental one taken from Ref. [33]. The corresponding simulation parameters are given in the Inset.

Again, the experimentally obtained and theoretically predicted *I-V* curves coincide very well. This proves that even if a D/A polymer blend in an OSC is changed, the V_{oc} can be reproduced by tuning of parameters $g, \mu_n, \mu_p, N_c, N_v,$ and ξ.

CONCLUSION

The experimental light *I-V* data extracted from literature showed that the V_{oc} can significantly differ for ITO/PEDOT:PSS/P3HT:PCBM/LiF/Al solar cells produced and tested under similar conditions. Three measured light *I-V* characteristics with $V_{oc} = 0.4$ V, $V_{oc} = 0.48$ V, and $V_{oc} = 0.59$ V were successfully reproduced by our DDM simulations by applying the same value of $V_{bi} = 0.9$ V corresponding to the difference between the LiF/Al and the ITO/PEDOT:PSS work functions, while the charge carrier photogeneration, transport, recombination, and extraction were varied. For the OSCs based on the PTB7:PCBM or MDMO-PPV:PCBM polymer-fullerene blends, our DDM simulations were, again, able to reproduce the measured *I-V* curves well. We concluded that the difference between the work functions of the electrodes is the source of the V_{oc} in OSCs and the difference between the acceptor's LUMO and the donor's HOMO influences the V_{oc} through charge carrier photogeneration, recombination, transport, and extraction. These processes have a significant impact on the V_{oc} value. Future work will be dedicated to research of how the LUMO and HOMO energy levels of the polymer-fullerene D/A blend as well as the CT states formed at the D/A interfaces influence the V_{oc}.

REFERENCES

[1] N. K. Elumalai and A. Uddin, "Open circuit voltage of organic solar cells: an in-depth review," *Energy Eviron. Sci*, vol. 9, no. 2, pp. 391–410, Feb. 2016, doi: https://doi.org/10.1039/C5EE02871J

[2] Q. Liu, Y. Jiang, K. Jin, J. Qin, J. Xu, W. Li, J. Xiong, J. Liu, Z. Xiao, K. Sun, S. Yang, X, Zhang, and L. Ding, "18% Efficiency organic solar cells," *Science Bulletin*, vol. 65, no. 4, pp. 272–275, Feb. 2020, doi: https://doi.org/10.1016/j.scib.2020.01.001

[3] A. Distler, C. J. Brabec, and H-J. Egelhaaf, "Organic photovoltaic modules with new world record efficiencies," *Prog. Photovoltaics Res. App.*, vol. 29, no. 1, pp. 24–31, Jan. 2021, doi: https://doi.org/10.1002/pip.3336

[4] W. Chen, Y. Zhu, J. Xiu, G. Chen, H. Liang, S. Liu, H. Xue, E. Birgersson, J. W. Ho, X. Qin, J. Lin, R. Ma, T. Liu, Y. He, A. M-C. Ng, X. Guo, Z. He, H. Yan, A. B. Djurišić, and Y. Hou, "Monolithic perovskite/organic tandem solar cells with 23.6% efficiency enabled by reduced voltage losses and optimized interconnecting layer," *Nat Energy*, vol. 7, no. 3, pp. 229–237, Mar. 2022, doi: https://doi.org/10.1038/s41560-021-00966-8

[5] A. Karki, A. J. Gillett, R. H. Friend and T-Q Nguyen, "The Path to 20% Power Conversion Efficiencies in Nonfullerene Acceptor Organic Solar Cells," *Adv. Energy Mater.*, vol. 11, no. 15, Apr. 2021, Art. no. 2003441, doi: https://doi.org/10.1002/aenm.202003441

[6] C. Anrango-Camacho, K. Pavón-Ipiales, B. A. Frontana-Uribe, and A. Palma-Cando, "Recent Advances in Hole-Transporting Layers for Organic Solar Cells," *Nanomaterials*, vol. 12, no. 3, p. 443, Jan. 2022, doi: https://doi.org/10.3390/nano12030443.

[7] L. J. A. Koster, E. C. P. Smits, V. D. Mihailetchi, and P. W. M. Blom, "Device model for the operation of polymer/fullerene bulk heterojunction solar cells," *Phys. Rev. B*, vol. 72, no. 8, Aug. 2005, Art. no. 085205, doi: https://link.aps.org/doi/10.1103/PhysRevB.72.085205

[8] M. C. Scharber, D. Mühlbacher, M. Koppe, P. Denk, C. Waldauf, A. J. Heeger, and C. J. Brabec, "Design Rules for Donors in Bulk-Heterojunction Solar Cells – Towards 10% Energy-Conversion Efficiency," *Adv. Mater.*, vol. 18, no. 6, pp. 789–794, Mar. 2006, doi: https://doi.org/10.1002/adma.200501717

[9] G. Garcia-Belmonte, "Temperature dependence of open-circuit voltage in organic solar cells from generation–recombination kinetic balance," *Sol. Energy Mater. Sol. cells*, vol. 94, no. 12, pp. 2166–2169, Dec. 2010, doi: https://doi.org/10.1016/j.solmat.2010.07.006

[10] R. Signerski, "On the light intensity dependence of short-circuit current of bilayer organic photovoltaic cells," *J. Non-Cryst. Solids*, vol. 354, no. 35, pp. 4465–4468, Oct. 2008, doi: https://doi.org/10.1016/j.jnoncrysol.2008.06.076

[11] W. J. Potscavage Jr., S. Yoo, and B. Kippelen, "Origin of the open-circuit voltage in multilayer heterojunction organic solar cells," *Appl. Phys. Lett.*, vol. 93, no. 19, Nov. 2008, Art. no. 193308, doi: http://dx.doi.org/10.1063/1.3027061

[12] S. R. Cowan, A. Roy, and A. J. Heeger, "Recombination in polymer-fullerene bulk heterojunction solar cells," *Phys. Rev. B*, vol. 82, no. 24, Dec. 2010, Art. no. 245207, doi: https://link.aps.org/doi/10.1103/PhysRevB.82.245207

[13] D. Credgington and J. R. Durrant, "Insights from Transient Optoelectronic Analyses on the Open-Circuit Voltage of Organic Solar Cells," *J. Phys. Chem. Lett.*, vol. 3, no. 11, pp. 1465–1478, Jun. 2012, doi: https://doi.org/10.1021/jz300293q

[14] J. C. Blakesley and D. Neher, "Relationship between energetic disorder and open-circuit voltage in bulk heterojunction organic solar cells," *Phys. Rev. B*, vol. 84, no. 7, Aug. 2011, Art. no. 075210, doi: https://link.aps.org/doi/10.1103/PhysRevB.84.075210

[15] V. Coropceanu, X-K. Chen, T. Wang, Z. Zheng, and J-L. Brédas, "Charge-transfer electronic states in organic solar cells," *Nat. Rev. Mater.*, vol. 4, no. 11, pp. 689–707, Nov. 2019, doi: https://doi.org/10.1038/s41578-019-0137-9

[16] K. Vandewal, J. Widmer, T. Heumueller, C. J. Brabec, M. D. McGehee, K. Leo, M. Riede, and A. Salleo, "Increased Open-Circuit Voltage of Organic Solar Cells by Reduced Donor-Acceptor Interface Area," *Adv. Mater.*, vol. 26, no. 23, pp. 3839–3843, Jun. 2014, doi: https://doi.org/10.1002/adma.201400114

[17] A. Zampetti, A. H. Fallahpour, M. Dianetti, L. Salamandra, F. Santoni A. Gagliardi, M. Auf der Maur, F. Brunetti, A. Reale, T. M. Brown, and A. Di Carlo, "Influence of the Interface Material Layers and Semiconductor Energetic Disorder on the Open Circuit Voltage in Polymer Solar Cells," *J. Polym. Sci., Part B: Polym. Phys.*, vol. 53, no. 10, pp. 690–699, May 2015, doi: https://doi.org/10.1002/polb.23685

[18] M. Erray, M. Hanine, El-M. Boufounas, and A. El Amrani, "Combined effects of carriers charge mobility and electrodes work function on the performances of polymer/fullerene P3HT:PCBM based organic photovoltaic solar cell," *Eur. Phys. J. Appl. Phys.*, vol. 82, no. 3, June 2018, Art. no. 30201, doi: https://doi.org/10.1051/epjap/2018180070

[19] Z. Çaldıran, Ü. Erkem, A. Baltakesmez, and M. Biber, "Effects of the PENTACENE as doping material on the power conversion efficiency of P3HT:PCBM based ternary organic solar cells,"*Physica B: Condensed Matter*, vol. 607, Apr. 2021, Art. no. 412859, doi: https://doi.org/10.1016/j.physb.2021.412859

[20] T. J. Whitcher, N. A. Talik, K. Woon, N. Chanlek, H. Nakajima, T. Saisopa, and P. Songsiriritthigul, "Determination of energy levels at the interface between O_2 plasma treated ITO/P3HT:PCBM and PEDOT:PSS/P3HT:PCBM using angular-resolved x-ray and ultraviolet photoelectron spectroscopy*," J. Phys. D: Appl. Phys.,* vol. 47, no. 5, Jan. 2014, Art. no. 055109, doi:https://doi.org/10.1088/0022-3727/47/5/055109

[21] S. Arora, S. K. Rajouria, P. Kumar, P. K. Bhatnagar, M. Arora, and R. P. Tandon, "Role of donor–acceptor domain formation and interface states in initial degradation of P3HT:PCBM-based solar cells," *Phys. Scr.,* vol. 83, no. 3, Mar. 2011, Art. no. 035804, doi: https://doi.org/10.1088/0031-8949/83/03/035804

[22] H-T. Chien, M. Pölzl, G. Koller, S. Challinger, C. F. I. Baikie, M. Kratzer, C. Teichert, B. Friedel, "Effects of Hole-Transport Layer Homogeneity in Organic Solar Cells – A Multi-Length Scale Study," *Surf. Interfaces*, vol. 6, pp. 72–80, Mar. 2017, doi: https://doi.org/10.1016/j.surfin.2016.11.008

[23] H. Kwon, J. Ham, D. Y. Kim, S. J. Oh, S. Lee, S. H. Oh, E. F. Schubert, K-G. Lim, T-W. Lee, S. Kim, J-L. Lee, and J. K. Kim, "Three-Dimensional Nanostructured Indium-Tin Oxide Electrodes for Enhanced Performance of Bulk Heterojunction Organic Solar Cells," *Adv. Energy Mater.*, vol. 4, no. 7, May 2014, Art. no. 1301566, doi: https://doi.org/10.1002/aenm.201301566

[24] H. Kaçuş and Ş. Aydoğan, "The power conversion efficiency optimization of the solar cells by doping of (Au:Ag) nanoparticles into P3HT:PCBM active layer prepared with chlorobenzene and chloroform solvents," *Mater. Res. Express,* vol. 6, no. 9, July 2019, Art. no. 095104, doi: https://doi.org/10.1088/2053-1591/ab309a

[25] Y. Galagan and R. Andriessen, "Organic Photovoltaics: Technologies and Manufacturing," in *Third Generation Photovoltaics*, London, United Kingdom:IntechOpen,2012, ch. 3 [Online]. Available: https://www.intechopen.com/chapters/32590 doi: 10.5772/25901

[26] Ç. K. Kurukavak and S. Polat, "Influence of the volume of EGME-DMSO mixed co-solvent doping on the characteristics of PEDOT:PSS and their application in polymer solar cells,"*Polym. Polym. Compos.*, vol. 29, no. 8, pp. 1222–1228, Oct. 2021, doi: https://doi.org/10.1177/0967391120963470

[27] M. Wang, Q. Tang, J. An, F. Xie, J. Chen, S. Zheng, K. Y. Wong, Q. Miao, and J. Xu, "Performance and Stability Improvement of P3HT:PCBM-Based Solar Cells by Thermally Evaporated Chromium Oxide (CrOx) Interfacial Layer," *ACS Appl. Mater. Interfaces*, vol. 2, no. 10, pp. 2699–2702, Oct. 2010, doi: https://doi.org/10.1021/am100541d

[28] F. Li, L. Kou, W. Chen, C. Wu, and T. Guo, "Enhancing the short-circuit current and power conversion efficiency of polymer solar cells with graphene quantum dots derived from double-walled carbon nanotubes," *NPG Asia Materials*, vol. 5, no. 8, Aug. 2013, doi: https://doi.org/10.1038/am.2013.38

[29] M-S. Kim, B-G. Kim, and J. Kim, "Effective Variables To Control the Fill Factor of Organic Photovoltaic Cells," *ACS Appl. Mater. Interfaces*, vol. 1, no. 6, pp. 1264–1269, June 2009, doi: https://doi.org/10.1021/am900155y

[30] S. H. Oh, S. J. Heo, J. S. Yang, and H. J. Kim, "Effects of ZnO Nanoparticles on P3HT:PCBM Organic Solar Cells with DMF-Modulated PEDOT:PSS Buffer Layers," *ACS Appl. Mater. Interfaces*, vol. 5, no. 22, pp. 11530–11534, Nov. 2013, doi: https://doi.org/10.1021/am4046475

[31] S. Shanin, "Engineering the performance of optical devices using plasmonics and nonlinear organic chromophores," Ph.D. dissertation, Department of Optical Sciences, University of Arizona, Tucson, Arizona, 2014.

[32] K. Yao, L. Chen, Y. Chen, F. Li, and P. Wang, "Influence of water-soluble polythiophene as an interfacial layer on the P3HT/PCBM bulk heterojunction organic photovoltaics," *J. Mater. Chem.*, vol. 21, no. 36, pp. 13780–13784, Sep. 2011, doi: https://doi.org/10.1039/C1JM12016F

[33] F. Li, J. Zhao, K. Yao, and Y. Chen, "Origin of the efficiency improvement in pre-annealed P3HT/PCBM solar cells with LiF/Al electrodes," *Chem. Phys. Lett.*, vol. 553, pp. 36–40, Nov. 2012, doi: https://doi.org/10.1016/j.cplett.2012.10.006

[34] B. Arredondo, C. de Dios, R. Vergaz, A.R. Criado, B. Romero, B. Zimmermann, and U. Würfel, "Performance of ITO-free inverted organic bulk heterojunction photodetectors: Comparison with standard

device architecture," *Org. Electron.*, vol. 14, no. 10, pp. 2484–2490, Oct. 2013, doi: https://doi.org/10.1016/j.orgel.2013.06.018

[35] M. Girtan and M. Rusu, "Role of ITO and PEDOT:PSS in stability/degradation of polymer: fullerene bulk heterojunctions solar cells," *Sol. Energy Mater. Sol. Cells*, vol. 94, no. 3, pp. 446–450, Mar. 2010, doi: https://doi.org/10.1016/j.solmat.2009.10.026

[36] F. Yakuphanoglua and R.S. Anand, "Charge transport properties of an organic solar cell," *Synth. Met.*, vol. 160, no. 21, pp. 2250–2254, Nov. 2010, doi: https://doi.org/10.1016/j.synthmet.2010.08.015

[37] Y. Park, S. Noh, D. Lee, J. Y. Kim, and C. Lee, "Temperature and Light Intensity Dependence of Polymer Solar Cells with MoO_3 and PEDOT:PSS as a Buffer Layer," *J. Korean Phys. Soc.*, vol. 59, no. 2, pp. 362–366, Aug. 2011, doi: https://doi.org/10.3938/jkps.59.362

[38] M. D. Irwin, D. B. Buchholz, A. W. Hains, R. P. H. Chang, and T. J. Marks, "p-Type semiconducting nickel oxide as an efficiency-enhancing anode interfacial layer in polymer bulk-heterojunction solar cells," *Proc. Natl. Acad. Sci. USA*, vol. 105, no. 8, pp. 2783–2787, Feb. 2008, doi: https://doi.org/10.1073/pnas.0711990105

[39] H. Kaçuş, M. Biber, and Ş. Aydoğan, "Role of the Au and Ag nanoparticles on organic solar cells based on P3HT:PCBM active layer," *Appl. Phys. A*, vol. 126, no. 10, Sep. 2020, Art. no. 815, doi: https://doi.org/10.1007/s00339-020-03992-7

[40] X. Liu, L. J. Guo, and Y. Zheng, "5-nm LiF as an Efficient Cathode Buffer Layer in Polymer Solar Cells Through Simply Introducing a C_{60} Interlayer," *Nanoscale Res. Lett.*, vol. 12, no. 1, Sep. 2017, Art. no. 543, doi: https://doi.org/10.1186/s11671-017-2299-y

[41] W. Lu, Y. Peng, Q. Chen, W. Tang, T. Pang, S. Zhang, Z. Liu, L. Yan, and X. Wang, "Hole transport layer free bulk heterojunction organic solar cells with high work function ITO anodes," *AIP Adv.*, vol. 8, no. 9, Aug. 2018, Art. no. 095027, doi: https://doi.org/10.1063/1.5049424

[42] C. J. Brabec, S. E. Shaheen, C. Winder, and N. S. Sariciftci, "Effect of LiF/metal electrodes on the performance of plastic solar cells," *Appl. Phys. Lett.*, vol. 80, no. 7, pp. 1288–1290, Feb. 2002, doi: https://doi.org/10.1063/1.1446988

[43] S. Park, J. Jeong, G. Hyun, M. Kim, H. Lee, and Y. Yi, "The origin of high PCE in PTB7 based photovoltaics: proper charge neutrality level and free energy of charge separation at PTB7/PC71BM interface," *Sci. Rep.*, vol. 6, no. 1, Oct. 2016, Art. no. 35262, doi: https://doi.org/10.1038/srep35262

[44] S. Alem, J. Gao, and G. Wantz, "Photovoltaic response of symmetric sandwich polymer cells with identical electrodes," *J. Appl. Phys.*, vol. 106, no. 4, Aug. 2009, Art. no. 044505, doi: https://doi.org/10.1063/1.3207769

[45] J. Gao, J. Hui, Y. Hou, and S. Alem, "Planar polymer photovoltaic cells with millimeter interelectrode spacing," *J. Appl. Phys.*, vol. 104, no. 8, Oct. 2008, Art. no. 084512, doi: https://doi.org/10.1063/1.3003082

[46] M. Girtan, "On the stability of the electrical and photoelectrical properties of P3HT and P3HT:PCBM blends thin films," *Org. Electron.*, vol. 14, no. 1, pp. 200–205, Jan. 2013, doi: https://doi.org/10.1016/j.orgel.2012.10.023

[47] V. D. Mihailetchi, P. W. M. Blom, J. C. Hummelen, and M. T. Rispens, "Cathode dependence of the open-circuit voltage of polymer:fullerene bulk heterojunction solar cells," *J. Appl. Phys.*, vol. 94, no. 10, pp. 6849–6854, Nov. 2003, doi: https://doi.org/10.1063/1.1620683

[48] A. R. Khalf, J. P. Gojanović, N. A. Ćirović, S. Živanović, and P. S. Matavulj, "The Impact of Surface Processes on the J–V Characteristics of Organic Solar Cells," in *IEEE Journal of Photovoltaics*, vol. 10, no. 2, pp. 514-521, Mar. 2020, doi: https://doi.org/10.1109/JPHOTOV.2020.2965401

[49] D. Li, L. Song, Y. Chen, and W. Huang, "Modeling Thin Film Solar Cells: From Organic to Perovskite," *Adv. Sci.*, vol. 7, no. 1, Jan. 2020, Art. no. 1901397, doi: https://doi.org/10.1002/advs.201901397

[50] F. Laquai, D. Andrienko, R. Mauer, and P. W. M. Blom, "Charge Carrier Transport and Photogeneration in P3HT:PCBM Photovoltaic Blends," *Macromol. Rapid Comm.*, vol. 36, no. 11, pp. 1001–1025, June 2015, doi: https://doi.org/10.1002/marc.201500047

[51] J. A. Garrido, E. Monroy, I. Izpura, and E. Muñoz, "Photoconductive gain modelling of GaN photodetectors," *Semicond. Sci. Technol.,* vol. 13, no. 6, pp. 563–568, June 1998, doi: https://doi.org/10.1088/0268-1242/13/6/005

[52] T. M. Burke, S. Sweetnam, K. Vandewal, and M. D. McGehee, "Beyond Langevin Recombination: How Equilibrium Between Free Carriers and Charge Transfer States Determines the Open-Circuit Voltage of Organic Solar Cells," *Adv. Energy Mater.*, vol. 5, no. 11, June 2015, Art. no. 1500123, doi: https://doi.org/10.1002/aenm.201500123

[53] O. J. Sandberg, A. Sundqvist, M. Nyman, and R. Österbacka, "Relating Charge Transport, Contact Properties, and Recombination to Open-Circuit Voltage in Sandwich-Type Thin-Film Solar Cells," *Phys. Rev.*

Appl., vol. 5, no. 4, Apr. 2016, Art. no. 044005, doi: https://link.aps.org/doi/10.1103/PhysRevApplied.5.044005

Design Consideration for Low-Power Step-Up Converter

Jana Vračar, *Student Member*, *IEEE*, Milan Stojanović, *Student Member*, *IEEE*, Zoran Prijić, *Member*, *IEEE*, Aneta Prijić, *Member*, *IEEE* and Ljubomir Vračar

Abstract— **This paper describes the comparison of different MOSFETs and transformers used in a step-up circuit under initial voltages of 50 mV and 100 mV. Two MOSFETs, BSP149 and CPC3701CTR, and two transformers, CST-100LC and MID-SNS CS, were cross-connected, and the results of charging a 2200 μF capacitor were shown. This circuit consists of a Meissner oscillator and a voltage doubler circuit. Experimentally, the time it takes for different MOSFETs and transformers to increase the voltage and charge the capacitor at the circuit's output was measured, as well as the maximum output voltage generated by the circuit, and the resonant frequency for each of the given pairs of MOS transistors and transformers.**

Index Terms—**step-up converter, transformers, MOSFET, power management.**

I. INTRODUCTION

In recent years, the WSNs technology create more interest in researching from macro to micro-level to develop systems without using conventional power supplies and exploring alternative power sources for WSNs (Wireless Sensor Nodes). Energy harvesting is a viable option for replacing low-power devices batteries or power supply. Energy harvesting necessitates the collaboration of three distinct technologies. For developing systems based on energy harvesting, there must be three separate technologies combined in working together: energy harvesters - used to convert ambient energy into electrical energy, power management - for amplifying and regulating the generated energy and energy storage - for powering low power consumption systems, such as sensors, actuators, microcontrollers, RF transceivers, etc. [1].

Jana Vračar is with the Department of Microelectronics, University of Niš, Faculty of Electronic Engineering, Aleksandra Medvedeva 14, 18000 Niš, Serbia, e-mail: jana.vracar@elfak.ni.ac.rs

Milan Stojanović is with the Department of Microelectronics, University of Niš, Faculty of Electronic Engineering, Aleksandra Medvedeva 14, 18000 Niš, Serbia, e-mail: milan.stojanovic@elfak.ni.ac.rs

Zoran Prijić is with the Department of Microelectronics, University of Niš, Faculty of Electronic Engineering, Aleksandra Medvedeva 14, 18000 Niš, Serbia, e-mail: zoran.prijic@elfak.ni.ac.rs

Aneta Prijić is with the Department of Microelectronics, University of Niš, Faculty of Electronic Engineering, Aleksandra Medvedeva 14, 18000 Niš, Serbia, e-mail: aneta.prijic@elfak.ni.ac.rs

Ljubomir Vračar is with the Department of Microelectronics, University of Niš, Faculty of Electronic Engineering, Aleksandra Medvedeva 14, 18000 Niš, Serbia, e-mail: ljubomir.vracar@elfak.ni.ac.rs
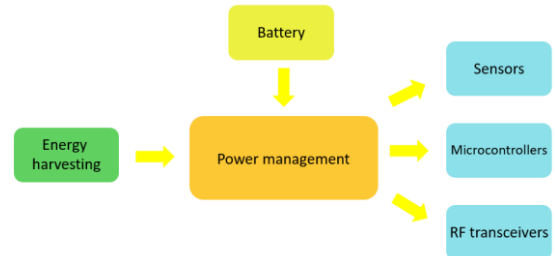
Fig. 1. Block scheme of energy harvesting system.

The block diagram of this kind of system is shown in Fig. 1. Low voltage and ultra-low power circuit design have become increasingly important recently. Low-power systems, such as those used in energy harvesting systems, wearable electronic devices, autonomous sensor nodes powered by non-conventional energy sources, the Internet of Things, and other similar applications, may require even lower supply voltage [2].

II. VOLTAGE STEP-UP CIRCUIT AND EXPERIMENTAL SETUP

A. *Voltage step-up circuit*

For the supply of an embedded system, it is required to employ an electrical boost converter to boost the harvested voltage to a voltage of higher values. When used in combination with energy harvesting, a step-up converter should be self-starting from as low as feasible input voltages without the usage of additional power. A low-voltage start circuit with an oscillator followed by a voltage multiplier is used to meet these design constraints. The electric circuit of a step-up circuit is shown in Fig 2.
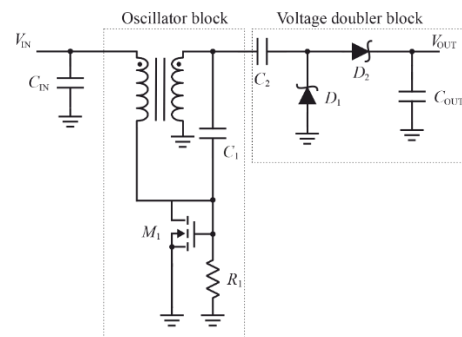

Fig. 2. Electric circuit of a voltage booster without energy harvesting block

The minimal input voltage may be amplified significantly by changing the input DC energy into an AC form via an oscillator, then converting it back to DC with a boosted level by a voltage multiplier [3]. The oscillator block in this paper consists of a Meissner oscillator. It is needed to have an appropriate step-up ratio and have an adequate power conversion efficiency also.

At low input voltages, with the appropriate selection of MOS transistors and transformers, the Meissner oscillator begins to oscillate. If the input voltage is high enough, it undergoes a transition from its linear into a non-linear operation regime. The Meissner oscillator serves as a start-up circuit providing the supply voltage for a separate, inductor-based step-up converter from an input voltage of 50 mV and 100 mV for this experiment, followed by a voltage doubler circuit. When comparing different step-up converters, the parameters of start-up voltage and self-supply, as well as the employed circuit idea, are key factors to take into account. Low-voltage step-up converters are a popular subject of research, and of course, there are commercially produced devices. These converters have start-up voltages as low as 20 mV in some cases [4]. The capacitor C_2, which is part of the voltage doubler circuit, influences the maximum output current value. When utilizing a transformer with a ratio of 1:100 and working from very low input voltages, a minimum value of 1 nF is advised [4]. When operating at low input voltage or with high resistance sources, a large capacitor value may affect circuit performance. In this circuit, the gate coupling capacitor C_1 is employed. When the input voltage surpasses 50 mV, the capacitor's voltage value capacitor is increased to the point where oscillations occur rapidly. The experimentally established value for capacitor C_1 is 4.7 nF. Because of resistor R_1, the circuit's oscillations start consistently. The resistor R_1 of 2.2 MΩ is the predefined value. Schottky diodes are being used in this circuit for the voltage doubler (D_1 and D_2). The selected diodes have better frequency response and lower forward voltage than standard Si diode due to the lower forward voltage, and that is the reason for their implementation in this circuit. The energy is stored in the electrolytic capacitor C_{OUT}, which has a capacitance of 2200 µF. The choice of transformer is crucial in the circuit design process, and it will be considered in the experimental setup. High quality factor Q, compact footprint area, and high turns ratio are the main characteristics of the transformer for low voltage step-up oscillators. The step-up oscillator is coupled to the voltage source that drives the current through the primary trnasformer winding L_1 and the depletion-mode MOSFET. This current causes a positive voltage to be induced on the secondary transformer winding L_2, which raises the gate voltage of transistor M_1 and hence the primary winding current. The secondary winding voltage begins to diminish when this current reaches core saturation. The transistor begins to switch off the current via the transformer's main winding, resulting in a voltage reversal at the secondary winding and a negative gate voltage. The transistor is promptly turned on and remains active until the primary winding current reaches saturation, at which point the oscillation process restarts. The signal from the step-up oscillator is received by a half wave voltage doubler (V_{OSC}).

In the voltage doubler circuit, capacitor C_2 and diode D_1 create a clamp, while the diode D_2 and capacitor C_{OUT} create a peak rectifier. Diode D_1 conducts during the negative half cycle of an input voltage signal, charging capacitor C_2 to the voltage $V_{C2} = V_{D1} - V_{OSC}$. Diode D_1 is turned off during the positive half cycle of the input signal, while diode D_2 conducts charging capacitor C_{OUT} [5]. The output voltage will be:

$$V_{OUT} = V_{OSC} - V_{C2} - V_{D2} = 2(V_{OSC} - V_D) \qquad (1)$$

B. Experimental setup

The major purpose of this study is to see how different pairings of transformers and transistors affect the generation of output voltage in the stated circuit, depending on whether a 50 mV or 100 mV voltage is provided to the circuit's input. The BSP149 and CPC3701CTR NMOS depletion mode transistors were used for the experiment. Since of its negative threshold voltage (V_{th}), the depletion mode n-type MOSFET BSP149 (M_1) was chosen because it is in a normally-on state at low voltages [6]. The transistor's low drain-source on-state resistance, which ranges from 1.7 Ω to 3.5 Ω, is the transistor's second advantage.

The CPC3701CTR transistor has lower drain-source on-state resistance of 1 Ω than transistor BSP149 [7]. The drain-source on-state resistance is an important characteristic of the depletion mode n-type MOSFET for the reason that this resistance affects power loss, and can be calculated as:

$$R_{DS(ON)} = \frac{1}{\mu_n \cdot C_{OX}\frac{W}{L}(V_{GS} - V_{th})} \qquad (2)$$

where is μ_n – carrier mobility, C_{OX} – oxide capacitance, W – channel width, L – channel length, V_{GS} – gate-source voltage, and V_{th} – threshold voltage.

As previously noted in the paper, the micro transformer with a ratio of 1:100 was chosen. For this experiment, transformers from different manufacturers were taken, but with similar characteristics and the same transformation ratio. The first transformer is CST-100LC, which has an inductance of 2 mH and a resistance of 5 Ω [8], while the second is a MID-SNS-CS with an inductance of 5.6 mH and a resistance of 0.85 Ω [9].

Since it is necessary to use a pair of transistor and transformer in the circuit, based on an input voltage of 50 mV in the first case and 100 mV in the second, it was decided to test all possible transistor and transformer combinations and then compare the output values of various parameters. These combinations are BSP149 MOSFET and CST-100LC transformer, BSP149 MOSFET and MID-SNS CS transformer, CPC3701CTR MOSFET and CS-100LC transformer, and CPC3701CTR MOSFET and MID-SNS CS transformer.

The expected results are that the MOS transistor CPC3701CTR in combination with some of the transformers can generate the highest output voltage since it has better characteristics than the BSP149 transistor, specified in the datasheet.

III. RESULTS AND DISCUSSION

The input voltage V_{IN} simulates the generated voltage given by one of the energy harvesting block. In this case, DC voltage input is generated by a voltage supply at 50 mV and 100 mV instead of an energy harvesting voltage source. Fig. 3 shows the time that elapsed until the voltage on the capacitor reached 3.3 V and 5 V. The result of this measurement shows that the CPC3701CTR MOSFET and CST-100LC transformer take the longest time to generate specified output voltages. The shortest time to generate these values of voltage is measured for CPC3701CTR MOSFET and MID-SNS CS transformer, which indicates that they are the most efficient MOSFET-transformer pair in this research.
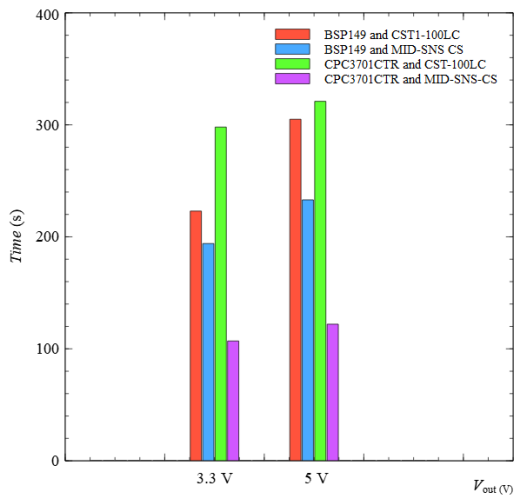
Fig. 3 Measured time for generating 3.3 V and 5 V on the output capacitor C_{OUT} (2200 μF) for different pairs of transformers and MOS transistors.

Fig. 4 shows the maximum output voltage at the capacitor C_{OUT} when the circuit reaches a steady-state and the given results are for 50 mV and 100 mV of the input voltage.
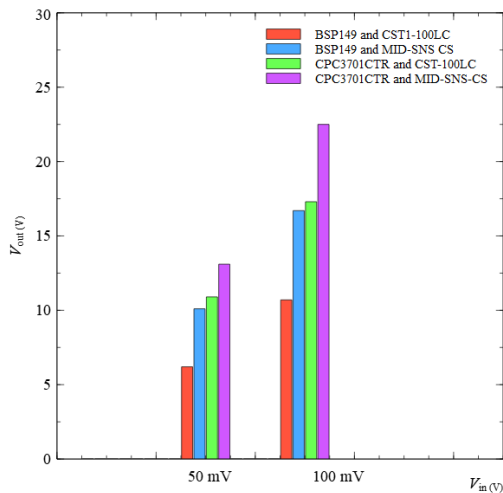
Fig. 4 Maximum generated output voltage on the capacitor C_{OUT} for different pairs of transformers and MOS transistors at the input voltages of 50 mV and 100 mV.

It is measured that CPC3701CTR along with MID-SNS CS transformer can generate the biggest output voltage at the capacitor C_{OUT}, and the lowest produced voltage in these combinations of MOSFETs and transformers is for BSP149 MOSFET in pair with CST-100LC transformer. For the stated measurements, the best performances of the MOSFET-transformer pair are for the CPC3701CTR MOSFET and MID-SNS CS transformer, as expected. The resonate frequency of each MOSFET-transformer pair is presented in Fig 5. The highest resonating frequency is measured for CPC3701 MOSFET and CST-100LC transformer, and the lowest resonating frequency is measured for BSP149 MOSFET with MID-SNS CS transformer. Fig. 6 – Fig. 9 represent the output voltage generation for all of the measured MOSFET-transformer pairs, at the initial voltage of 100 mV, captured by the Tektronix DPO4034 oscilloscope.
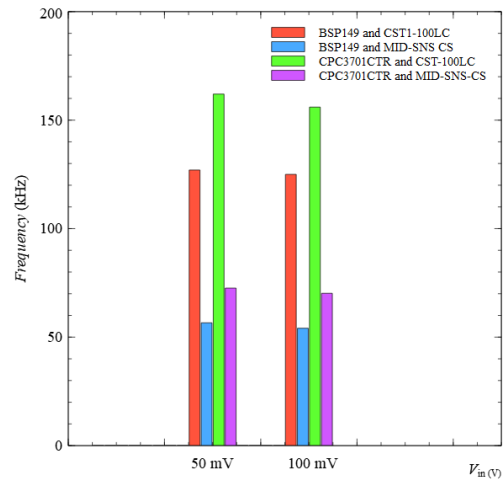
Fig. 5 Measured resonant freaquency for generating 3.3 V and 5 V on the output capacitor (2200 μF) for different pairs of transformers and MOS transistors.
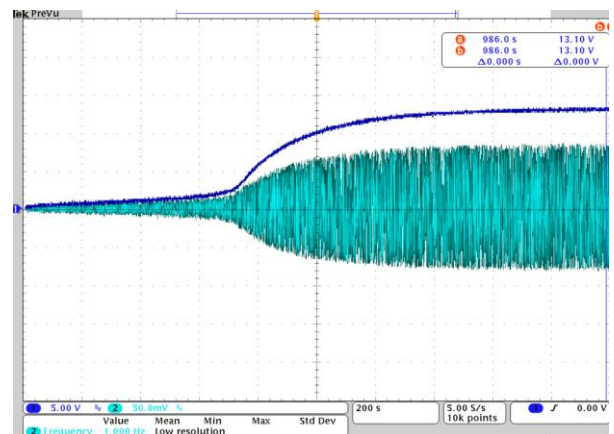
Fig. 6 BSP149 MOSFET and CST-100LC transformer pair: The oscillator voltage (light blue) and the voltage at the output capacitor C_{OUT} (deep blue) as a function of time for the initial voltage of 100 mV. X-axis: 200 s/div, Y-axis: 5 V/div for V_{OUT} and 50 mV for V_{OSC}.
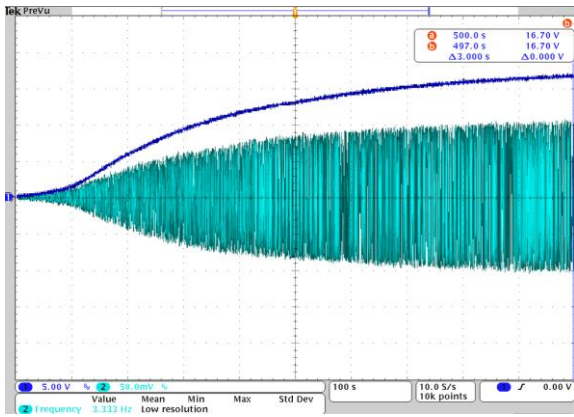
Fig. 7 BSP149 MOSFET and MID-SNS CS transformer pair: The oscillator voltage (light blue) and the voltage at the output capacitor C_{OUT} (deep blue) as a function of time for the initial voltage of 100 mV. X-axis: 100 s/div, Y-axis: 5 V/div for V_{OUT} and 50 mV for V_{OSC}.
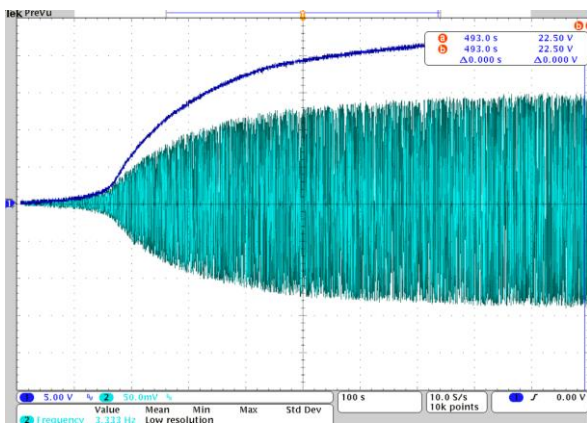

Fig. 8 CPC3701CTR MOSFET and CST-100LC transformer pair: The oscillator voltage (light blue) and the voltage at the output capacitor C_{OUT} (deep blue) as a function of time for the initial voltage of 100 mV. X-axis: 100 s/div, Y-axis: 5 V/div for V_{OUT} and 50 mV for V_{OSC}.
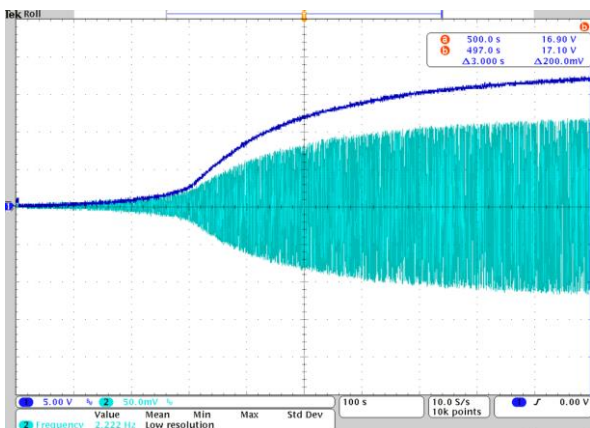

Fig. 9 CPC3701CTR MOSFET and MID-SNS CS transformer pair: The oscillator voltage (light blue) and the voltage at the output capacitor C_{OUT} (deep blue) as a function of time for the initial voltage of 100 mV. X-axis: 100 s/div, Y-axis: 5 V/div for V_{OUT} and 50 mV for V_{OSC}.

IV. CONCLUSION

It is a great challenge to choose the components that will provide the highest efficiency of the power management circuit, but it is one that must be addressed depending on the purpose of the circuit behind the power management block. Depending on that, it is necessary to pay attention to how the components affect the power loss, which ones generate the highest output voltage, which ones reach a certain value of the output voltage for the shortest time, etc. This paper shows how different transformers and MOS transistors affect all of the parameters stated above, and it is possible to choose a pair depending on the needs of the circuit powered by such a system. In terms of generating the highest possible output voltage on the C_{OUT} capacitor it is best to use a CPC3701CTR MOSFET with a MID-SNS CS transformer, for a lower input voltage at 50 mV but at 100 mV as well. If the user needs a power management circuit that generates an output voltage in the shortest time, the best option is a pair of CPC3701CTR MOSFET and a MID-SNS CS transformer. The pair of a CPC3701CTR MOSFET and CST-100LC transformer is the second-best for generating maximum output voltage, but it needs the longest time to generate the desired voltage. In the future, this type of step-up converter will be improved by adding and testing additional components to the circuit in order to give the shortest time for the oscillation process.

REFERENCES

[1] Khan, Farid Ullah; Khattak, Muhammad Umair (2016). Contributed Review: Recent developments in acoustic energy harvesting for autonomous wireless sensor nodes applications. Review of Scientific Instruments, 87(2), 021501–. doi:10.1063/1.4942102.

[2] Calautit, K., Nasir, D. S. N. M., & Hughes, B. R. (2021). Low power energy harvesting systems: State of the art and future challenges. Renewable and Sustainable Energy Reviews, 147, 111230. doi:10.1016/j.rser.2021.111230

[3] Weng, Po-Shuan; Tang, Hao-Yen; Ku, Po-Chih; Lu, Liang-Hung (2013). 50 mV-Input Batteryless Boost Converter for Thermal Energy Harvesting. IEEE Journal of Solid-State Circuits, 48(4), 1031–1041. doi:10.1109/JSSC.2013.2237998.

[4] LTC3108 ultralow voltage step-up converter and power manager, Linear Technology Corporation, 2010, datasheet. [Online]. Available: https://www.infineon.com

[5] J. Vračar, M. Marjanović, A. Stojković, Z. Prijić, A. Prijić, Lj. Vračar, "Application of a Low-Voltage Step-Up Circuit for Thermal Energy Harvesting Under Natural Convection" Proceedings of papers IcETRAN 2019, 6th International Conference on Electrical, Electronic and Computing Engineering, Srebrno Jezero, 2019, pp. 564-569, ISBN 978-86-7466-785-9

[6] BSP149 Small-Signal-Transistor, Infineon, 2012, Datasheet., Infineon, 2012. [Online]. Available: https://www.infineon.com/

[7] CPC3701 Depletion-Mode, N-Channel VDMOSFET, IXYS Integrated Circuits Division, 2015, Datasheet., IXYS Integrated Circuits Division 2015. [Online]. Available: https://www.ixysic.com/

[8] CST1-100LC Current Sense Transformers, Coilcraft Inc, 2021, Datasheet., Coilcraft Inc, 2021. [Online]. Available: www.coilcraft.com

[9] MID-SNS CS Current Sense Transformers, Würth Elektronik [Online]. Available: https://www.we-online.com

Osnovi teorije diferencnih jednačina sa primenom na analizu svojstava nanostruktura

Akademik, prof. dr Jovan P. Šetrajčić,

prof. dr Vjekoslav D. Sajfert i prof. dr Siniša M. Vučenović

Apstrakt— **Trend naglog razvoja nanotehnologija je uzrokovan otkrićima da nanostrukture poseduju fizičke karakteristike koje se znatno razlikuju od istih koje poseduju strukture velikih dimenzija (balk). Nanostrukture karakteriše i serija kvalitativno sasvim novih i izmenjenijih efekata. Npr. superkonduktivne, termoizolacione, akustičke i druge osobine koje karakterišu nanomaterijale su bolje ili sasvim drugačije od onih u balk-strukturi. Posebno je intrigantna potencijalna primena u inoviranoj farmaciji i medicini uopšte. Na neki način nanostrukturni efekti su povezani sa efektima u masivnoj strukturi slično kao što su povezani kvantni i klasični efekti. Teorijsko izučavanje balk-struktura uglavnom zahteva rešavanje diferencijalnih jednačina sa kontinualnim promenljivama. U istraživanju mehanizama u nanostrukturama, koji su vinovnici drastičnih izmena njihovih svojstava, pojavljuju se diferencne jednačine, ali sa koeficijentima koji zavise od prostornih koordinata zbog neophodnosti da se obračunaju dimenzioni – kvantni i granični (konfajnment) uslovi, kao i uticaj vakancija i primesa. Zbog tog uvećanog interesovanja i velikih iščekivanja za korist od novootkrivenih efekata, a posebno zbog nerazvijene teorije, mi smo ovde izložili teoriju koja ima za cilj da prezentuje tehniku izračunavanja diferencnih jednačina i da to demonstrira na seriji primena u analizama različitih – otkrivenih i još neotkrivenih fizičkih svojstava nanostruktura.**

Ključne reči—**diferencne jednačine; dimenziona kvantizacija, konfajnment efekti, fizička svojstva nanostruktura.**

I. Uvod

Fizika nanostruktura doživljava intenzivan razvoj i predstavlja jedan od udarnih frontova istraživanja u savremenoj fizici [1–5]. Osnovni matematički instrument teorijskih proračuna osobina nanostuktura je diferencni račun. U skladu sa ovim, ovu prezentaciju posvećujemo diferencnom računu i njegovoj primeni na analize struktura sa narušenom translacionom simetrijom.

Osnovni trend ovde je isticanje operacionih računskih moći diferencnog računa. Zbog toga su i pri izlaganju osnova diferencnog računa i u nizu njegovih primena na nanostrukture, najčešće korišćeni translacioni operatori. Preko njih se najbrže dolazi do željenog rezultata. Udarni deo izlaganja je, zbog toga, posvećen isključivo diferencnom računu i on je operativan, bez matematičkih fundamenata tipa korolara,

teorema i komplikovanih dokaza (koji se mogu naći u literaturi, npr. [6–11]).

Manji deo sadrži primene diferencnog računa u analizi fizičkih pojava u sistemima sa narušenom simetrijom, tačnije primenu te metodologije na ispitivanje nanostruktura koje su translaciono invarijantne. Uglavnom je korišćen metod Grinovih funkcija (GF) zbog toga što je ovaj metod samousaglašen, tj. on rešava i dinamiku i termodinamiku problema.

Treba naglasiti da je ovde razvijena posebna metodologija izračunavanja GF u uslovima narušene simetrije, pri čemu ovo narušenje simetrije može biti duž jednog, dva pravca i duž sva tri prostorna pravca. Problem izračunavanja GF struktura sa narušenom simetrijom je u tome što one zavise od prostornih promenljivih ponaosob, a ne od njihove razlike, kao što je to kod struktura idealne simetrije, gde GF zavisi od razlike prostornih promenljivih, a zbog homogenosti sredine pri računima se može koristiti zakon održanja impulsa [12–14]. Ovaj zakon ne važi za strukture sa narušenom simetrijom, što unosi glavnu matematičku poteškoću. Ovde je to prevaziđeno reprezentacijom stojećih talasa za Kronekerov simbol, umesto ravnih talasa kao za analize balk-struktura.

Jedan od najznačajnijih uspeha u analizi narušene simetrije u strukturama sa vodoničnim vezama je objašnjenje Krik-Votsonove teorije [15] o raspadu DNK dvostrukog lanca i objašnjenje daljeg ponašanja dva DNK makromolekula dobijena u ovom procesu. Analize difuzije eksitona u nanofilmovima [16,17] ukazuju na tačnost Sent Đerđijevih ideja [18] da eksitonski mehanizam igra značajnu ulogu u transportu elektromagnetne energije kroz biostrukture [19]. Analize elektrona u provodnim nanofilmovima i u kvantnim gredama [20,21] predstavljaju dokaz egzistencije skin-efekta. Rezultat od velikog praktičnog interesa je postojanje energijskog gepa u fononskom spektru ultratankog filma [22,23]. Poznato je da fononi u balk-strukturama nemaju gep, pa pojava u ultratankom filmu, koji je za troslojni film reda preko 100 k_B, navodi na ideju da bi on mogao da bude superprovodan i preko 100 K.

II. Elementi diferencnog računa

Diferencije i diferencne jednačine pojavljuju se u prebrojivim skupovima varijabli ([6–12]). Poznato je da se u skupovima kontinualnih varijabli pojavljuju diferencijali i diferencijalne jednačine i ta teorija je mnogo razrađenija od teorije diferencnih jednačina. S'druge strane, diferencne jednačine su bliže praksi, naročito kada se radi o problemima vezanim za kristalnu nanostrukturu. U krajnjem, celokupna materija u prirodi je diskretan entitet, pa je prirodno da se u njenom izučavanju koriste diskretne zakonitosti sa diskretnim veličinama.

Jovan P. Šetrajčić – Akademija nauka i umjetnosti Republike Srpske, Bana Lazarevića 1, 78000 Banja Luka, Republika Srpska – BiH (e-mail: jovan.setrajcic@gmail.com).

Vjekoslav D.Sajfert – Inđija, Srbija (e-mail: sajfert.vjekoslav@gmail.com)

Siniša M.Vučenović – Univerzitet u Banjoj Luci, Prirodno-matematički fakultet, Mladena Stojanovića 2, 78000 Banja Luka, Republika Srpska – BiH (e-mail: sinisa.vucenovic@pmf.unibl.org).

Po analogiji sa izvodima u neprebrojivim skupovima, koje ćemo zvati kontinualnim izvodima, uvešćemo diskretne izvode u prebrojivim skupovima. Probleme rešavanja diferencnih jednačina vezaćemo za probleme rešavanja diferencijalnih jednačina, da bismo koristili prilaze i postupke iz ove poslednje, bolje razvijene oblasti.

A. Diferencije i diskretni izvodi

Kod diskretnih varijabli, priraštaj argumenta jednak je jedinici, pa se ovaj priraštaj ne piše u formulama. Formalna oznaka za priraštaj argumenta koristi se samo da bi se znalo po kojoj promenljivoj se diferencira.

Diskretan izvod funkcije diskretne promenljive n, dakle F_n, definiše se kao:

$$\frac{\Delta}{\Delta n} F_n = F_{n+1} - F_n \tag{II.1}$$

i on je linearan operator. Na osnovu toga mogu se potražiti i viši izvodi, npr. za drugi izvod imamo:

$$\frac{\Delta^2}{\Delta n^2} F_n = \frac{\Delta}{\Delta n} \frac{\Delta}{\Delta n} F_n = \frac{\Delta}{\Delta n}(F_{n+1} - F_n) =$$
$$= F_{n+2} - 2F_{n+1} + F_n; \tag{II.2}$$
$$\Rightarrow \frac{\Delta^m}{\Delta n^m} F_n = \sum_{k=0}^{m}(-1)^k \binom{m}{k} F_{n+m-k}.$$

Sada ćemo potražiti diskretan izvod proizvoda dve funkcije:

$$\frac{\Delta}{\Delta n} F_n H_n = F_{n+1}H_{n+1} - F_n H_n =$$
$$= F_{n+1}H_{n+1} - F_{n+1}H_n + F_{n+1}H_n - F_n H_n =$$
$$= F_{n+1}\frac{\Delta H_n}{\Delta n} + H_n \frac{\Delta F_n}{\Delta n}.$$

Međutim, vidljivo je da se ovo može izraziti i kao:

$$\frac{\Delta}{\Delta n} F_n H_n = F_{n+1}H_{n+1} - F_n H_n =$$
$$= F_{n+1}H_{n+1} - F_n H_{n+1} + F_n H_{n+1} - F_n H_n =$$
$$= H_{n+1}\frac{\Delta F_n}{\Delta n} + F_n \frac{\Delta H_n}{\Delta n}.$$

Zbog toga se izvod proizvoda definiše preko aritmetičke sredine ova dva izraza, pa nakon sređivanja sledi:

$$\frac{\Delta}{\Delta n} F_n H_n = H_n \frac{\Delta F_n}{\Delta n} + F_n \frac{\Delta H_n}{\Delta n} + \frac{\Delta F_n}{\Delta n}\frac{\Delta H_n}{\Delta n}. \tag{II.3}$$

Drugi izvod proizvoda funkcija je onda jednak:

$$\frac{\Delta^2}{\Delta n^2} F_n H_n = H_n \frac{\Delta^2 F_n}{\Delta n^2} + F_n \frac{\Delta^2 H_n}{\Delta n^2} + 2\frac{\Delta H_n}{\Delta n}\frac{\Delta^2 F_n}{\Delta n^2} +$$
$$+ 2\frac{\Delta F_n}{\Delta n}\frac{\Delta^2 H_n}{\Delta n^2} + 2\frac{\Delta F_n}{\Delta n}\frac{\Delta H_n}{\Delta n} + \frac{\Delta^2 F_n}{\Delta n^2}\frac{\Delta^2 H_n}{\Delta n^2}. \tag{II.4}$$

Zatim, potrebno je naći i izvod količnika dve funkcije:

$$\frac{\Delta}{\Delta n}\frac{F_n}{H_n} = \frac{F_{n+1}}{H_{n+1}} - \frac{F_n}{H_n} = \frac{F_{n+1}H_n - F_n H_{n+1}}{H_{n+1}H_n} =$$
$$= \frac{F_{n+1}H_n - F_n H_n - F_n H_{n+1} + F_n H_n}{H_{n+1}H_n} = \tag{II.5}$$
$$= \frac{H_n \frac{\Delta F_n}{\Delta n} - F_n \frac{\Delta H_n}{\Delta n}}{H_{n+1}H_n}.$$

I konačno, potrebno je naći izvod složene diskretne funkcije:

$$\frac{\Delta}{\Delta n} F_{\varphi_n} = \frac{\Delta F_{\varphi_n}}{\Delta \varphi_n}\frac{\Delta \varphi_n}{\Delta n}. \tag{II.6}$$

B. Translacioni operatori i diskretna integracija

Pomoću translacionog operatora sa osobinama:

$$\hat{T}_k F_n = F_{n+k};$$
$$\hat{T}_k^{-1} = \hat{T}_{-k}; \quad \hat{T}_k = (\hat{T}_1)^k; \quad (\hat{T}_k)^n = \hat{T}_{nk}, \tag{II.7}$$

može se redefinisati diskretni izvod iz (II.1):

$$\frac{\Delta}{\Delta n} F_n = F_{n+1} - F_n = (\hat{T}_1 - 1)F_n;$$
$$\Rightarrow \frac{\Delta^m}{\Delta n^m} F_n = (\hat{T}_1 - 1)^m F_n = \tag{II.8}$$
$$= \sum_{k=0}^{m}(-1)^k \binom{m}{k} \hat{T}_{m-k} F_{n+m-k}.$$

Uvođenje translacionih operatora korisno je u prvom redu zbog toga što se pomoću njih može definisati operacija diskretne integracije: $\frac{\Delta^{-1}}{\Delta n}$, kao inverznu operaciju u odnosu na diskretno diferenciranje. Pošto se diskretni izvod dobija primenom operatora $\hat{T}_1 - 1$ na funkciju diskretne promenljive F_n, očigledno je da se primenom operatora $(\hat{T}_1 - 1)^{-1}$ na tu istu funkciju dobija njen diskretni integral:

$$\frac{\Delta^{-1}}{\Delta n} F_n = (\hat{T}_1 - 1)^{-1} F_n, \tag{II.9}$$

ali je sada potrebno naći odgovarajuću operativnu formulu za operator: $(\hat{T}_1 - 1)^{-1}$, posebno jer se može napisati u dve forme:

$$(\hat{T}_1 - 1) = \begin{cases} \hat{T}_1(1 - \hat{T}_{-1}), \\ -(1 - \hat{T}_1). \end{cases} \Rightarrow$$
$$\Rightarrow (\hat{T}_1 - 1)^{-1} = \begin{cases} (1 - \hat{T}_{-1})^{-1}\hat{T}_{-1} = \sum_{k=0}^{\infty} \hat{T}_{-k-1}, \\ -(1 - \hat{T}_1)^{-1} = -\sum_{k=0}^{\infty} \hat{T}_k. \end{cases} \tag{II.10}$$

Zbog ovoga i diskretni integral funkcije F_n ima dve forme:

$$\hat{J}_1 F_n \equiv \frac{\Delta^{-1}}{\Delta n} F_n = \sum_{k=0}^{\infty} \hat{T}_{-k-1} F_n =$$

$$= F_{n-1} + F_{n-2} + F_{n-3} + ... \qquad \text{(II.11a)}$$

$$\hat{J}_2 F_n \equiv \frac{\Delta^{-1}}{\Delta n} F_n = -\sum_{k=0}^{\infty} \hat{T}_k F_n =$$

$$= -F_n - F_{n+1} - F_{n+2} - ... \qquad \text{(II.11b)}$$

Ukoliko red iz (II.11a) ne konvergira, onda se može koristiti (II.11b) jer će on konvergirati. Važi i obrnuto.

Definisanje diskretnog integrala pomoću translacionih operatora pogodno je jer daje gotove recepte po kojima se mogu izračunavati. Metod računa sa translacionim operatorima primenljiv je na eksponencijalne, logaritamske, trigonometrijske i hiperbolične funkcije, ali i na stepene funkcije. Kod ovih poslednjih postoje izvesne specifičnosti u računu, na koje ćemo posebno ukazati. Razmotrićemo sada nekoliko diskretnih izvoda i diskretnih integrala navedenih tipičnih funkcija.

1) *Eksponencijalna funkcija* tipa: $F_n = A^{\alpha n}$; $A > 1$; $\alpha > 0$.

Diskretni izvod jednak je:

$$\frac{\Delta}{\Delta n} A^{\alpha n} = A^{\alpha(n+1)} - A^{\alpha n} = A^{\alpha n}\left(A^{\alpha} - 1\right), \qquad \text{(II.12)}$$

a diskretni integral, korišćenjem (II.11a):

$$\frac{\Delta^{-1}}{\Delta n} A^{\alpha n} \equiv \hat{J}_1 A^{\alpha n} = A^{\alpha(n-1)} + A^{\alpha(n-2)} + A^{\alpha(n-3)} + ...$$

$$= A^{\alpha n}\left[-1 + \sum_{k=0}^{\infty}\left(A^{-\alpha}\right)^k\right] = \frac{A^{\alpha n}}{A^{\alpha} - 1}. \qquad \text{(II.13)}$$

Za funkciju $Ae^{-\alpha n}$; $A > 1$; $\alpha > 0$, sa (II.11a) red bi bio divergentan, zato se mora primeniti formula (II.11b):

$$\frac{\Delta^{-1}}{\Delta n} Ae^{-\alpha n} = \hat{J}_2 Ae^{-\alpha n} \equiv -\sum_{k=0}^{\infty} \hat{T}_k Ae^{-\alpha n} =$$

$$= -Ae^{-\alpha n}\left(1 + e^{-\alpha} + e^{-2\alpha} + ...\right) = -\frac{Ae^{-\alpha n}}{1 - e^{-\alpha}}. \qquad \text{(II.14)}$$

2) *Logaritamska funkcija* tipa: $F_n = \log_A n$.

Diskretni izvod ove funkcije je:

$$\frac{\Delta}{\Delta n} \log_A n = \log_A(n+1) - \log_A n = \log_A \frac{n+1}{n}, \qquad \text{(II.15)}$$

a diskretni integral ove funkcije će biti:

$$\frac{\Delta^{-1}}{\Delta n} \log_A n = \log_A(n-1) + \log_A(n-2) +$$

$$+ \log_A(n-3) + ... + \log_A 2 = \log_A[(n-1)!] \qquad \text{(II.16)}$$

3) *Trigonometrijska funkcija* tipa: $F_n = \cos n\alpha$.

Prema definiciji, diskretni izvod ove funkcije je:

$$\frac{\Delta}{\Delta n} \cos n\alpha = \cos(n+1)\alpha - \cos n\alpha =$$

$$= \cos n\alpha \cos\alpha - \sin n\alpha \sin\alpha - \cos n\alpha =$$

$$= -2\sin\frac{\alpha}{2}\sin\left(n+\frac{1}{2}\right)\alpha, \qquad \text{(II.17)}$$

a njen diskretni integral se nalazi:

$$\frac{\Delta^{-1}}{\Delta n}\cos\alpha\, n = \left(\hat{T}_1 - 1\right)^{-1}\cos\alpha\, n = \sum_{k=0}^{\infty} \hat{T}_{-k-1}\cos\alpha\, n =$$

$$= \left(\hat{T}_{-1} + \hat{T}_{-2} + \hat{T}_{-3} + ...\right)\frac{1}{2}e^{i\alpha n} + \left(\hat{T}_{-1} + \hat{T}_{-2} + \hat{T}_{-3} + ...\right)\frac{1}{2}e^{-i\alpha n} =$$

$$= \frac{1}{2}e^{i(n-1)\alpha}\left(1 + e^{-i\alpha} + e^{-2i\alpha} + ...\right) + \frac{1}{2}e^{-i(n-1)\alpha}\left(1 + e^{i\alpha} + e^{2i\alpha} + ...\right)$$

U prvoj zagradi se uzme $\alpha \to \alpha - i\delta$, a u drugoj $\alpha \to \alpha + i\delta$, pa se traži granična vrednost sume kada $\delta \to +0$:

$$\frac{\Delta^{-1}}{\Delta n}\cos\alpha\, n = \frac{1}{2}e^{in\alpha}\frac{1}{e^{i\alpha}}\frac{1}{1 - e^{-i\alpha}} + \frac{1}{2}e^{-in\alpha}e^{i\alpha}\frac{1}{1 - e^{i\alpha}} =$$

$$= \mathrm{Re}\left\{e^{in\alpha}\frac{1}{e^{i\alpha} - 1}\right\} = \frac{\cos(n-1)\alpha - \cos n\alpha}{4\sin^2\frac{\alpha}{2}} = \frac{\sin\left(n - \frac{1}{2}\right)\alpha}{2\sin\frac{\alpha}{2}}. \qquad \text{(II.18)}$$

4) *Hiperbolična funkcija* tipa: $F_n = \cosh n\alpha$.

Diskretni izvod ove funkcije nalazi se preko kombinacije dve eksponencijalne funkcije:

$$\frac{\Delta}{\Delta n}\cosh n\alpha = \frac{1}{2}\frac{\Delta}{\Delta n}e^{\alpha n} + \frac{1}{2}\frac{\Delta}{\Delta n}e^{-\alpha n} = \frac{1}{2}\left[e^{\alpha(n+1)} - e^{\alpha n} + \right.$$

$$\left. + e^{-\alpha(n+1)} - e^{-\alpha n}\right] = 2\sinh\frac{\alpha}{2}\sinh\left(n+\frac{1}{2}\right)\alpha. \qquad \text{(II.19)}$$

Diskretan integral ove funkcije mora se, takođe nalaziti preko eksponencijalnih funkcija, ali za eksponencijalnu funkciju sa pozitivnim predznakom mora se primeniti operator $\hat{J}_1$, dok za onu sa negativnim predznakom $\hat{J}_2$:

$$\frac{\Delta^{-1}}{\Delta n}\cosh n\alpha = \left(\frac{\Delta^{-1}}{\Delta n}\right)_1 \frac{1}{2}e^{\alpha n} + \left(\frac{\Delta^{-1}}{\Delta n}\right)_2 \frac{1}{2}e^{-\alpha n} \equiv$$

$$\equiv \frac{1}{2}\left(\hat{J}_1 e^{\alpha n} + \hat{J}_2 e^{-\alpha n}\right) =$$

$$= \frac{1}{2}\left[\left(\hat{T}_{-1} + \hat{T}_{-2} + \hat{T}_{-3} + ...\right)e^{\alpha n} - \right.$$

$$\left. - \left(\hat{T}_1 + \hat{T}_2 + \hat{T}_3 + ...\right)e^{-\alpha n}\right] =$$

$$= \frac{1}{2}\left[\frac{e^{\alpha n}}{e^{\alpha}}\left(1 + e^{-\alpha} + e^{-2\alpha} + ...\right) - \right.$$

$$\left. - e^{-\alpha n}\left(1 + e^{-\alpha} + e^{-2\alpha} + ...\right)\right] = \qquad \text{(II.20)}$$

$$= \frac{1}{2}\left(\frac{e^{\alpha n}}{e^{\alpha} - 1} + \frac{e^{-\alpha n}}{e^{-\alpha} - 1}\right) =$$

$$= \left(2\sinh\frac{\alpha}{2}\right)^{-1}\sinh\left(n - \frac{1}{2}\right)\alpha.$$

Sličnim postupkom mogu se odrediti diskretni izvodi i diskretni integrali za funkciju tipa $F_n = \sinh n\alpha$:

$$\frac{\Delta}{\Delta n}\sinh n\alpha = 2\sinh\frac{\alpha}{2}\cosh\left(n+\frac{1}{2}\right)\alpha. \qquad (II.21)$$

$$\frac{\Delta^{-1}}{\Delta n}\sinh n\alpha = \left(2\sinh\frac{\alpha}{2}\right)^{-1}\cosh\left(n-\frac{1}{2}\right)\alpha. \qquad (II.22)$$

5) *Stepena funkcija* tipa: $F_n = n^{-\alpha\cdot}; \; \alpha > 0$.

Diskretni izvod ove funkcije nalazi se preko definicije:

$$\frac{\Delta}{\Delta n}n^{-\alpha} = (\hat{T}_1-1)n^{-\alpha} = (n+1)^{-\alpha} - n^{-\alpha} = -n^{-\alpha}\left[1-\left(\frac{n}{n+1}\right)^{\alpha}\right], \qquad (II.23)$$

a diskretni integral obavezno se mora računati pomoću operatora $\hat{J}_2$, jer bi se u računu pomoću operatora $\hat{J}_1$, pojavili singulariteti:

$$\frac{\Delta^{-1}}{\Delta n}n^{-\alpha} = \hat{J}_2 n^{-\alpha} = -\sum_{k=0}^{\infty}\hat{T}_k n^{-\alpha} = \\ = n^{\alpha} + (n+1)^{-\alpha} + (n+2)^{-\alpha} + ... = -\sum_{k=0}^{\infty}(n+k)^{-\alpha}. \qquad (II.24)$$

U slučaju da je: $f_n = n^{\alpha\cdot}; \; \alpha > 0$, onda je diskretni izvod:

$$\frac{\Delta}{\Delta n}n^{\alpha} = (\hat{T}_1-1)n^{\alpha} = (n+1)^{\alpha} - n^{\alpha} = (n+1)^{\alpha}\left[1-\left(\frac{n}{n+1}\right)^{\alpha}\right], \qquad (II.25)$$

A za izračunavanje diskretnog integrala mora primeniti operatora $\hat{J}_1$:

$$\frac{\Delta^{-1}}{\Delta n}n^{\alpha} = \hat{J}_1 n^{\alpha} = \sum_{k=0}^{\infty}\hat{T}_{-k-1}n^{\alpha} = (n-1)^{\alpha} + (n-2)^{\alpha} + ... = \\ = \sum_{q=1}^{\infty}(n-q)^{\alpha} \Rightarrow = \sum_{q=1}^{n-1}(n-q)^{\alpha}. \qquad (II.26)$$

(beskonačni red morao je da se "preseče" za $q = n$).

C. Diferencne jednačine prvog reda

U ovom delu posmatraćemo linearne diferencne jednačine sa promenljivim koeficijentima.

1) *Homogena linearna diferencna jednačina* je tipa:

$$\frac{\Delta Y_n}{\Delta n} + a_n Y_n = 0. \qquad (II.27)$$

Rešavanje ove diferencne jednačine svodi se na nalaženje rekurentnog obrasca sa jednom diferencijom:

$$Y_{n+1} - Y_n + a_n Y_n = 0 \;\; \Rightarrow \;\; Y_{n+1} = (1-a_n)Y_n,$$

a odatle:

$$Y_1 = (1-a_0)Y_0; \; Y_2 = (1-a_1)Y_1 = (1-a_0)(1-a_1)Y_0; \; \cdots$$

$$Y_n = (1-a_0)(1-a_1)(1-a_2)...(1-a_{n-1})Y_0 = \\ = Y_0\prod_{s=0}^{n-1}(1-a_s). \qquad (II.28)$$

2) *Nehomogena linearna diferencna jednačina* ima oblik:

$$\frac{\Delta Y_n}{\Delta n} + a_n Y_n = b_n \qquad (II.29)$$

i ona se rešava operatorskim putem:

$$\left[(\hat{T}_1-1)+a_n\right]Y_n = b_n \;\; \Rightarrow \;\; Y_n = \left[(\hat{T}_1-1)+a_n\right]^{-1}b_n. \qquad (II.30)$$

Operator $(\hat{T}_1-1)+a_n$ može se izraziti na dva nezavisna načina:

$$(\hat{T}_1-1)+a_n = \begin{cases} a_n\left[1+a_n^{-1}(\hat{T}_1-1)\right]; \\ (\hat{T}_1-1)\left[1+(\hat{T}_1-1)^{-1}a_n\right], \end{cases}$$

pa imamo i dve forme inverznih operatora:

$$\hat{J}_1 = \sum_{k=0}^{\infty}(-1)^k\left[a_n^{-1}(\hat{T}_1-1)\right]^k a_n^{-1}; \\ \hat{J}_2 = \sum_{k=0}^{\infty}(-1)^k\left[(\hat{T}_1-1)^{-1}a_n\right]^k(\hat{T}_1-1)^{-1}. \qquad (II.31)$$

Pošto operator $\hat{T}_1$ i multiplikativni operator a_n ne komutiraju, imamo:

$$(\hat{T}_1-1)a_n F_n = a_{n+1}F_{n+1} - a_n F_n; \\ a_n(\hat{T}_1-1)F_n = a_n(F_{n+1}-F_n) = a_n F_{n+1} - a_n F_n,$$

pa se stepeni iz (II.29) moraju uzeti u formi:

$$\left[a_n^{-1}(\hat{T}_1-1)\right]^k = \underbrace{a_n^{-1}(\hat{T}_1-1)a_n^{-1}(\hat{T}_1-1)...a_n^{-1}(\hat{T}_1-1)}_{k\,\text{puta}};$$

$$\left[(\hat{T}_1-1)^{-1}a_n\right]^k = \underbrace{(\hat{T}_1-1)^{-1}a_n(\hat{T}_1-1)^{-1}a_n...(\hat{T}_1-1)^{-1}a_n}_{k\,\text{puta}}.$$

Rešenje jednačine (II.27) dobija se primenom samo jednog od operatora $\hat{J}_1$, odnosno $\hat{J}_2$ i to onog koji primenjen na b_n daje konvergentan red. Znači, rešenje jednačine (II.30) je:

$$Y_n = \hat{J}_1 b_n, \quad \text{ili} \quad Y_n = \hat{J}_2 b_n. \qquad (II.32)$$

Ako funkcije *a* i *b* ne zavise od promenljive *n* onda se ovim operatorskim metodom relativno jednostavno mogu rešiti nehomogene diferencne jednačine prvog reda. Ukoliko pak obe funkcije *a* i *b* zavise od promenljive *n*, rešenje je glomazno, ali se i ono lako nalazi. Tu nam uvek pomaže smena funkcije:

$$Y_n = U_n Z_n \Rightarrow \frac{\Delta Y_n}{\Delta n} = U_n\frac{\Delta Z_n}{\Delta n} + Z_n\frac{\Delta U_n}{\Delta n} + \frac{\Delta U_n}{\Delta n}\frac{\Delta Z_n}{\Delta n}, \qquad (II.33)$$

jer se polazna jednačina (II.29) uprosti: ona se rešava po Z_n, a funkciju U_n odredimo tako da jednačina za Z_n bude uprošćena. Zamenom smene u (II.29) i deobom sa U_n, dobija se:

$$\left(1 + \frac{1}{U_n}\frac{\Delta U_n}{\Delta n}\right)\frac{\Delta Z_n}{\Delta n} + \left(\frac{1}{U_n}\frac{\Delta U_n}{\Delta n} + a_n\right)Z_n = \frac{b_n}{U_n}.$$

I sada se U_n određuje da „otpadne" član uz Z_n:

$$\frac{1}{U_n}\frac{\Delta U_n}{\Delta n} = -a_n \Rightarrow \frac{\Delta U_n}{\Delta n} = -a_n U_n \Rightarrow$$

$$\Rightarrow U_{n+1} - U_n = -a_n U_n \Rightarrow U_{n+1} = (1 - a_n)U_n,$$

odnosno, za $n = 0, 1, 2, \ldots$:

$$U_1 = (1 - a_0)U_0,$$
$$U_2 = (1 - a_1)U_1 = (1 - U_0)(1 - a_1)U_0,$$
$$U_3 = (1 - a_2)U_2 = (1 - U_0)(1 - a_1)(1 - a_2)U_0,$$
$$\ldots \qquad \ldots \qquad \ldots \qquad \ldots$$
$$U_n = U_0 \prod_{k=0}^{n-1}(1 - a_k).$$

Dalje ćemo uzeti da je $U_0 = 1$, pa jednačina za Z_n postaje:

$$(1 - a_n)\frac{\Delta Z_n}{\Delta n} = \frac{b_n}{U_n} \Rightarrow \frac{\Delta Z_n}{\Delta n} = \frac{b_n}{1 - a_n}\frac{1}{U_n} \Rightarrow$$

$$\Rightarrow \frac{\Delta Z_n}{\Delta n} = \frac{b_n}{1 - a_n}\frac{1}{\prod_{k=0}^{n-1}(1 - a_k)} \Rightarrow$$

$$\Rightarrow Z_n = \frac{\Delta^{-1}}{\Delta n}\left\{\frac{b_n}{1 - a_n}\left[\prod_{k=0}^{n-1}(1 - a_k)\right]^{-1}\right\} + C.$$

Nakon zamene u (II.33), rešenje polazne jednačine je:

$$Y_n = C\prod_{k=0}^{n-1}(1 - a_k) + $$
$$+ \prod_{k=0}^{n-1}(1 - a_k)\frac{\Delta^{-1}}{\Delta n}\left\{\frac{b_n}{1 - a_n}\left[\prod_{k=0}^{n-1}(1 - a_k)\right]^{-1}\right\}. \qquad \text{(II.34)}$$

D. Snižavanje reda diferencne jednačine drugog reda

U opštem slučaju, diferencne jednačine drugog reda sadrže argument funkcije, diskretnu funkciju, prvi izvod diskretne funkcije i drugi izvod diskretne funkcije.

Jedan od načina rešavanja diferencnih jednačina drugog reda je njihovo svođenje na diferencne jednačine prvog reda. Red diferencne jednačine može se sniziti ako u njoj figurišu argument, kao i prvi i drugi diskretni izvod funkcije. Drugi slučaj, kada je moguće snižavanje reda, predstavljaju diferencne jednačine u kojima figurišu funkcija diskretne promenljive i njen prvi i drugi diskretni izvod.

Prvi pomenuti slučaj je zadat relacijom:

$$\Phi\left(n, \frac{\Delta Y_n}{\Delta n}, \frac{\Delta^2 Y_n}{\Delta n^2}\right) = 0, \qquad \text{(II.35)}$$

koja smenom:

$$\frac{\Delta Y_n}{\Delta n} = p_n \Rightarrow \frac{\Delta^2 Y_n}{\Delta n^2} = \frac{\Delta p_n}{\Delta n},$$

prelazi u diferencnu jednačinu prvog reda:

$$\Phi\left(n, p_n, \frac{\Delta p_n}{\Delta n}\right) = 0. \qquad \text{(II.36)}$$

Drugi pomenuti slučaj je jednačina ovog oblika:

$$\Psi\left(Y_n, \frac{\Delta Y_n}{\Delta n}, \frac{\Delta^2 Y_n}{\Delta n^2}\right) = 0. \qquad \text{(II.37)}$$

I ovde se uzima ista smena: $\frac{\Delta Y_n}{\Delta n} = p_n$, ali se drugi izvod nalazi na sledeći način:

$$\frac{\Delta^2 Y_n}{\Delta n^2} = \frac{\Delta p_n}{\Delta n} = \frac{\Delta Y_n}{\Delta Y_n}\frac{\Delta p_n}{\Delta n} = \frac{\Delta Y_n}{\Delta n}\frac{\Delta p_n}{\Delta Y_n} = p_n\frac{\Delta p_n}{\Delta Y_n},$$

čime (II.35) prelazi u diferencnu jednačinu prvog reda:

$$\Psi\left(Y_n, p_n, \frac{\Delta p_n}{\Delta Y_n}\right) = 0. \qquad \text{(II.38)}$$

E. Linearne diferencne jednačine sa stalnim koeficijentima

1) *Nehomogena linearna diferencna jednačina I reda*
je oblika:

$$\frac{\Delta Y_n}{\Delta n} + aY_n = 0, \qquad \text{(II.39)}$$

a rešava se prema definiciji (II.1):

$$Y_{n+1} - Y_n + aY_n = 0 \Rightarrow Y_{n+1} - (1 - a)Y_n = 0$$

i uvođenjem smene: $Y_n = x^n$, pa sledi:

$$x^{n+1} - (1 - a)x^n = 0 \Rightarrow x = 1 - a.$$

Konačno rešenje je onda:

$$Y_n = (1 - a)^n. \qquad \text{(II.40)}$$

2) *Nehomogena linearna diferencna jednačina II reda*
ima oblik:

$$\frac{\Delta^2 Y_n}{\Delta n^2} + a_1\frac{\Delta Y_n}{\Delta n} + a_2 Y_n = 0 \qquad \text{(II.41)}$$

i ona se, prema definiciji (II.1) i (II.2) svodi na:

$$Y_{n+2} - (2 - a_1)Y_{n+1} + (1 - a_1 + a_2)Y_n = 0,$$

koja se rešava istom smenom: $Y_n = x^n$, te sledi:

$$x^2 - (2 - a_1)x + (1 + a_2) = 0 \Rightarrow x_{1,2} = 1 - \frac{a_1}{2} \pm \sqrt{\frac{a_1^2}{4} - a_1 - a_2}.$$

To znači da polazna jednačina ima dva partikularna integrala:

$$Y_n^{(1)} = x_1^n = \left(1 - \frac{a_1}{2} + \sqrt{\frac{a_1^2}{4} - a_1 - a_2}\right)^n, \qquad \text{(II.42)}$$

$$Y_n^{(2)} = x_2^n = \left(1 - \frac{a_1}{2} - \sqrt{\frac{a_1^2}{4} - a_1 - a_2}\right)^n.$$

3) *Primer iz fizike kristala*

Jednačina kojom se opisuje jednodimenziono prostiranje poremećaja u kristalima sa pravilnom rešetkom je oblika [24]:

$$Y_{n+1} + Y_{n-1} + \rho\, Y_n = 0, \qquad \text{(II.43)}$$

gde je parametar $\rho \neq \rho(n) = \text{const}$ – za neograničene kristale sa translacionom simetrijom (idealne balk kristalne strukture). Ukazanom smenom $Y_n = x^n$, jednačina (II.43) prelazi u:

$$x + x^{-1} + \rho = 0 \Rightarrow x^2 + \rho\, x + 1 = 0 \Rightarrow x_{1,2} = -\frac{\rho}{2} \pm \sqrt{\frac{\rho^2}{4} - 1}.$$

Dva partikularna rešenja jednačine (II. 43) su onda:

$$Y_n^{(1)} = \left(-\frac{\rho}{2} + \sqrt{\frac{\rho^2}{4} - 1}\right)^n; \quad Y_n^{(2)} = \left(-\frac{\rho}{2} - \sqrt{\frac{\rho^2}{4} - 1}\right)^n,$$

a opšte rešenje:

$$Y_n = C_1 Y_n^{(1)} + C_2 Y_n^{(2)}, \qquad \text{(II.44)}$$

gde se konstante C_1 i C_2 određuju iz početnih uslova.

III. OPERATORSKO REŠAVANJE DIFERENCNIH JEDNAČINA DRUGOG REDA I PRIMENA

A. Opšti slučaj – pristup rešavanja

Posmatramo diferencnu jednačinu oblika:

$$\frac{\Delta^2 Y_n}{\Delta n^2} + \hat{f}_n Y_n = 0, \qquad \text{(III.1)}$$

koja se, s´obzirom na (II.2) može napisati kao:

$$\left[\left(\hat{T}_1 - 1\right)^2 + \hat{f}_n\right] Y_n = 0. \qquad \text{(III.2)}$$

Sada formiramo odgovarajuću nehomogenu jednačinu:

$$\left[\left(\hat{T}_1 - 1\right)^2 + \hat{f}_n\right] y_n = \Phi_n \Rightarrow y_n = \left[\left(\hat{T}_1 - 1\right)^2 + \hat{f}_n\right]^{-1} \Phi_n. \quad \text{(III.3)}$$

Ovo je formalno rešenje polaznog problema, a prema opštoj teoriji diferencnih jednačina, treba da ima dva nezavisna partikularna integrala: $y_n^{(1)}$ i $y_n^{(2)}$:

$$\left[\left(\hat{T}_1 - 1\right)^2 + \hat{f}_n\right] y_n^{(1)} = \Phi_n; \quad \left[\left(\hat{T}_1 - 1\right)^2 + \hat{f}_n\right] y_n^{(2)} = \Phi_n. \quad \text{(III.4)}$$

Lako je uočiti da se oduzimanjem ove dve jednačine dobija traženo rešenje jednačine u formi (III.2):

$$\left[\left(\hat{T}_1 - 1\right)^2 + \hat{f}_n\right]\left(y_n^{(1)} - y_n^{(2)}\right) = 0 \Rightarrow Y_n \equiv y_n^{(1)} - y_n^{(2)}. \quad \text{(III.5)}$$

To znači da je potrebno odrediti ova dva partikularna rešenja.

Kako se operator $\left(\hat{T}_1 - 1\right)^2 + \hat{f}_n$ može se napisati na dva potpuno različita načina:

$$\left(\hat{T}_1 - 1\right)^2 + \hat{f}_n = \begin{cases} \hat{f}_n\left[1 + \hat{f}_n^{-1}\left(\hat{T}_1 - 1\right)^2\right]; \\ \left(\hat{T}_1 - 1\right)^2\left[1 + \left(\hat{T}_1 - 1\right)^{-2}\hat{f}_n\right], \end{cases}$$

onda i operator $\left[\left(\hat{T}_1 - 1\right)^2 + \hat{f}_n\right]^{-1}$ ima sledeće dve forme:

$$\left[\left(\hat{T}_1 - 1\right)^2 + \hat{f}_n\right]^{-1} = \begin{cases} \hat{J}_1 \equiv \left[1 + \hat{f}_n^{-1}\left(\hat{T}_1 - 1\right)^2\right]^{-1}\hat{f}_n^{-1} = \\ \quad = \sum_{k=0}^{\infty}(-1)^k\left[\hat{f}_n^{-1}\left(\hat{T}_1 - 1\right)^2\right]^k \hat{f}_n^{-1}; \\ \hat{J}_2 \equiv \left[1 + \left(\hat{T}_1 - 1\right)^{-2}\hat{f}_n\right]^{-1}\left(\hat{T}_1 - 1\right)^{-2} = \\ \quad = \sum_{k=0}^{\infty}(-1)^k\left[\left(\hat{T}_1 - 1\right)^{-2}\hat{f}_n\right]^k\left(\hat{T}_1 - 1\right)^{-2}. \end{cases} \quad \text{(III.6)}$$

Operatori $\hat{J}_1$ i $\hat{J}_2$ napisani u eksplicitnoj formi su:

$$\hat{J}_1 = \left[1 - \hat{f}_n^{-1}\left(\hat{T}_1 - 1\right)^2 + \hat{f}_n^{-1}\left(\hat{T}_1 - 1\right)^2 \hat{f}_n^{-1}\left(\hat{T}_1 - 1\right)^2 - ...\right]\hat{f}_n^{-1};$$

$$\hat{J}_2 = \left[1 - \left(\hat{T}_1 - 1\right)^{-2}\hat{f}_n + \left(\hat{T}_1 - 1\right)^{-2}\hat{f}_n\left(\hat{T}_1 - 1\right)^{-2} - ...\right]\left(\hat{T}_1 - 1\right)^{-2}$$

i moraju se pisati i računati u datom poretku, jer operatori $\hat{f}_n$ i $\hat{T}_1 - 1$ ne komutiraju! Dva partikularna integrala nalaze se onda kao:

$$y_n^{(1)} = \hat{J}_1 \Phi_n; \quad y_n^{(2)} = \hat{J}_2 \Phi_n. \qquad \text{(III.7)}$$

Sada treba konkretizovati funkciju Φ_n, a treba je odabrati tako da se jedan od dva beskonačna reda iz (III.6) preseče. Pošto je: $\left(\hat{T}_1 - 1\right)^2 C = 0$, biramo: $\Phi_n = f_n$, pa su onda:

$$y_n^{(1)} = \left[1 - \hat{f}_n^{-1}\left(\hat{T}_1 - 1\right)^2 + \hat{f}_n^{-1}\left(\hat{T}_1 - 1\right)^2 \hat{f}_n^{-1}\left(\hat{T}_1 - 1\right)^2 - ...\right]\hat{f}_n^{-1} f_n = 1;$$

$$y_n^{(2)} = \left[1 - \left(\hat{T}_1 - 1\right)^{-2}\hat{f}_n + \left(\hat{T}_1 - 1\right)^{-2}\hat{f}_n\left(\hat{T}_1 - 1\right)^{-2} - ...\right]\left(\hat{T}_1 - 1\right)^{-2} f_n,$$

a ukupno traženo rešenje polazne jednačine je:

$$Y_n = 1 - \left(\hat{T}_1 - 1\right)^{-2}\hat{f}_n + \left(\hat{T}_1 - 1\right)^{-2}\hat{f}_n\left(\hat{T}_1 - 1\right)^{-2}\hat{f}_n - ... = $$
$$= \sum_{k=0}^{\infty}(-1)^k\left[\left(\hat{T}_1 - 1\right)^{-2}\hat{f}_n\right]^k. \qquad \text{(III.8)}$$

B. Diferencna jednačina stanja kristalnih nano-struktura

Kao što je rečeno, u problemima fizike kristala [24-28] često se pojavljuje diferencna jednačina tipa:

$$Y_{n+1} + Y_{n-1} + \rho_n Y_n = 0, \qquad \text{(III.9)}$$

koja se od (II.41) razlikuje po tome što parametar ρ (bitno!) zavisi od argumenta *n*, tj. $\rho = \rho_n$, čime se opisuje translaciona

neinvarijantnost (realnih i posebno nano) kristala, a argument definiše položaj molekula (atoma, jona) u kristalu.

Upotrebom translacionih operatora ova jednačina može se napisati u sledećem obliku:

$$\left(\hat{T}_1 + \hat{T}_{-1} + \hat{\rho}_n\right)Y_n = 0. \tag{III.10}$$

U prethodnom paragrafu je naglašeno da se krucijalan zahtev za nalaženje rešenja ovom metodom sastojao u tome da jedan od operatora primenjen na konstantu u rezultatu daje nulu. Ovde imamo operatore $\hat{T}_1 + \hat{T}_{-1}$ i $\hat{\rho}_n$. Ni jedan od njih primenjen na konstantu, ne može dati nulu. Zato izraz (III.10) moramo transformisati u:

$$\left[\left(\hat{T}_1 + \hat{T}_{-1} - 2\right) + \left(\hat{\rho}_n + 2\right)\right]Y_n = 0,$$

jer operator $\left(\hat{T}_1 + \hat{T}_{-1} - 2\right)$, primenjen na konstantu, daje nulu:

$$\left(\hat{T}_1 + \hat{T}_{-1} - 2\right)C = \hat{T}_1 C + \hat{T}_{-1} C - 2C = C + C - 2C = 0.$$

Radi pojednostavljenja, uvedemo oznake:

$$\hat{a} = \hat{T}_1 + \hat{T}_{-1} - 2; \quad \hat{b}_n = \hat{\rho}_n + 2,$$

pa jednačina (III.10) postaje:

$$\left(\hat{a} + \hat{b}_n\right)Y_n = 0, \tag{III.11}$$

pri čemu je $\hat{a}\,C = 0$.

Pošto je ova jednačina homogena, njeno rešenje ćemo tražiti, kao i u prethodnom paragrafu, preko odgovarajuće pomoćne nehomogene jednačine:

$$\left(\hat{a} + \hat{b}_n\right)y_n = \Phi_n, \tag{III.12}$$

koja ima dva linearno nezavisna rešenja: $y_n^{(1)} = \hat{J}_1\Phi_n$ i $y_n^{(2)} = \hat{J}_2\Phi_n$, a pomoću kojih je traženo opšte rešenje jednako: $Y_n \equiv y_n^{(1)} - y_n^{(2)}$. Ostaje da nađemo ove partikularne integrale. Na osnovu dvostrukog razvoja operatora:

$$\hat{a} + \hat{b}_n = \begin{cases} \hat{b}_n\left(1 + \hat{b}_n^{-1}\hat{a}\right), \\ \hat{a}\left(1 + \hat{a}^{-1}\hat{b}_n\right). \end{cases}$$

odnosno inverznog operatora:

$$\left(\hat{a} + \hat{b}_n\right)^{-1} = \left(1 + \hat{b}_n^{-1}\hat{a}\right)\hat{b}_n^{-1} =$$
$$= \sum_{k=0}^{\infty}(-1)^k\left(\hat{b}_n^{-1}\hat{a}\right)^k \hat{b}_n^{-1} \equiv \hat{J}_1 :$$
$$\left(\hat{a} + \hat{b}_n\right)^{-1} = \left(1 + \hat{a}^{-1}\hat{b}_n\right)^{-1} \hat{a}^{-1} =$$
$$= \sum_{k=0}^{\infty}(-1)^k\left(\hat{a}^{-1}\hat{b}_n\right)^k \hat{a}^{-1} \equiv \hat{J}_2,$$

dobijamo:

$$y_n^{(1)} = \hat{J}_1\Phi_n = \left(1 - \hat{b}_n^{-1}\hat{a} + \hat{b}_n^{-1}\hat{a}\hat{b}_n^{-1}\hat{a} + ...\right)\hat{b}_n^{-1}\Phi_n;$$
$$y_n^{(2)} = \hat{J}_2\Phi_n = \left(1 - \hat{a}^{-1}\hat{b}_n + \hat{a}^{-1}\hat{b}_n\hat{a}^{-1}\hat{b}_n - ...\right)\hat{a}^{-1}\Phi_n.$$

Ukoliko sada specificiramo funkciju Φ_n – uzmemo da je: $\Phi_n = \hat{b}_n$, onda se prvo rešenje dobija u vidu:

$$y_n^{(1)} = \left(1 - \hat{b}_n^{-1}\hat{a} + \hat{b}_n^{-1}\hat{a}\hat{b}_n^{-1}\hat{a} - ...\right)\hat{b}_n^{-1}\hat{b}_n = 1,$$

a dobijen je zahvaljujući činjenici da je $\hat{a}\cdot 1 = 0$.

Drugo rešenje se izražava kao:

$$y_n^{(2)} = \hat{a}^{-1}\hat{b}_n - \hat{a}^{-1}\hat{b}_n\hat{a}^{-1}\hat{b}_n + \hat{a}^{-1}\hat{b}_n\hat{a}^{-1}\hat{b}_n\hat{a}^{-1}\hat{b}_n - ...$$

i da bi se izračunalo treba naći eksplicitnu formu operatora $\hat{a}^{-1}$. Kako operator $\hat{a}$ ima dva oblika:

$$\hat{a} = \hat{T}_1 + \hat{T}_{-1} - 2 = \begin{cases} -2\left[1 - \frac{1}{2}\left(\hat{T}_1 + \hat{T}_{-1}\right)\right], \\ \left(\hat{T}_1 + \hat{T}_{-1}\right)\left[1 - 2\left(\hat{T}_1 + \hat{T}_{-1}\right)^{-1}\right]. \end{cases}$$

onda postoje i dve forme njemu inverznog operatora:

$$\hat{a}^{-1} = -\left[1 - \frac{1}{2}\left(\hat{T}_1 + \hat{T}_{-1}\right)\right]^{-1} = -\sum_{k=0}^{\infty}\frac{1}{2^{k+1}}\left(\hat{T}_1 + \hat{T}_{-1}\right)^k \equiv \hat{A}_1;$$

$$\hat{a}^{-1} = \left[1 - 2\left(\hat{T}_1 + \hat{T}_{-1}\right)^{-1}\right]^{-1}\left(\hat{T}_1 + \hat{T}_{-1}\right)^{-1} =$$
$$= -\sum_{k=0}^{\infty} 2^k\left(\hat{T}_1 + \hat{T}_{-1}\right)^{-k-1} \equiv \hat{A}_2, \tag{III.13}$$

ali se i operator $\left(\hat{T}_1 + \hat{T}_{-1}\right)^{-1}$ može napisati u dve različite forme, jer je:

$$\hat{T}_1 + \hat{T}_{-1} = \begin{cases} \hat{T}_1\left(1 + \hat{T}_{-2}\right); \\ \hat{T}_{-1}\left(1 + \hat{T}_2\right), \end{cases}$$

pa su:

$$\left(\hat{T}_1 + \hat{T}_{-1}\right)^{-1} = \left(1 + \hat{T}_{-2}\right)^{-1}\hat{T}_{-1} = \sum_{k=0}^{\infty}(-1)^k\hat{T}_{-2k-1} \equiv \hat{\theta}_1;$$

$$\left(\hat{T}_1 + \hat{T}_{-1}\right)^{-1} = \left(1 + \hat{T}_2\right)^{-1}\hat{T}_1 = \sum_{k=0}^{\infty}(-1)^k\hat{T}_{2k+1} \equiv \hat{\theta}_2.$$

Operatorske forme $\hat{A}_1$, $\hat{A}_2$, $\hat{\theta}_1$ i $\hat{\theta}_2$ biraju se tako da rezultat njihove primene na datu funkciju diskretne promenljive bude konvergentan red. Kada je taj izbor napravljen, može se izračunati $y_n^{(2)}$. Rešenje polazne homogene jednačine biće dato preko:

$$Y_n = y_n^{(1)} - y_n^{(2)} = 1 - \hat{a}^{-1}\hat{b}_n + \hat{a}^{-1}\hat{b}_n\hat{a}^{-1}\hat{b}_n - ... =$$
$$= \sum_{k=0}^{\infty}(-1)^k\left(\hat{a}^{-1}\hat{b}_n\right)^k. \tag{III.14}$$

C. Jedan karakterisičan primer

Kao primer posmatraćemo slučaj kada je: $\rho_n = Ae^{n\alpha} - 2$, tj. diferencnu jednačinu:

$$Y_{n+1} + Y_{n-1} + \left(A\mathrm{e}^{n\alpha} - 2\right)Y_n = 0, \qquad \text{(III.15)}$$

gde zaključujemo da je: $\hat{b}_n = A\,\mathrm{e}^{n\alpha}$, pa zbog toga što je to eksponencijalna funkcija, neke od operatora ne moramo tražiti preko beskonačnih redova. Tako se vidi da je:

$$\left(\hat{T}_1 + \hat{T}_{-1}\right)A\mathrm{e}^{n\alpha} = 2\cosh\alpha\;A\mathrm{e}^{n\alpha},$$

a kako je: $\left(\hat{T}_1 + \hat{T}_{-1}\right)^{-1}\left(\hat{T}_1 + \hat{T}_{-1}\right) = 1$, znači da je:

$$\left(\hat{T}_1 + \hat{T}_{-1}\right)^{-1} A\mathrm{e}^{n\alpha} = \frac{1}{2\cosh\alpha}\,A\mathrm{e}^{n\alpha}.$$

S obzirom da je $\cosh\alpha > 1$, moramo koristiti one operatorske redove u kojima figuriše operator $\left(\hat{T}_1 + \hat{T}_{-1}\right)^{-1}$. Takav je red (III.13). To znači da će u (III.14) operator $\hat{a}^{-1}$, primenjen na funkciju $A\mathrm{e}^{n\alpha}$, dati rezultat:

$$\hat{a}^{-1}\hat{b}_n = \hat{a}^{-1}A\mathrm{e}^{n\alpha} = \sum_{k=0}^{\infty} 2^k \left(\hat{T}_1 + \hat{T}_{-1}\right)^{-k-1} A\mathrm{e}^{n\alpha} =$$

$$= A\mathrm{e}^{n\alpha}\sum_{k=0}^{\infty} 2^k \frac{1}{2^{k+1}\cosh^{k+1}\alpha} = \frac{A\mathrm{e}^{n\alpha}}{2\cosh\alpha}\sum_{k=0}^{\infty}\frac{1}{(\cosh\alpha)^k} =$$

$$= \frac{A\mathrm{e}^{n\alpha}}{2(\cosh\alpha - 1)},$$

pa dalje sledi:

$$\hat{a}^{-1}\hat{b}_n\hat{a}^{-1}\hat{b}_n = \hat{a}^{-1}A\mathrm{e}^{n\alpha}\frac{A\mathrm{e}^{n\alpha}}{2(\cosh\alpha - 1)} =$$

$$= \frac{A^2\mathrm{e}^{2n\alpha}}{2^2(\cosh\alpha - 1)(\cosh 2\alpha - 1)}.$$

Prema tome, izraz (III.15) se može pisati kao:

$$Y_n = 1 - \frac{A\mathrm{e}^{n\alpha}}{2(\cosh\alpha - 1)} + \frac{A^2\mathrm{e}^{2n\alpha}}{2^2(\cosh\alpha - 1)(\cosh 2\alpha - 1)} - \cdots =$$

$$= \sum_{k=1}^{\infty}(-1)^k\left(\frac{A\mathrm{e}^{n\alpha}}{2}\right)^k \frac{1}{\prod_{s=1}^{k}(\cosh s\,\alpha - 1)}. \qquad \text{(III.16)}$$

Sada treba pokazati da ovo rešenje zadovoljava polaznu jednačinu (III.15). Kada se rešenje (III.16) uvrsti u tu jednačinu, lako se vidi da suma prvog, drugog i četvrtog člana iznosi:

$$\sum_{k=1}^{\infty}(-1)^k\left(\frac{A\mathrm{e}^{n\alpha}}{2}\right)^k \frac{2(\cosh k\alpha - 1)}{\prod_{s=0}^{k}(\cosh, s\alpha - 1)}$$

a treći član se može napisati na sledeći način:

$$-\sum_{k=1}^{\infty}(-1)^k\left(\frac{A\mathrm{e}^{n\alpha}}{2}\right)^{k+1}\frac{2[\cosh(k+1)\alpha - 1]}{\prod_{s=0}^{q}(\cosh s\,\alpha - 1)}$$

i on, posle zamene sumacionog indeksa $k+1 = q$, postaje:

$$-\sum_{q=1}^{\infty}(-1)^q\left(\frac{A\mathrm{e}^{n\alpha}}{2}\right)^q \frac{2(\cosh\alpha q - 1)}{\prod_{s=0}^{q}(\cosh s\,\alpha - 1)}.$$

Vidi se da je ovaj rezultat jednak onom od sume prvog, drugog i četvrtog člana, ali sa suprotnim znakom, što znači da je njihov zbir jednak nuli. Dakle, rešenje (III.16) upravo predstavlja rešenje polazne jednačine (III.15).

Na kraju ćemo potražiti konkretan fizički sistem kod koga se pojavljuje jednačina tipa (III.15). Ako se posmatra oscilovanje jednodimenzionog lanca molekula [12,13,22,23,29,30], onda je popravka potencijalne energije lanca, koja potiče od oscilovanja molekula, data sa:

$$V = \frac{C}{2}\sum_m \left(u_m - u_{m-1}\right)^2, \qquad \text{(III.17)}$$

gde je u_m pomeraj molekula iz ravnotežnog položaja čija je koordinata označena sa m, dok je C – Hukova konstanta istezanja i predstavlja drugi izvod međumolekulske interakcije po rastojanju između molekula. Torzione konstante (i odgovarajući modovi!) se zanemaruju. Oscilatorna sila, koja deluje na molekul u tački n, definiše se klasično preko:

$$F_n = -\frac{\partial V}{\partial u_n}, \text{ odnosno: } F_n = -\frac{\Delta V}{\Delta u_n} \qquad \text{(III.18)}$$

i jednaka je proizvodu između mase molekula M i njegovog ubrzanja: $M\ddot{u}_n = F_n$. Na osnovu (III.17) i (III.18) sledi:

$$M\ddot{u}_n = C\left(u_{n+1} + u_{n-1} - 2u_n\right) \Rightarrow \frac{M}{C}\ddot{u}_n = u_{n+1} + u_{n-1} - 2u_n. \quad \text{(III.19)}$$

Ovo je jednačina kretanja fononskog poremećaja. Kako pomeraj mora biti realan, uzećemo da je:

$$u_n(t) = \psi_n\cos\omega t;\;\; \psi_n = u_n(0);$$

što znači da je $\ddot{u}_n = -\omega^2\psi_n\cos\omega t$. Ako se ovo uvrsti u izraz (III.19), dobija se sledeća diferencna jednačina:

$$\psi_{n+1} + \psi_{n-1} + \left(\frac{M\omega^2}{C} - 2\right)\psi_n = 0. \qquad \text{(III.20)}$$

U slučaju idealne (translaciono invarijantne) strukture, pod normalnim pritiskom, veličina $\frac{M\omega^2}{C} \equiv \rho$ ne zavisi od indeksa čvora n. Ako u graničnim delovima lanca dođe do njegovog sabijanja i to tako da međumolekulsko rastojanje eksponencijalno opada ka drugom kraju lanca, onda se može uzeti da se Hukova konstanta ponaša po zakonu:

$$C = C_0\,\mathrm{e}^{-\alpha n},$$

što znači da se ρ može napisati u obliku $A(\omega)\mathrm{e}^{\alpha n}$, gde je

$$A(\omega) = \frac{M\omega^2}{C} = \frac{\omega^2}{\Omega_\mathrm{D}^2}, \text{ a } \Omega_\mathrm{D} = \sqrt{\frac{C_0}{M}}. \text{ Na osnovu ovoga}$$

jednačina (III.20) postaje:

$$\psi_{n+1} + \psi_{n-1} + \left[A(\omega)e^{\alpha n} - 2\right]\psi_n = 0, \qquad \text{(III.21)}$$

i ona je po obliku identična sa (III.15). Prema tome, rešenje tipa (III.16) može se koristiti za izračunavanje molekulskih pomeraja u 1D lancu u kome su molekuli na jednom kraju sabijeni.

IV. Elektroni u ultratankim filmovima

Na konferencijama ETRAN još od početka ovog veka predstavljali smo različite metode za analizu sistema elementarnih pobuđenja uglavnom u ultratankim kristalnim filmovima, npr. fonone i termodinamičke osobine 2003. – 2021., eksitone i optička svojstva 2004. – 2013, te elektrone i provodnost 2003. – 2013. Ovde ćemo demonstrirati primenu izložene teorije na elektronski sistem, a u posebnom radu i eksitonsku difuziju u modelu filma sa nanoskopskom debljinom.

A. Model elektrona u ultratankom metalnom filmu

Ultratanki metalni filmovi (UTF) jesu strukture sa narušenom simetrijom, pa se kao glavni problem analize UTF pojavljuje problem korektnog nalaženja Grinove funkcije (GF) filma. Kako je već ranije napomenuto, ovaj problem nije trivijalan, jer GF u strukturi sa narušenom simetrijom duž jednog pravca zavise od dva prostorna indeksa ponaosob, a ne od njihove razlike kao u balk-strukturi [31,32]. Zbog toga je cilj ove analize razvijanje takve tehnike sa GF koja će korektno reprodukovati karkateristike konkretnog UTF.

U analizi elektrona u UTF, koristićemo uprošćeni Habardov model [34,35], uzet u aproksimaciji najbližih suseda. Pretpostavićemo da je film „isečen" iz idealne proste kubne stukture, pa hamiltonijan ovog podsistema ima oblik:

$$H = \sum_{\vec{n},\vec{\lambda}} W_{\vec{n},\vec{n}+\vec{\lambda}} A_{\vec{n}}^+ A_{\vec{n}} - \sum_{\vec{n},\vec{\lambda}} W_{\vec{n},\vec{n}+\vec{\lambda}} A_{\vec{n}+\vec{\lambda}}^+ A_{\vec{n}} + \sum_{\vec{n},\vec{\lambda}} W_{\vec{n},\vec{n}+\vec{\lambda}} A_{\vec{n}}^+ A_{\vec{n}+\vec{\lambda}}. \quad \text{(IV.1)}$$

U ovoj formuli W predstavlja energiju elektronskog transfera, tj. jon-jon interakciju, vektor $\vec{\lambda}$ spaja najbliže susede sa onim koji se nalazi u tački rešetke označenoj sa $\vec{n}$, a Fermi operatori A^+ i A kreiraju i aniliraju elektrone, respektivno. Dakle, UTF je translaciono invarijantan u XY ravnima, a simetrija je narušena samo u z-pravcu. U skladu sa ovim, vrednosti ideksa n_x, n_y i n_z kreću se u sledećim intervalima:

$$-\frac{N_i}{2} + 1 \leq n_i \leq \frac{N_i}{2}; N_i \sim 10^8; i = x, y;$$

$$n_z = 0, 1, 2, \cdots, N_z; N_z \leq 10.$$

B. GF i korelaciona funkcija ultratankog metalnog filma

U analizi biće korišćena antikomutatorska GF [24,12–14]:

$$G_{\vec{n},\vec{m}}(t) \equiv \left\langle\left\langle A_{\vec{n}} \,\|\, A_{\vec{m}}^+ \right\rangle\right\rangle = \theta(t)\left\langle\left\{A_{\vec{n}}, A_{\vec{m}}^+\right\}\right\rangle, \qquad \text{(IV.2)}$$

gde je $\theta(t)$ Hevisajdova step-funkcija ($\theta = 0$, za $t < 0$ i $\theta = 1$, za $t > 0$). Diferencirajući po vremenu (IV.2) uz korišćenje jednačina kretanja dolazimo do sledeće jednačine:

$$i\hbar\frac{d}{dt}G_{n_x,n_y,n_z;m_x,m_y,m_z}(t) = i\hbar\delta(t)\delta_{n_x,m_x}\delta_{n_y,m_y}\delta_{n_z,m_z} + 6W G_{n_x,n_y,n_z;m_x,m_y,m_z}(t) -$$
$$- W\Big[G_{n_x+1,n_y,n_z;m_x,m_y,m_z}(t) + G_{n_x-1,n_y,n_z;m_x,m_y,m_z}(t) + G_{n_x,n_y+1,n_z;m_x,m_y,m_z}(t) +$$
$$+ G_{n_x,n_y-1,n_z;m_x,m_y,m_z}(t) + G_{n_x,n_y,n_z+1;m_x,m_y,m_z}(t) + G_{n_x,n_y,n_z-1;m_x,m_y,m_z}(t)\Big]$$

$$\text{(IV.3)}$$

U ovoj jednačini biće izvršene Furije-tansformacije vreme – frekvencija: $G_{n_x,n_y,n_z;m_x,m_y,m_z}(t) = \int\limits_{-\infty}^{+\infty} d\omega\, e^{-i\omega t} G_{n_x,n_y,n_z;m_x,m_y,m_z}(\omega);$

$\delta(t) = \int\limits_{-\infty}^{+\infty} d\omega\, e^{-i\omega t};\ \hbar\omega = E,$ nakon čega ona prelazi u:

$$(E - 6W) G_{n_x,n_y,n_z;m_x,m_y,m_z}(\omega) = \frac{i\hbar}{2\pi}\delta_{n_x,m_x}\delta_{n_y,m_y}\delta_{n_z,m_z} -$$
$$- W\Big[G_{n_x+1,n_y,n_z;m_x,m_y,m_z}(\omega) + G_{n_x-1,n_y,n_z;m_x,m_y,m_z}(\omega) + G_{n_x,n_y+1,n_z;m_x,m_y,m_z}(\omega) +$$
$$+ G_{n_x,n_y-1,n_z;m_x,m_y,m_z}(\omega) + G_{n_x,n_y,n_z+1;m_x,m_y,m_z}(\omega) + G_{n_x,n_y,n_z-1;m_x,m_y,m_z}(\omega)\Big]$$

$$\text{(IV.4)}$$

Na ovom mestu moramo uzeti u obzir da je simetrija narušena u z-pravcu, što znači da u račun moramo uvesti granične uslove u ovom pravcu, a koristićemo najjedostavnije – koji su u odsustvu slojeva za $n_z = -1$ i $n_z = N_z + 1$ jednaki:

$$W_{n_x,n_y,0;m_x,m_y,-1} = W_{n_x,n_y,N_z+1;m_x,m_y,N_z} = 0.$$

Treba naglasiti da realističniji granični uslovi treba da uključe promene interakcija u graničnim slojevima i promenu interakcija između graničnog sloja i prvog unutrašnjeg sloja. Ovi opštiji granični uslovi bili su korišćeni u analizi sistema Frenkelovih eksitona [24,34,35]. U skladu sa usvojenim graničnim uslovima jednačina (IV.4) raspada se na sistem od 3^l jednačina, gde je l broj pravaca narušenja simetrije (u razmatranom slučaju je $l = 1$), pa sledi:

$\underline{n_z = 0:}$
$$(E - 5W) G_{n_x,n_y,0;m_x,m_y,m_z} = \frac{i\hbar}{2\pi}\delta_{0,m_x}\delta_{0,m_y}\delta_{n_z,m_z} -$$
$$- W\big(G_{n_x+1,n_y,0;m_x,m_y,m_z} + G_{n_x-1,n_y,0;m_x,m_y,m_z}\big) -$$
$$- W\big(G_{n_x,n_y+1,0;m_x,m_y,m_z} + G_{n_x,n_y-1,0;m_x,m_y,m_z}\big) -$$
$$- W G_{n_x,n_y,1;m_x,m_y,m_z};$$

$$\text{(IV.5a)}$$

$\underline{1 \leq n_z \leq N_z - 1:}$
$$(E - 6W) G_{n_x,n_y,n_z;m_x,m_y,m_z} = \frac{i\hbar}{2\pi}\delta_{n_x,m_x}\delta_{n_y,m_y}\delta_{n_z,m_z} -$$
$$- W\big(G_{n_x+1,n_y,n_z;m_x,m_y,m_z} + G_{n_x-1,n_y,n_z;m_x,m_y,m_z}\big) -$$
$$- W\big(G_{n_x,n_y+1,n_z;m_x,m_y,m_z} + G_{n_x,n_y-1,n_z;m_x,m_y,m_z}\big) -$$
$$- W\big(G_{n_x,n_y,n_z+1;m_x,m_y,m_z} + G_{n_x,n_y,n_z-1;m_x,m_y,m_z}\big);$$

$$\text{(IV.5b)}$$

$\underline{n_z = N_z:}$
$$(E - 5W) G_{n_x,n_y,N_z;m_x,m_y,m_z} = \frac{i\hbar}{2\pi}\delta_{n_x,m_x}\delta_{n_y,m_y}\delta_{N_z,m_z} -$$
$$- W\big(G_{n_x+1,n_y,N_z;m_x,m_y,m_z} + G_{n_x-1,n_y,N_z;m_x,m_y,m_z}\big) -$$
$$- W\big(G_{n_x,n_y+1,N_z;m_x,m_y,m_z} + G_{n_x,n_y-1,N_z;m_x,m_y,m_z}\big) -$$
$$- W G_{n_x,n_y,N_z-1;m_x,m_y,m_z}.$$

$$\text{(IV.5c)}$$

Imajući u vidu da je film translatorno invarijantan u svim XY ravnima izvršićemo delimičnu transformaciju prostor-impuls:

$$G_{n_x,n_y,n_z;m_x,m_y,m_z}(\omega) = \frac{1}{N_x N_y} \sum_{k_x,k_y} e^{iak_x(n_x-m_x)+iak_y(n_y-m_y)} G_{k_x,k_y}(\omega) \alpha_{n_z,m_z}(\omega),$$

sa Kronekerovim simbolima u reprezentaciji ravnih talasa:

$$\delta_{n_x;m_x} = \frac{1}{N_x} \sum_{k_x} e^{iak_x(n_x-m_x)}; \quad \delta_{n_y;m_y} = \frac{1}{N_y} \sum_{k_y} e^{iak_y(n_y-m_y)},$$

gde je a kostanta kristalne rešetke. Posle zamena ovih transformacija ovaj sistem jednačina se uprošćava i postaje:

$\underline{n_z = 0:}$

$$G_{k_x,k_y}\left[W\alpha_{1,m_z} + (\varepsilon+W)\alpha_{0,m_z}\right] = \frac{i\hbar}{2\pi}\delta_{0,m_z}; \tag{IV.6a}$$

$\underline{1 \le n_z \le N_z - 1:}$

$$G_{k_x,k_y}\left[W(\alpha_{n_z+1,m_x} + W\alpha_{n_z-1,m_x}) + \varepsilon\alpha_{n_z,m_z}\right] = \frac{i\hbar}{2\pi}\delta_{n_z,m_z}; \tag{IV.6b}$$

$\underline{n_z = N_z:}$

$$G_{k_x,k_y}\left[W\alpha_{Nz-1,m_x} + (\varepsilon+W)\alpha_{N_z,m_x}\right] = \frac{i\hbar}{2\pi}\delta_{N_z,m_z}, \tag{IV.6c}$$

gde je: $\varepsilon = E - 2W - 4W\sin^2\frac{ak_x}{2} - 4W\sin^2\frac{ak_y}{2}$. Funkciju α podobno je uzeti u sledećem obliku:

$$\alpha_{n_z,m_z}(\omega) = \sum_\nu a_\nu(m_z,\omega)\left[\sin(n_z+1)\varphi_\nu - \sin n_z\,\varphi_\nu\right],$$

u kojem se nepoznate funkcije određuju tako da granične jednačine (IV.6a) i (IV.6c) budu zadovoljene. Ako se ovo zameni u (IV.6b) dobija se:

$$\sum_\nu G_{k_x,k_y}(2W\cos\varphi_\nu + \varepsilon)\,a_\nu \times$$
$$\times\left[\sin(n_z+1)\varphi_\nu - \sin n_z\varphi_\nu\right] = \frac{i\hbar}{2\pi}\delta_{n_z,m_z}, \tag{IV.7}$$

a zamenom u (IV.6a), ona postaje:

$$\sum_\nu G_{k_x,k_y}(2W\cos\varphi_\nu + \varepsilon)\,a_\nu\,\sin\varphi_\nu = \frac{i\hbar}{2\pi}\delta_{0,m_z}.$$

Lako se uočava da ova jednačina predstavlja specijalan slučaj jednačine (IV.7) za nultu vrednost indeksa n_z. Ako se izraz za $\alpha_{n_z,m_z}(\omega)$ zameni u (IV.6c), dobija se jednačina koja predstavlja specijalan slučaj izraza (IV.7) za $n_z = N_z$, pod uslovom:

$$(1-\cos\varphi_\nu)\sin(N_z+1)\varphi_\nu = 0 \Rightarrow \varphi_\nu = \frac{\nu\pi}{N_z+1}, \tag{IV.8}$$

gde je $\nu = 1,2,3,...,N_z$.

Konačan izraz za GF onda postaje:

$$G_{n_x,n_y,n_z;m_x,m_y,m_z}(\omega) = \frac{i}{2\pi}\frac{1}{N_x}\frac{1}{N_y}\sum_{k_x}\sum_{k_y}\sum_{\nu=1}^{N_z}\frac{e^{iak_x(n_x-m_x)+iak_y(n_y-m_y)}}{\omega-\omega_{k_x,k_y,\nu}}\times \tag{IV.9}$$
$$\times\left[\sin(n_z+1)\frac{\nu\pi}{N_z+1} - \sin n_z\frac{\nu\pi}{N_z+1}\right]\sum_{\nu'=1}^{N_z}L^z_{\nu\nu'}\sin(m_z+\nu')\frac{\nu\pi}{N_z+1},$$

a koeficijenti $L^z_{\nu\nu'}$ određuju se iz algebarske jednačine:

$$\delta_{n_z,m_z} = \sum_{\nu=1}^{N_z}\left[\sin(n_z+1)\frac{\nu\pi}{N_z+1} - \sin n_z\frac{\nu\pi}{N_z+1}\right]\times$$
$$\times\sum_{\nu'=1}^{N_z}L^z_{\nu\nu'}\sin(m_z+\nu')\frac{\nu\pi}{N_z+1},$$

tako da ona bude zadovoljena kada je: $\delta_{n_z,m_z} = 1$ za $n_z = m_z$ i $\delta_{n_z,m_z} = 0$ za $n_z \ne m_z$.

Na osnovu definicije, npr. iz [36], spektralna intenzivnost elektronske GF će biti:

$$I_G = \frac{G(\omega+i\delta) - G(\omega-i\delta)}{e^{\frac{\hbar\omega}{\Theta}} + 1}\Bigg|_{\delta\to 0^+} = \tag{IV.10}$$
$$= \frac{1}{N_x}\frac{1}{N_y}\sum_{k_x}\sum_{k_y}\sum_{\nu=1}^{N_z}\frac{e^{iak_x(n_x-m_x)+iak_y(n_y-m_y)}}{e^{\frac{\hbar\omega}{\Theta}}+1}\delta(\omega-\omega_{k_x,k_y,\nu})\times$$
$$\times\left[\sin(n_z+1)\frac{\nu\pi}{N_z+1} - \sin n_z\frac{\nu\pi}{N_z+1}\right]\sum_{\nu'=1}^{N_z}L^z_{\nu\nu'}\sin(m_z+\nu')\frac{\nu\pi}{N_z+1},$$

a ona je potrebna radi proračuna korelacione funkcije [12-14]:

$$\left\langle A^+_{m_x,m_y,m_z}(0)A_{n_x,n_y,n_z}(t)\right\rangle = \int_{-\infty}^{+\infty}d\omega\,e^{-i\omega t}I_G(\omega) = \tag{IV.11}$$
$$= \frac{1}{N_x}\frac{1}{N_y}\sum_{k_x}\sum_{k_y}\sum_{\nu=1}^{N_z}\frac{e^{-i\omega_{k_x,k_y,\nu}t}}{e^{\frac{E_{k_x,k_y,\nu}}{\Theta}}+1}e^{iak_x(n_x-m_x)+iak_y(n_y-m_y)}\times$$
$$\times\left[\sin(n_z+1)\frac{\nu\pi}{N_z+1} - \sin n_z\frac{\nu\pi}{N_z+1}\right]\cdot\sum_{\nu'=1}^{N_z}L^z_{\nu\nu'}\sin(m_z+\nu')\frac{\nu\pi}{N_z+1},$$

gde je:

$$E_{k_x,k_y,\nu} \equiv \hbar\omega_{k_x,k_y,\nu} = 4W\left(\sin^2\frac{ak_x}{2} + \sin^2\frac{ak_y}{2} + \sin^2\frac{\nu}{N_z+1}\frac{\pi}{2}\right), \tag{IV.12}$$

energija elektronskih stanja.

C. Elektronske koncentracije u uskom sloju oko E_F

Izraz za elektronsku koncentraciju dobija se preko (IV.11) ako se uzme $t = 0$ i $m_i = n_i$, $i = x,y,z$. Međutim, elektronske koncentracije moraju se računati u reprezentaciji hemijskog potencijala, tj. po statističkim formulama velikog kanonskog ansambla, zbog toga što se broj elektrona u sistemu održava. Hemijski potencijal biće uzet [13,24] kao najveća vrednost energije elektronskih stanja u prvoj Briluenovoj zoni [14], tj.

$$\mu = \left(E_{k_x,k_y,\nu}\right)_{max} = 4W\left(2 + \sin^2\frac{N_z}{N_z+1}\frac{\pi}{2}\right).$$

Vodeći računa o ovoj napomeni, u (IV.11) mora se izvršiti zamena $E_{kx,ky,\nu} \to E_{kx,ky,\nu} - \mu$. Osim toga, elektroni koji se nalaze u uskom impulsnom sloju oko Fermi-površi najaktivniji su u fizičkim procesima [12,13], pa ćemo odrediti koncentracije u ovom sloju i to u formi:

$$C_{n_z} \equiv \left\langle A^+_{n_x,n_y,n_z}(0)A_{n_x,n_y,n_z}(0)\right\rangle. \tag{IV.13}$$

s´tim da se sumiranje po k_x i k_y zamenjuje odgovarajućom integracijom: $\dfrac{1}{N_x}\dfrac{1}{N_y}\sum_{k_x}\sum_{k_y} \rightarrow \dfrac{a^2}{(2\pi)^2}\iint dk_x dk_y$ u aproksimaciji malih talasnih vektora.

Posmatraćemo ilustrativni primer: troslojni film (film sa tri XY paralelne neograničene kristalografske ravni – dve granične i jedna u sredini filma), dakle $N_z = 2$.

Na osnovu prethodnih rezultata upadljivo je da impulsni indeks ν uzima jednu vrednost manje nego konfiguracioni indeks n_z. Za izabrani primer: $n_z \in [0,1,2]$, dok $\nu \in [1,2]$. To fizički znači da u jednom sloju troslojnog filma nema provodnih elektrona sa zakonom disperzije (IV.12). U ovom slučaju elektroni ostaju lokalizovani ili se, eventualno, film jonizuje tako što elektroni iz jednog sloja napuste film. Na osnovu ovoga očigledno je da se troslojni film ponaša kao jedan od tri navedena subfilma. Ti subfilmovi su: subfilm sa $n_z = 0$ i $n_z = 1$ (u daljem tekstu oznaka 0-1), subfilm sa $n_z = 1$ i $n_z = 2$ (oznaka 1-2) i subfilm sa $n_z = 0$ i $n_z = 2$ (oznaka 0-2). Za svaki od pomenutih subfilmova ćemo izračunati koncentracije elektrona uz podatke da je: $W = 1{,}885 \cdot 10^{-19}$ J, a temperatura sobna, dakle: $\Theta = k_B T = 4{,}14 \cdot 10^{-21}$ J. Na osnovu ovoga, izračunali smo raspodelu koncentracija uzduž (nano)debljine filma za:

− subfilm 0-1	1 ———————	$C_1 = 0{,}011$
	0 ———————	$C_0 = 0{,}025$
− subfilm 1-2	2 ———————	$C_2 = 0{,}025$
	1 ———————	$C_1 = 0{,}011$
− subfilm 0-2	2 ———————	$C_2 = 0{,}025$
	0 ———————	$C_0 = 0{,}025$

Rezultati analize pokazuju da se troslojni metalni film ponaša kao dvoslojni, jer se provodni elektroni pojavljuju samo u dva sloja. Za troslojni film postoje tri dvoslojna subfilma i to 0-1, 1-2 i 0-2, pri čemu su 0-1 i 1-2 fizički identični. Pošto su ti subfilmovi isti, verovatnoća njihovog pojavljivanja u eksperimentu iznosi 2/3, dok verovatnoća pojavljivanja filma 0-2 iznosi 1/3.

U svim subfilmovima zapaža se skin efekat. Kod subfilmova 0-1 i 1-2 skin efekat je asimetričan, dok je kod subfilma 0-2 simetričan. Skin efekat kod subfilma 0-2 može se nazvati pravim skin efektom, jer su koncentracije na granicama jednake, a u srednjem sloju nema provodnih elektrona. Mišljenje je da ova varijanta subfilma ima najbolje aplikativne perspektive.

V. ZAKLJUČAK

Teorijsko izučavanje stuktura velikih dimenzija uglavnom zahteva rešavanje diferencijalnih jednačina sa konstantnim koeficijentima. U istraživanjima nanostruktura javljaju se diferencne jednačine, ali i njihovi koeficijenti zavise od prostornih koordinata zbog neophodnosti da se u račun uvedu granični uslovi, kao i uticaj vakancija i primesa. Zbog povećanog interesovanja za ove probleme naša namera je da doprinesemo ovoj tematici. Cilj je da se prikaže kompletna tehnika izračunavanja diferencnih jednačina i demonstrira primena

diferencnog računa u analizama fizičkih karakteristika savremenih nanostruktura.

Udarni trend ovog rada je čisto operativan, tj. ima za cilj da se razvije sposobnost za opisivanje i rešavanje konkretnih problema uvođenjem teorije diferencnog računa. Matematički fundamenti diferencnog računa u vidu korolara, teorema i komplikovanih dokaza nekih stavova ispušteni su jer se sve to može naći u predloženoj matematičkoj literaturi. Treba još napomenuti da se za niz rešenja različitih problema lako dokazuje da ona stvarno zadovoljavaju početnu jednačinu. Ovo je učinjeno prvenstveno zbog toga da se čitalac privikne na operativnu tehniku diferencnog računa. Najčešće korišćena matematička struktura u rešavanju problema diferencnog računa je ovde zastupljena uvođenjem translacionih operatora, jer se njihovim korišćenjem najefikasnije dolazi do rešenja opisanog problema. Dakle, ova prikazana teorija daje neophodno oruđe istraživačima – teoretičarima kako bi se iznašla odgonetka na pitanja kako i zašto dolazi do tako drastičnih izmena svojstava struktura kada se oni proizvedu sa nano-dimenzijama.

Najveći doprinos ove teorije diferencija i antidiferencija je mogućnost opisivanja vrlo specifičnih i bitno različitih osobina nanoskopskih u odnosu na balkovske kristalne strukture. Na konferencijama ETRAN još od početka ovog veka predstavljali smo različite metode za analizu sistema elementarnih pobuđenja uglavnom u ultratankim kristalnim filmovima i njihove karakteristične osobine, a ovde smo demonstrirali primenu izložene teorije na elektronski i eksitonski sistem. Od rezultata treba istaći upečatljiv skin-efekat i različitu prostornu distribuciju i različitu koncentraciju elementarnih pobuđenja.

LITERATURA

[1] G. Cao, *Nanostructures and Nanomaterials: Synthesis, Properties and Applications*, 2nd ed. London, UK: Imperial College Press, 2004.

[2] E.L. Wolf, *Nanophysics and Nanotechnology*, 2nd ed. Weinheim, UK: Wiley-VCH, 2006.

[3] R.W. Kelsall, I.W. Hamley, M. Geoghegan (Eds.), *Nanoscale Science and Technology*, Chichester, UK: J. Wiley & Sons, 2005.

[4] A.G. Davies, J.M.T. Thompson (Eds.), *Advances in Nanoengineering – Electronics, Materials and Assembly*, London, UK: Imperial College, 2007.

[5] C.N.R. Rao, P.J. Thomas, G.U. Kulkarni, *Nanocrystals: Synthesis, Properties and Applications*, New York, USA: Springer, 2007.

[6] S.N. Elaydi, S. Axler, F.W. Gehring, K.A. Ribet, *An Introduction to Difference Equations*, Berlin, Germany: Springer, 1999.

[7] S. Goldberg, *Introduction to Difference Equations*, New York, USA: Dover, 1986.

[8] J.J. Abdul, *Linear Difference Equations with Discrete Transforms Method*, London, UK: Clarkson University, Kluwer AP, 1996.

[9] R.P. Agarwal, *Difference Equations and Inequalities: Theory, Methods and Applications*, New York, USA: Marcel Dekker, 2000.

[10] L. Brand, *Differential and Difference Equations*, New York, USA: John Wiley, 1966.

[11] L.M. Milne-Thomson, *The Calculus of Finite Differences*, London, UK: Macmillan, 1960.

[12] B.S. Tošić, V.D. Sajfert, J.P. Šetrajčić, D. Popov, D. Ćirić, *Primena diferencnog računa u analizi nanostruktura*, Novi Sad Srbija: Vojvođanska akademija nauka i umetnosti, 2005.

[13] B.S. Tošić, J.P. Šetrajčić i S.K. Jaćimovski, *Metodi teorijske fizike*, Zemun – Beograd, Srbija: Kriminalističko-policijska akademija, 2018.

[14] V.D. Sajfert and J.P. Šetrajčić, "Application of Green's Functions and Difference Equations in Theoretical Analyses of Nanostructures", in: *Monograph Series on the Foundations of Natural Science and Technology*, Vol. 15: *Topics in Nanoscience*, Part I: *Basic Views, Complex Nanosystems: Typical Results and Future*, Ed. Schomers W., Ch. 7, pp. 311-412, Singapore, Singapore: World Scientific, 2022.

[15] J.D. Watson and F.H.S. Crick, "Molecular Structure of Nucleic Acids: A Structure for Deoxyribose Nucleic Acid", *Nature*, vol. 171, pp. 737-738, 1953.

[16] V.M. Agranovich, *Theory of Excitons*, Moscow, SSSR: Nauka, 1978.

[17] A.J. Šetrajčić-Tomić, D. Rodić, I.J. Šetrajčić, V.D. Sajfert and J.P. Šetrajčić, "Basics of Optical Engineering – Analysis of Environmental and Quantum Size Effects on the Optical Characteristics of Molecular Crystalline Nanofilms", *Photonic Nanostruct*. vol. 31, pp. 115–128, 2018.

[18] A.J.Šetrajčić-Tomić, M. Vojnović, J.P. Šetrajčić, S.M. Vučenović and N.R. Vojnović, "Theoretical Basis of Optical Engineering of Ultrathin Crystalline Film-Structures", *Opt. Quant. Electron.* vol. 52, no 4, 251 [1-18], 2020.

[19] L. Edelstein-Keshet, *Mathematical Models in Biology*, New York, USA: Random House, 1988.

[20] J.P. Šetrajčić, S. Armaković, I.J. Šetrajčić and Lj.D. Džambas, "Surface Localization of Electrons in Ultrathin Crystalline Structures", *Mod. Phys. Lett*. B, vol. 28, no.), 1450023 [8 pages], 2014.

[21] J.P.Šetrajčić, S.K.Jaćimovski i S.M.Stojković, *Uticaj elektronskog podsistema na posebne odlike kristalni nanostruktura*, Zemun – Beograd, Srbija: Kriminalističko-policijska akademija, 2018.

[22] J.P. Šetrajčić, D.I.Ilić and S.K.Jaćimovski, "The Influence of the Surface Parameter Changes onto the Phonon States in Ultrathin Crystalline Films", *Physica* A vol. 496, pp. 434-445, 2018.

[23] J.P. Šetrajčić, D.I. Ilić, S.K. Jaćimovski and S.M. Vučenović, "Impact of Surface Conditions Changes on Changes in Thermodynamic Properties of Quasi 2D Crystals", *Physica* A vol. 566, pp. 125650, 2021.

[24] Ch. Kittel, *Introduction to Solid State Physics*, New York, USA: Wiley, 2004.

[25] P. Hoffmann, *Solid State Physics*, New York, USA: Wiley, 2015.

[26] S.M. Girvin and K. Yang, *Modern Condensed Matter Physics*, Cambridge, UK: Cambridge Univ. Press, 2019.

[27] V.D. Sajfert, B.S. Tošić, "The Research of Nanoscience Progress", *J. Comput. Theor. Nanosci.* vol. 7, no. 1, pp. 15–84, 2010.

[28] V.D. Sajfert, B.S. Tošić, "Order–Disorder Excitations in Nanostructures", in: *Encyclopedia of Nanoscience and Nanotechnology*, vol. 20, pp. 281–350, 2011. (American Scientific Publishers, Ed. H.S. Nalwa, Valencia, California 2011).

[29] J.P. Šetrajčić, V.D. Sajfert, S.K. Jaćimovski, "Fundamental Preferences of the Phonon Engineering for Nanostructural Samples", *Rev. Theor. Sci.* vol. 4, no. 4, pp. 353-401, 2016.

[30] V.D. Sajfert, J.P. Šetrajčić, S.K. Jaćimovski, D.Popov, "Theoretical Basis for Phonon Engineering of Nanostructures", *Quantum Matter*, vol. 6, no. 1, pp. 18-27, 2017.

[31] V.D. Sajfert, J.P. Šetrajčić, B.S. Tošić, R.P. Đajić," Excitonic Diffusion in Thin Molecular Films", *Czechoslovak J.Phys*. vol. 54, no. 9, pp. 975-988, 2004.

[32] V.D. Sajfert, J.P. Šetrajčić, S.K. Jaćimovski, B.S. Tošić, "Thermodynamic and Kinetic Properties of Phonons in Cylindrical Quantum Dots", *Physica* E, vol. 353, pp. 479-491, 2005.

[33] H. Ibach and H. Lüth, *Solid State Physics, An Introduction to Principles of Material Science*, 4th ed. Berlin, Germany: Springer Nature, 2009.

[34] S. Doniach and E.H. Sondheimer, *Green's Functions for Solid State Physisists*, London, UK: Imperial College Press, 1999.

[35] G. Strobl, *Condensed Matter Physics, Crystals, Liquid Crystals and Polymers*, Berlin, Germany: Springer, 2004

[36] D. Popov, S.K. Jaćimovski, B.S. Tošić, J.P. Šetrajčić, "Kinetics of Thin Films Mechanical Oscillations", *Physica* A, vol. 317, pp. 129-139, 2003.

ABSTRACT

The trend of rapid development of nanotechnologies is caused by the discovery of nanostructures – materials that have significantly different physical characteristics when compared with large structures (balk). Nanostructures also have a series of qualitatively completely new and changed effects. For example, superconductive, thermal insulation, acoustic and other properties of nanomaterials are better or completely different from those properties in bulk structures. In general, the potential application in innovative pharmacy and medicine is particularly intriguing. In a way, differences between effects in nanostructures and massive structures can be compared to differences between quantum and classical effects. Theoretical study of balk structures generally requires solving differential equations with continuous variables. In the study of mechanisms in nanostructures, which are the culprits of drastic changes in their properties, differential equations have discrete variables. This is caused by the fact that coefficients depend on spatial coordinates due to the need to calculate dimensional – quantum and boundary (confinement) conditions, as well as the influence of vacancies and impurities. Due to increased interest and high expectations for the benefits of newly discovered effects, and especially due to undeveloped theory, we have presented a theory that aims to present the technique of calculating differential equations and to demonstrate this in a series of applications in the analysis of different – discovered and more undiscovered physical properties of nanostructures.Ovde dolazi prevod apstrakta na engleski. Srpski i engleski tekst apstrakta moraju se slagati.

Fundamentals of the Theory of Difference Equations Applied to the Analysis of the Properties of Nanostructures

Jovan P. Šetrajčić,
Vjekoslav D. Sajfert, Siniša M. Vučenović

Difuzija optičkih pobuđenja u tankim molekulskim filmovima

Jovan P. Šetrajčić i Siniša M. Vučenović

Apstrakt— Analizirana je difuzija Frenkelovih eksitona u ultratankom molekulskom filmu. Koeficijent difuzije je jedna od kinetičkih karakteristika materijala i zbog toga se analiza eksitonske difuzije može tretirati kao doprinos boljem poznavanju difuzionih procesa u molekulskim kristalima. Iz opšte teorije Grinovih funkcija izračunat je tenzor difuzije, a proračun testiran za primer molekulskog filma za 4 paralelna sloja. Pokazano je da su koeficijenti difuzije jednaki za unutrašnje slojeve, što je posljedica simetričnosti polja sila usljed dipol-dipol interakcije.

Ključne reči—Eksitoni; koeficijent difuzije, molekulski film.

I. UVOD

Eksitoni su pobuđenja koja u kristalima nastaju pod dejstvom svetlosti [1–4]. U poluprovodnicima pod dejstvom svetlosti nastaju eksitoni Vanije-Mota, koji se još nazivaju eksitoni velikog radijusa. Frenkelovi eksitoni su optička pobuđenja koja se javljaju u molekulskim kristalima (antracen, naftalin, naftacen, benzol u čvrstom stanju itd). Svetlosni kvant stvara par elektron-šupljina, ali ovaj par se, za razliku od situacije kod poluprovodnika, zadržava u molekulu u kome je stvoren. Ovo se dešava zbog toga što se elektronske talasne funkcije susednih molekula slabo prekrivaju. Pošto par ostaje u granicama molekula (u relativno malom prostoru u odnosu na prostor koji par zauzima u poluprovodnicima) ovi eksitoni su eksitoni malog radijusa.

Nastanak eksitonskog talasa može se opisati na sledeći način [1,2]: svetlosni kvant prevede elektron iz osnovnog stanja koje karakteriše skup kvantnih brojeva koji ćemo označiti indeksom 0 u pobuđeno stanje koje karakteriše skup kvantnih brojeva f. Pošto molekuli interaguju između sebe, pobuđenje se prenosi na susedni molekul i sa ovoga se prenosi dalje. Na taj način stvara se talas pobuđenja koji se naziva Frenkelov eksiton. Ako se posmatraju osnovno stanje elektrona i samo jedno pubuđeno stanje sa indeksom f, onda su očigledne sledeće mogućnosti: a) u osnovnom i u pobuđenom stanju nema elektrona; b) u osnovnom stanju se nalazi jedan elektron, a pobuđeno stanje je prazno; c) osnovno stanje je prazno, a u pobuđenom stanju se nalazi jedan elektron i d) osnovno i pobuđeno stanje sadrže po jedan elektron. To znači da je elektronski Hilbertov prostor u molekulu koji ćemo označiti sa h sadrži četiri vektora:

Akademik Jovan P. Šetrajčić, Akademija nauka i umjetnosti Republike Srpske, Bana Lazarevića 1, 78 000 Banja Luka, RS-BiH (e-mail: jovan.setrajcic@gmail.com).

Prof. dr Siniša M. Vučenović, Univerzitet u Banjoj Luci, PMF, Mladena Stojanovića 2, 78000 Banja Luka, RS-BiH (e-mail: sinisa.vucenovic@pmf.unibl.org)

$$\left|0_0 0_f\right\rangle; \ \left|1_0 0_f\right\rangle; \ \left|1_f 0_0\right\rangle; \ \left|1_0 1_f\right\rangle.$$

Prostor h može se razdvojiti na dva pot prostora:

$$h_1 = \left\{\left|0_0 0_f\right\rangle, \left|1_0 1_f\right\rangle\right\}; \quad h_2 = \left\{\left|1_0 0_f\right\rangle, \left|1_f 0_0\right\rangle\right\}.$$

S obzirom na opisani nastanak Frenkelovog eksitona očigledno je da proizvod elektronskih operatora $a_f^+ a_0$ odgovara stvaranju pobuđenja molekula, dok prozvod $a_0^+ a_f$ odgovara gašenju pobuđenja. Navedeni proizvodi elektronskih operacija ostaju zavoreni u potprostoru h_2 što znači da delujući na vektore iz potprostora h_2 daju vektore koji takođe pripadaju potprostoru h_2. Svojstvene vrednosti operatora $a_f^+ a_0$ i $a_0^+ a_f$ jednake su nuli u potprostoru h_1. Takođe je očigledno da je zbir svojstvenih vrednosti operatora brojeva elektrona $a_f^+ a_f$ i $a_0^+ a_0$ jednak jedinici u potprostoru h_2.

Proizvod operatora $a_f^+ a_0$ obeležava se sa P^+ i predstavlja operator kreacije eksitona, dok se operator $a_0^+ a_f$ označava sa P i predstavlja operator anihilacije eksitona. Operatori P^+ i P nazivaju se Pauli-operatori i ne zadovoljavaju ni bozonske ni fermionske komutatorske relacije. Njihove komutacione relacije su date [1] sa:

$$\left[P_{\vec{n}}, P_{\vec{m}}^+\right] = \left(1 - 2P_{\vec{n}}^+ P_{\vec{n}}\right)\delta_{\vec{n},\vec{m}}; \ \left[P_{\vec{n}}, P_{\vec{m}}\right] = \left[P_{\vec{n}}^+, P_{\vec{m}}^+\right] = 0;$$

$$P_{\vec{n}}^2 = \left(P_{\vec{n}}^+\right)^2 = 0,$$

gde su $\vec{n}$ i $\vec{m}$ vektori kristalne rešetke molekulskog kristala. Vidi se da su komutacione relacije za Pauli-operatore delimično bozonskog, a delimično fermionskog tipa.

Do otkrića lasera pobuđivanje molekulskih kristala svetlošću iz standardnih izvora (živina lampa na primer) stvaralo je male koncentracije eksitona reda 10^{-15}, pa je analiza eksitonskog sistema sa kvadratnim bozonskim hamiltonijanom davala rezultate koji su se slagali sa eksperimentom.

Laseri velike snage stvaraju eksitonske koncentracije reda 10^{-3} i tada se mora uzeti u obzir i kinematička i dinamička interakcija eksitona, da bi se objasnili eksperimenti. Posle otkrića lasera [2], naglo se razvila tzv. nelinearna optika, koja je proučavala efekte eksiton-eksiton interakcije, kao što su stvaranje viših harmonika, pomeraj eksitonskih energetskih nivoa i multifotonska apsorpcija. Posebno je bio interesantan efekat multifotonske apsorpcije, koji se sastojao u tome što je molekulski kristal, osvetljen crvenom svetlošću, emitovao ljubičastu svetlost. Ovo se moglo objasniti time što je zbog visokih koncentracija eksitona i njihove međusobne interakcije dolazilo do fuzije dva crvena eksitona u jedan novi eksiton sa približno dvostrukom energijom. U današnjoj etapi

izučavanja eksitona uglavnom se radi na problemima nelinearne optike.

Pretpostavićemo da je molekulski kristal "isečen" iz anizotropne kubne strukture (ortorombičke strukture) [5–9] i da su mu konstante rešetke u pravcima x, y i z: a_x, a_y i a_z, respektivno. Takođe ćemo pretpostaviti da padajući na molekul, svetlosni kvanti prevode elektron iz osnovnog stanja u samo jedno pobuđeno stanje (dvonivoska šema molekulskih pobuđenja [10–16]). Tada su eksitonski operatori-Pauli-operatori.

Tenzor difuzije je dat izrazom:

$$D_{\vec{m},\vec{n}} = \int_0^\infty \mathrm{d}t e^{-\varepsilon t} < v_{\vec{m}}(0) v_{\vec{n}}(t) > ; \quad \delta \to 0 + \tag{1}$$

gde je $< v_{\vec{m}}(0) v_{\vec{n}}(t) >$ korelaciona funkcija eksitonskih brzina.

II. KORELACIONA FUNKCIJA BRZINA EKSITONA U MOLEKULSKOM FILMU

Brzina eksitona definiše se kao izvod po vremenu vektora rešetke koji je dat u operatorskoj formi [10–13]. Vektor rešetke je jednočestični operator, pa se preko elektronskih operatora a_s^+ i $a_{s'}$ daje u obliku kvadratne forme:

$$\hat{\vec{n}} = \sum_{s,s'} \vec{M}_{ss'} a_{\vec{n}s}^+ a_{\vec{n}s'} , \tag{2}$$

gde su: $\vec{M}_{ss'} = \int d^3\xi_{\vec{n}} \psi_s^+ (\xi_{\vec{n}}) \hat{\vec{n}} \psi_{s'}(\xi_{\vec{n}})$ matrični elementi operatora $\hat{\vec{n}}$, dok su $\xi_{\vec{n}}$ unutrašnje koordinate molekula.

Pošto je pretpostavljeno da je šema molekulskih pobuđenja dvonivoska, indeksi s i s' uzimaju vrednosti 0 i f. Dijagonalni matrični elementi $\vec{M}_{0,0}$ i $\vec{M}_{f,f}$ jednaki su nuli, pa zbog toga formulu (2) možemo napisati na sledeći način:

$$\hat{\vec{n}} = \vec{M}_{0,f} a_{\vec{n}0}^+ a_{\vec{n}f} + \vec{M}_{f,0} a_{\vec{n}f}^+ a_{\vec{n}0} = \vec{M}_{0,f} P_{\vec{n}} + \vec{M}_{f,0} P_{\vec{n}}^+ ;$$
$$\vec{M}_{f,0} = \vec{M}_{0,f}^* . \tag{3}$$

Naglašavamo da je poslednji stav u ovoj formuli dobijen na osnovu definicije da je $P_{\vec{n}}^+ = a_{\vec{n}f}^+ a_{\vec{n}0}$, tj. $P_{\vec{n}} = a_{\vec{n}0}^+ a_{\vec{n}f}$.

Na osnovu definicije operatora brzine, može se pisati:

$$\vec{v}_{\vec{n}} = \dot{\hat{\vec{n}}} = \frac{1}{i\hbar}[\vec{n}, H], \tag{4}$$

a kombinujući sa (3), dobijamo:

$$\vec{v}_{\vec{n}}(t) = \frac{1}{i\hbar}\left\{ \vec{M}_{0,f}\left[P_{\vec{n}}(t), H\right] + \vec{M}_{0,f}^*\left[P_{\vec{n}}^+(t), H\right]\right\} .$$

U trenutku $t = 0$ i $\vec{n} \to \vec{m}$, ovaj izraz postaje:

$$\vec{v}_{\vec{m}}(0) = \frac{1}{i\hbar}\left\{ \vec{M}_{0,f}\left[P_{\vec{m}}(0), H\right] + \vec{M}_{0,f}^*\left[P_{\vec{m}}^+(0), H\right]\right\} .$$

Kombinacijom dve poslednje formule dobija se izraz za korelacionu funkciju eksitonskih brzina:

$$< v_{\vec{m}}(0) v_{\vec{n}}(t) > = \frac{1}{\hbar^2}\left\{ M_{0f}^2 < \left[P_{\vec{m}}(0), H\right] \cdot \left[P_{\vec{n}}(t), H\right]_t > + \right.$$
$$+ \left(M_{f0}^*\right)^2 < \left[P_{\vec{m}}^+(0), H\right] \cdot \left[P_{\vec{n}}^+(t), H\right] > + \tag{5}$$
$$\left. + \left|M_{0f}\right|^2 < \left[P_{\vec{m}}^+(0), H\right] \cdot \left[P_{\vec{n}}(t), H\right] >\right\} .$$

Korelacione funkcije koje figurišu u ovom izrazu mogu se odrediti preko paulionskih Grinovih funkcija [15,16] i to:

– napredne (retardovane): $\Gamma_R = << P_{\vec{n}}(t) | P_{\vec{m}}^+(0) >>$ (6)

– nazadne (avansovane): $\Gamma_A = << P_{\vec{n}}^+(t) | P_{\vec{m}}(0) >>$ (7)

Pošto operatori P^+ i P kreiraju i anihiliraju eksitone, funkcije Γ biće dalje nazivane eksitonske Grinove funkcije.

III. EKSITONSKE GRINOVE FUNKCIJE U TANKOM MOLEKULSKOM FILMU

Za dvonivosku šemu molekulskih pobuđenja, hamiltonijan Frenkelovih eksitona ima oblik:

$$H = \sum_{\vec{n},\vec{m}} A_{\vec{n},\vec{m}} P_{\vec{n}}^+ P_{\vec{n}} + \sum_{\vec{n},\vec{m}} B_{\vec{n},\vec{m}} P_{\vec{n}}^+ P_{\vec{m}} + \sum_{\vec{n},\vec{m}} C_{\vec{n},\vec{m}} P_{\vec{n}}^+ P_{\vec{n}} P_{\vec{m}}^+ P_{\vec{m}}, \tag{8}$$

sa: $A_{\vec{n},\vec{m}} = \Delta\delta_{\vec{n},\vec{m}} + D_{\vec{n},\vec{m}}$; $D_{\vec{n},\vec{m}} = D_{\vec{m},\vec{n}}$; $B_{\vec{n},\vec{m}} = B_{\vec{m},\vec{n}}$; $C_{\vec{n},\vec{m}} = C_{\vec{m},\vec{n}}$.

Prvo ćemo potražiti nazadnu Grinovu funkciju:

$$\Gamma_{\vec{n},\vec{m}} = << P_{\vec{n}}(0) | P_{\vec{m}}^+(0) >> = \theta(t) < [P_{\vec{n}}(t), P_{\vec{m}}^+(0)] >, \tag{9}$$

gde je $\theta(t) = \begin{cases} 1, & t > 0 ; \\ 0, & t < 0 , \end{cases}$ – Hevisajdova step-funkcija.

Diferencirajući izraz (9) po vremenu, dobijamo:

$$\frac{\mathrm{d}}{\mathrm{d}t}\Gamma_{\vec{n},\vec{m}} = \delta_{\vec{n},\vec{m}}\delta(t)\left(1 - 2 < P^+ P >\right) +$$
$$+ \theta(t) < \left[\frac{\mathrm{d}P_{\vec{n}}(t)}{\mathrm{d}t}, P_{\vec{m}}^+(0)\right] > \tag{10}$$

Jednačine kretanja za operatore P su: $\frac{\mathrm{d}P_{\vec{n}}(t)}{\mathrm{d}t} = \frac{1}{i\hbar}[P_{\vec{n}}(t), H]$, pa se posle zamene ovoga u (10) dobija:

$$i\hbar\frac{\mathrm{d}}{\mathrm{d}t}\Gamma_{\vec{n},\vec{m}} = i\hbar\delta_{\vec{n},\vec{m}}\delta(t)\left(1 - 2P^+ P\right) + << [P_{\vec{n}}, H]_t | P_{\vec{m}}^+(0) >> \tag{11}$$

Pošto je, na osnovu (1) i (2):

$$[P_{\vec{n}}, H] = \Delta P_{\vec{n}} + D(0)P_{\vec{n}} + \sum_{\vec{g}} B_{\vec{n},\vec{g}} P_{\vec{g}} -$$
$$- 2\sum_{\vec{g}} B_{\vec{n},\vec{g}} P_{\vec{n}}^+ P_{\vec{n}} P_{\vec{g}} + 2\sum_{\vec{g}} C_{\vec{n},\vec{g}} P_{\vec{g}}^+ P_{\vec{g}} P_{\vec{n}} \tag{12}$$

jednačina (11) postaje:

$$i\hbar\frac{\mathrm{d}}{\mathrm{d}t}\Gamma_{\vec{n},\vec{m}} = i\hbar\delta_{\vec{n},\vec{m}}\delta(t)\left(1 - 2P^+ P\right) + \Delta\Gamma_{\vec{n},\vec{m}}(t) + D(0)\Gamma_{\vec{n},\vec{m}}(t) +$$
$$+ \sum_{\vec{g}} B_{\vec{n},\vec{g}} << P_{\vec{g}} | P_{\vec{m}}^+(0) >> - 2\sum_{\vec{g}} B_{\vec{n},\vec{g}} << P_{\vec{n}}^+ P_{\vec{n}} P_{\vec{g}} | P_{\vec{m}}^+(0) >> +$$
$$+ \sum_{\vec{g}} C_{\vec{n},\vec{g}} << P_{\vec{g}}^+ P_{\vec{g}} P_{\vec{n}} | P_{\vec{m}}^+(0) >> . \tag{13}$$

Analizom ovog izraza vidi se da, pored jednočestičnih paulionskih Grinovih funkcija, ovde figurišu i dvočestične paulionske Grinove funkcije. Dvočestične Grinove funkcije izrazićemo preko jednočestičnih koristeći aproksimaciju Tjablikova (vidi [14–16]):

$$<< P_{\vec{n}}^+(t) P_{\vec{n}}(t) P_{\vec{m}}(0) | P_{\vec{l}}^+(0) >> \approx$$
$$\approx < P_{\vec{n}}^+(t) P_{\vec{n}}(t) >< < P_{\vec{m}}(t) | P_{\vec{l}}^+(0) >> \tag{14}$$

Navedena aproksimacija praktično znači da se proces rasejanja eksitona na realom potencijalu zamenjuje procesom pre-

nosa na "umekšanom" potencijalu, koji predstavlja proizvod realnog potencijala i srednjeg broja eksitona. Koristeći ovu aproksimaciju, jednačinu (13) svodimo na:

$$i\hbar\frac{\mathrm{d}}{\mathrm{d}t}\Gamma_{\vec{n},\vec{m}} = i\hbar\delta_{\vec{n},\vec{m}}\delta(t) + \sigma[\Delta + D(0) + 2 < P^+P > C(0)]\Gamma_{\vec{n},\vec{m}}(t) +$$

$$+\sigma\sum_{\vec{g}}B_{\vec{n},\vec{g}}\Gamma_{\vec{g}\vec{m}}(t). \tag{15}$$

Pošto analiziramo film "isečen" iz ortorombičke strukture, veličine navedene u (15) moramo predstaviti u obliku:

$$C(0) = 2C_x + 2C_y + 2C_z, \; D(0) = 2D_x + 2D_y + 2D_z.$$

U toj jednačini figuriše i veličina σ, koja zapravo predstavlja parametar uređenosti eksitonskog sistema i koja je data (vidi [14–16]) sa: $1 - 2 < P_{\vec{n}}^+ P_{\vec{n}} >= \sigma$. U eksitonskom sistemu parametar uređenosti je blizak jedinici, pošto su najveće do sada postignute koncentracije eksitona $< P^+P >$ reda 10^{-3}.

Poslednji član na desnoj strani jednačine (15) uzećemo u aproksimaciji najbližih suseda (ostali članovi u ovoj jednačini već su uzeti u ovoj aproksimaciji. Posle ovoga ona postaje:

$$i\hbar\frac{\mathrm{d}}{\mathrm{d}t}\Gamma_{n_x,n_y,n_z;m_x,m_y,m_z}(t) = i\hbar\delta_{\vec{n},\vec{m}}\delta(t)\sigma +$$

$$\left[\Delta + 2(D_x + D_y + D_z) + 4 < P^+P > (C_x + C_y + C_z)\right]\Gamma_{n_x,n_y,n_z;m_x,m_y,m_z}(t) +$$

$$+\sigma\left\{\Delta B_x\left[\Gamma_{n_x+1,n_y,n_z;m_x,m_y,m_z}(t) + \Gamma_{n_x-1,n_y,n_z;m_x,m_y,m_z}(t)\right] + \tag{17}\right.$$

$$+B_y\left[\Gamma_{n_x,n_y+1,n_z;m_x,m_y,m_z}(t) + \Gamma_{n_x,n_y-1,n_z;m_x,m_y,m_z}(t)\right] +$$

$$+B_z\left[\Gamma_{n_x,n_y,n_z+1;m_x,m_y,m_z}(t) + \Gamma_{n_x,n_y,n_z-1;m_x,m_y,m_z}(t)\right]\right\},$$

gde su B interakcije koje odgovaraju prenosu eksitona sa čvora na čvor uzete u aproksimaciji najbližih suseda.

U jednačini (17) izvršićemo Furije transformacije tipa vreme-frekvencija:

$$f(t) = \int_{-\infty}^{+\infty}\mathrm{d}\omega e^{-i\omega t}f(\omega); \quad \delta(t) = \frac{1}{2\pi}\int_{-\infty}^{+\infty}\mathrm{d}\omega e^{-i\omega t},$$

a takođe i transformacije tipa prostor-talasni vektor:

$$\Gamma_{n_x,n_y,n_z;m_x,m_y,m_z}(\omega) = \frac{1}{N_xN_y}\sum_{k_x,k_y}\gamma_{n_z,m_z}(k_x,k_y,\omega)e^{ik_xa_x(n_x-m_x)+ik_ya_y(n_u-m_u)}$$

$$\delta_{n_x,m_x} = \frac{1}{N_x}\sum_{k_x}e^{ik_xa_x(n_x-m_x)}; \quad \delta_{n_y,m_y} = \frac{1}{N_y}\sum_{k_y}e^{ik_ya_y(n_y-m_y)},$$

u kojima je iskorišćena činjenica da je film translatorno invarijantan u *XY* ravnima. Na taj način jednačina (17) se svodi na:

$$b\gamma_{n_z+1,m_z} + b\gamma_{n_z-1,m_z} + \rho\gamma_{n_z,m_z} = f_{n_z,m_z}; f_{n_z,m_z} \equiv -\frac{i\hbar}{2\pi}\sigma\delta_{n_z,m_z} \tag{18}$$

gde su: $\sigma B_z = b$;

$$\rho \equiv \rho(k_x,k_y) = \Delta + 2(D_x + D_y + D_z) + 4 < P^+P > (C_x + C_y + C_z) +$$

$$+2\sigma(B_x\cos a_x k_y + B_y\cos a_y k_y) - E.$$

Dobijena jednačina (18) važi za idealnu balk-strukturu, jer u njoj nisu iskorišćeni granični uslovi duž *z* pravca. Uzećemo da se ovi granični uslovi sastoje u odsustvu slojeva $n_z = -1$ i $n_z = N_z + 1$. S obzirom na ovo, granični uslovi se mogu formulisati na sledeći način:

$$B_{n_x,n_y,0;n_x,n_y,-1} = B_{n_x,n_y,N_z;n_x,n_y,N_z+1} = 0 ;$$

$$C(0) = 2C_x + 2C_y + C_z ; \; D(0) = 2D_x + 2D_y + D_z.$$

Primenom navedenih graničnih uslova jednačina (18) se razbija na sistem od $(N_z + 1)$ diferencnih jednačina:

$$\underline{1 \le n_z \le N_z}: \quad b\gamma_{n_z+1,m_z} + b\gamma_{n_z-1,m_z} + \rho\gamma_{n_z,m_z} = f_{n_z,m_z} \tag{19a}$$

$$\underline{n_z = 0}: \quad b\gamma_{1,m_z} + (\rho - a_0)\gamma_{0,m_z} = f_{0,m_z} \tag{19b}$$

$$\underline{n_z = N_z}: \quad b\gamma_{N_z-1,m_z} + (\rho - a_0)\gamma_{N_z,m_z} = f_{N_z,m_z} \tag{19c}$$

U ovim formulama veličina a_0 je data sa:

$$a_0 = D_z + 2 < P^+P > C_z.$$

Treba naglasiti da parametar uređenosti takođe može da zavisi od n_z, jer zavisi od srednje vrednosti $< P^+P >$. Ova zavisnost je zanemarena zbog malih vrednosti koje u eksitonskom sistemu imaju veličine $< P^+P >$.

Rešenje sistema (19a–c) potražićemo u obliku [17–20]:

$$\gamma_{n_z,m_z} = \sum_{\mu=1}^{N_z'}\left[\alpha_{\mu,m_z}\sin(n_z+1)\phi_\mu + \beta_{\mu,m_z}\sin n_z\phi_\mu\right], \tag{20}$$

u kojoj će veličina gornje granice sume N_z' biti određena kasnije. Zamenom (20) u (19a) dobijamo:

$$\sum_{\mu=1}^{N_z'}(2b\cos\phi_\mu + \rho)\left[\alpha_{\mu,m_z}\sin(n_z+1)\phi_\mu + \beta_{\mu,m_z}\sin n_z\phi_\mu\right] = f_{n_z,m_z}, \tag{21}$$

a zamena u (19b) daje:

$$\sum_{\mu=1}^{N_z'}\left(2b\cos 2\phi_\mu + \rho + b\frac{\beta_{\mu,m_z}}{\alpha_{\mu,m_z}} - a_0\right)\alpha_{\mu,m_z}\sin\phi_\mu = f_{0,m_z}. \tag{22}$$

Odavde je lako zaključiti da (22) postaje analogno jednačini (21) ako je:

$$b\frac{\beta_{\mu,m_z}}{\alpha_{\mu,m_z}} - a_0 = 0 \Rightarrow \beta_{\mu,m_z} = \frac{a_0}{b}\alpha_{\mu,m_z}. \tag{23}$$

S obzirom na ovo, izraz (20) prelazi u:

$$\gamma_{n_z,m_z} = \sum_{\mu=1}^{N_z'}\alpha_{\mu,m_z}\left[\sin(n_z+1)\phi_\mu + \frac{a_0}{b}\sin n_z\phi_\mu\right], \tag{24}$$

a ako se ovaj izraz zameni u (19c) dobija se:

$$\sum_{\mu=1}^{N_z'}\left[\frac{b\sin N_z\phi_\mu + a_0\sin(N_z-1)\phi_\mu}{\sin(N_z-1)\phi_\mu + \frac{a_0}{b}\sin N_z\phi_\mu} + \rho - a_0\right]\alpha_{\mu,m_z}.$$

$$\cdot\left[\sin(N_z-1)\phi_\mu + \frac{a_0}{b}\sin N_z\phi_\mu\right] = f_{N_z,m_z}, \tag{25}$$

odakle je očigledno da ona postaje analogna relacijama (21) i (22), ako je ispunjen uslov

$$\frac{b\sin N_z\phi_\mu + a_0\sin(N_z-1)\phi_\mu}{\sin(N_z-1)\phi_\mu + \frac{a_0}{b}\sin N_z\phi_\mu} + \rho - a_0 = 2b\cos\phi_\mu,$$

koji se svodi na:

$$b^2\sin(N_z+2)\phi_\mu + a_0^2\sin N_z\phi_\mu + 2a_0b\sin(N_z+1)\phi_\mu = 0. \tag{26}$$

U opštem slučaju ova jednačina ima N'_z realnih rešenja. Može se pokazati da je $N'_z = N_z - 1$, ako je $\left|\dfrac{b}{a_0}\right| < 1$. Ukoliko je $\left|\dfrac{b}{a_0}\right| = 1$, broj N'_z jednak je N_z. Ukoliko je $\left|\dfrac{b}{a_0}\right| > 1$, dobija se da je $N'_z = N_z + 1$.

Rezime ove etape analize može se formulisati na sledeći način. Smena (21) svodi sve jednačine sistema (19a–c) na jednu jedinstvenu jednačinu:

$$\sum_{\mu=1}^{N'_z} \left(2b\cos\phi_\mu + \rho\right) \alpha_{\mu,m_z} \left(\sin\left(n_z+1\right)\phi_\mu + \frac{a}{b}\sin n_z \phi_\mu\right) = \tag{27}$$
$$= -\frac{i\hbar}{2\pi}\sigma\delta_{n_z,m_z}$$

koja važi za sve indekse $n_z = 0, 1, 2, ..., N_z$ ukoliko je ispunjen uslov (26). Pošto je kod eksitonskog sistema $\left|\dfrac{b}{a_0}\right| < 1$, gornja granica sume je $N'_z = N_z - 1$.

Dalje ćemo uzeti da je α_{μ,m_z} u (26), koje zavisi od k_x, k_y i ω dato sa:

$$\alpha_{\mu,m_z}\left(k_x,k_y,\omega\right) = G_\mu\left(k_x,k_y,\omega\right) \sum_{\nu=1}^{N'_z-1} L_{\mu\nu}\sin\left(m_z+\nu\right)\phi_\mu \tag{28}$$

a Kronekerov simbol u obliku:

$$\delta_{n_z,m_z} = \sum_{\mu=1}^{N'_z-1}\left(\sin\left(n_z+1\right)\phi_\mu + \frac{a_0}{b}\sin n_z\phi_\mu\right) \cdot \sum_{\mu=1}^{N'_z-1}L_{\mu\nu}\sin\left(m_z+\nu\right)\phi_\mu \tag{29}$$

Koeficijente $L_{\mu\nu}$ u ovim izrazima odredićemo kasnije.

Kombinujući (28), (29) i (26) dobijamo:

$$G_\mu\left(k_x,k_y,\omega\right) = -\frac{i\hbar}{2\pi}\sigma\frac{1}{2b\cos\phi_\mu + \rho}. \tag{30}$$

Izraz za funkciju G može se napisati u obliku [14,20]:

$$G_\mu\left(k_x,k_y,\omega\right) = -\frac{i\hbar}{2\pi}\sigma\frac{1}{E - E_k}, \tag{31}$$

gde je energija eksitona:

$$E_k = \Delta + 2\left(D_x + D_y + D_z\right) + 4 < P^+ P >\left(C_x + C_y + C_z\right) +$$
$$+ 2\sigma\left(B_x \cos a_x k_x + B_y \cos a_y k_y + B_z \cos\phi_\mu\right); \tag{32}$$

gde je $< P^+ P > = \dfrac{1-\sigma}{2}$.

Spektralnu intezivnost funkcije G nalazimo na osnovu opšte formule [1,2,15]:

$$I_G\left(\omega\right) = \frac{G_\mu\left(\omega + i\delta\right) - G_\mu\left(\omega - i\delta\right)}{e^{\frac{\hbar\omega}{\Theta}} - 1}; \quad \delta \to +0 ; \quad \omega_k = \frac{E_k}{\hbar},$$

gde je $\Theta = k_B T$ i dobijamo u obliku:

$$I_G\left(\omega\right) = \sigma\frac{\delta\left(\omega - \omega_{k_x,k_y,\mu}\right)}{e^{\frac{\hbar\omega_{k_x,k_y,\mu}}{\Theta}} - 1}. \tag{33}$$

Korelaciona funkcija u impulsnom prostoru, na osnovu definicionog izraza [1,2,15]:

$$< P^+_{k_x,k_y,\mu}\left(0\right) P_{k_x,k_y,\mu}\left(t\right) > = \int_{-\infty}^{+\infty} d\omega\, e^{-i\omega_{k_x,k_y,\mu} t} I_G\left(\omega\right),$$

postaje:

$$< P^+_{k_x,k_y,\mu}\left(0\right) P_{k_x,k_y,\mu}\left(t\right) > = \sigma\frac{e^{-it\omega_{k_x,k_y,\mu}}}{e^{\frac{\hbar\omega_{k_x,k_y,\mu}}{\Theta}} - 1}. \tag{34}$$

Izraz za korelacionu funkciju u konfiguracionom prostoru dobija se operatorskom primenom Kronekerovog simbola na korelacionu funkciju (34). Pod operatorskom primenom Kronekerovog simbola se podrazumeva sledeće: ako je Kronekerov simbol dat sa: $\delta_{n,m} = \dfrac{1}{N}\sum_{k=1}^{N} e^{ik(n-m)}$, onda njegova operatorska primena na funkciju $F\left(k\right)$ znači primenu operatora $\dfrac{1}{N}\sum_{k=1}^{N}$ na proizvod $e^{ik(n-m)} \cdot F\left(k\right)$. Za neku drugu reprezentaciju Kronekerovog simbola funkcija $F\left(k\right)$ se množi faktorom $f_{n,m}\left(k\right)$, koji definiše Kronekerov simbol, i na proizvod se primenjuje operator $\dfrac{1}{N'}\sum_{k=1}^{N}$. Tako dobijamo:

$$< P^+_m\left(0\right) P_n\left(t\right) > = \frac{\sigma}{N_z N_y} \sum_{k_z,k_y,\mu} \frac{e^{-it\omega_{k_x,k_y,\mu}}}{e^{\frac{\hbar\omega_{k_x,k_y,\mu}}{\Theta}} - 1} e^{i\left(n_x-m_x\right)a_x k_x + i\left(n_y-m_y\right)a_y k_y}.$$
$$\cdot\left[\sin\left(n_z+1\right)\phi_\mu + \frac{a}{b}\sin n_z\phi_\mu\right] \sum_{\nu=1}^{N'_z-1} L_{\mu\nu}\sin\left(m_z+\nu\right)\phi_\mu. \tag{35}$$

Pošto je Kronekerov simbol δ_{n_z,m_z} definisan relacijom (29), očigledno je da su koeficijenti $L_{\mu\nu}$ određeni sistemom algebarskih jednačina, tako da zadovolje definiciju:

$$\delta_{n_z,n_z} = \begin{cases} 1, n_z = m_z \\ 0, n_z \neq m_z \end{cases}$$

Formula (35) biće iskorišćena za nalaženje korelacione funkcije tipa brzina-brzina.

IV. Tenzor difuzije u tankom molekulskom filmu

Tenzor difuzije se izražava preko korelacione funkcije $< v_{\vec{m}}\left(0\right) v_{\vec{n}}\left(t\right) >$, koja je data formulom (5). Dva prva člana u tom izrazu jednaki su nuli, pošto su izraženi preko srednjih vrednosti koje ne sadrže jednak broj kreacionih i anihilacionih operatora. Srednja vrednost u četvrtom članu formule (5) može se odrediti preko nazadne Grinove funkcije (6). Srednje vrednosti u trećem članu (5) određuju se preko napredne Grinove funkcije (7).

Iz opšte teorije Grinovih funkcija poznato je da za Furijelikove funkcija Γ_R i Γ_A, koji su označeni sa G važi:

$$G_A\left(\omega\right) = G_R\left(-\omega\right).$$

Pošto je, na osnovu formule (31):

$$G_R\left(\omega\right) = \frac{i\sigma}{2\pi}\frac{1}{\omega - \omega_{k_x,k_y,\mu}}, \tag{36}$$

gde je $\omega_{k_x,k_y,\mu} \equiv \dfrac{E_k}{\hbar}$ – definisano izrazom (32), dobija se:

$$G_A(\omega) = -\frac{i\sigma}{2\pi}\frac{1}{\omega + \omega_{k_x,k_y,\mu}} \, . \qquad (37)$$

Spektralna intenzivnost napredne Grinove funkcije je onda:

$$I_G(\omega) = \frac{G(\omega+i\delta)-G(\omega-i\delta)}{e^{\frac{\hbar\omega}{\Theta}}-1} =$$

$$-\frac{i\sigma}{2\pi}\left(\frac{1}{\omega+\omega_0+i\delta}-\frac{1}{\omega+\omega_0-i\delta}\right).$$

$$\cdot\frac{1}{e^{\frac{\hbar\omega}{\Theta}}-1} = -\frac{\sigma}{e^{-\frac{\hbar\omega_{k_x,k_y,\mu}}{\Theta}}-1}\delta(\omega+\omega_{k_x,k_y,\mu}) \qquad (38)$$

dok je korelaciona funkcija u konfiguracionom prostoru:

$$<P_{\bar{m}}(0)P_{\bar{n}}^{+}(t)> = -\frac{\sigma}{N_x N_y}\sum_{k_z,k_y,\mu}\frac{e^{it\omega_{k_x,k_y,\mu}}}{e^{\frac{\hbar\omega_{k_x,k_y,\mu}}{\Theta}}-1}e^{-i(n_x-m_x)a_x k_x - i(n_y-m_y)a_y k_y}.$$

$$\cdot\left[\sin(n_z+1)\phi_\mu + \frac{a}{b}\sin n_z\phi_\mu\right]\cdot\sum_{\nu=1}^{M'}L_{\mu\nu}\sin(m_z+\nu)\phi_\mu . \qquad (39)$$

Korelaciona funkcija iz izraza (5), sadrži dvočestične korelacione funkcije, koje predstavljaju srednje vrednosti četiri operatora. Koristeći Tjablikovu aproksimaciju [1,2,6,7], mi ćemo izraziti ove korelacione funkcije preko jednočestičnih korelacionih funkcija, koje se određuju preko nazadne Grinove funkcije. Pri tome će svi članovi koji sadrže kvadrate eksitonskih koncentracija biti zanemareni.

U isto vreme za dvočestične korelacione funkcije, koje se pojavljuju u trećem članu formule (5), koristi se Tjablikova aproksimacija i one se izražavaju preko jednočestičnih naprednih korelacionih funkcija, koje su date izrazom (39).

Koristeći formule (35) i (39) i aproksimaciju, kojom se u izrazu za $<v_{\bar{m}}(0)v_{\bar{n}}(t)>$ zadržavaju samo članovi proporcionalni Δ^2, $D\cdot\Delta$ i $B\cdot\Delta$, za korelacionu funkciju $<v_{\bar{m}}(0)v_{\bar{n}}(t)>$ dobijamo sledeći izraz:

$$<v_{\bar{m}}(0)v_{\bar{n}}(t)> = \frac{(M_{f0})^2}{(i\hbar)^2}\frac{\sigma}{N_z N_y}\sum_{k_z,k_y,\mu}e^{i(n_x-m_x)a_x k_x + i(n_y-m_y)a_y k_y}.$$

$$\cdot\left[\sin(n_z+1)\phi_\mu + \frac{a_0}{b}\sin n_z\phi_\mu\right].$$

$$\cdot\sum_{\nu=1}^{N_z'}L_{\mu\nu}\sin(m_z+\nu)\phi_\mu\left(\frac{e^{-it\omega_{k_x,k_y,\mu}}}{e^{\frac{\hbar\omega_{k_x,k_y,\mu}}{\Theta}}-1} - \frac{e^{it\omega_{k_x,k_y,\mu}}}{e^{-\frac{\hbar\omega_{k_x,k_y,\mu}}{\Theta}}-1}\right)\cdot \quad (40)$$

$$\cdot\left\{\left[-\Delta^2 - 2\Delta D(0) - (D(0))^2\right] - \right.$$

$$\left. -2\left[\Delta - D(0)\right]\sigma\left[B_x\cos a_x k_x + B_y\cos a_y k_y + B_z\cos\phi_\mu\right]\right\}.$$

Na osnovu definicione formule:

$$\vec{D}_{\bar{n}\bar{m}} = \int_0^\infty dt\, e^{-\varepsilon t}<v_{\bar{m}}(0)v_{\bar{n}}(t)> ;\ \varepsilon \to 0$$

sledi da tenzor difuzije ima oblik:

$$\vec{D}_{\bar{n}\bar{m}} = \frac{2(M_{f0})^2}{\hbar\Delta}\frac{\sigma}{N_z N_y}\sum_{k_z,k_y,\mu}\frac{1}{\omega_{k_x,k_y,\mu}}e^{i(n_x-m_x)a_x k_x + i(n_y-m_y)a_y k_y}.$$

$$\cdot\left[\sin(n_z+1)\phi_\mu + \frac{a_0}{b}\sin n_z\phi_\mu\right].$$

$$\cdot\sum_{\nu=1}^{N_z'}L_{\mu\nu}\sin(m_z+\nu)\phi_\mu\left(\frac{1}{e^{\frac{\hbar\omega_{k_x,k_y,\mu}}{\Theta}}-1} - \frac{1}{e^{-\frac{\hbar\omega_{k_x,k_y,\mu}}{\Theta}}-1}\right)\cdot \quad (41)$$

$$\left\{\left[-\Delta^2 - 2\Delta D(0) - (D(0))^2\right] - \right.$$

$$\left. -2\left[\Delta - D(0)\right]\sigma\left[B_x\cos a_x k_x + B_y\cos a_y k_y + B_z\cos\phi_\mu\right]\right\}.$$

Dobijeni izraz je komplikovan, a radi dobijanja jasnije predstave o uticaju narušene simetrije na difuziju, izvršićemo dalja uprošćavanja. Zanemarićemo sve članove izuzev člana proporcionalnog Δ. Takođe ćemo bozonsku raspodelu zameniti bolcmanovskom, što se svodi na:

$$\frac{1}{e^{\frac{\hbar\omega_{k_x,k_y,\mu}}{\Theta}}-1} \approx e^{-\frac{\hbar\omega_{k_x,k_y,\mu}}{\Theta}}; \quad \frac{1}{e^{-\frac{\hbar\omega_{k_x,k_y,\mu}}{\Theta}}-1} \approx -1 .$$

Pored toga navešćemo samo dijagonalne elemente tenzora difuzije:

$$|D| = \frac{(M_{f0})^2}{\hbar}\sigma\Delta\left\{1 + e^{-\frac{\Delta}{\Theta}}\left(1 - \frac{6D + 12<P^+P>C}{\Theta}\right) + \right.$$

$$+ \frac{2\sigma B_0}{\Theta}e^{-\frac{\Delta}{\Theta}}\sum_{\mu=1}^{N_z'}\left[\sin(n_z+1)\phi_\mu + \frac{a_0}{b_0}\sin n_z\phi_\mu\right]\cdot \quad (42)$$

$$\left. \cdot\cos\phi_\mu\sum_{\mu=1}^{N_z'}L_{\mu\nu}\sin(n_z+\nu)\phi_\mu\right\}.$$

Pošto su svi dijagonalni elementi tenzora difuzije međusobno jednaki, dalje možemo govoriti o koeficijentu difuzije eksitona. U izrazu (42) je pretpostavljeno da eksitoni imaju pozitivnu disperziju, pa je zbog toga b iz formule (41) zamenjeno sa $-b_0$, gde je $b_0 > 0$, dok je B zamenjeno sa $-B_0$.

Kao ilustrativni primer ispitaćemo koeficijent difuzije u ultratankom molekulskom filmu koji sadrži četiri molekulska sloja. Ovi slojevi označeni su sa $n_z = 0,1,2$ i 3. Uzećemo da je $\dfrac{a_0}{b_0} = 8$. Za navedeni izbor parametara jednačina (26), u kojoj je b zamenjeno sa $-b_0$, ima dva realna rešenja:

$$\phi_1 = 1.12635\,\text{rad} ;\ \phi_2 = 2.15902\,\text{rad} . \qquad (43)$$

To znači da se u četvoroslojnom filmu pojavljuju samo dva eksitona. Ova dva eksitona, ako pretpostavimo da se oni nalaze u dva susedna sloja, mogu se nalaziti u slojevima $n_z = 0$ i $n_z = 1$, ili u slojevima $n_z = 1$ i $n_z = 2$ ili u slojevima $n_z = 2$ i $n_z = 3$. Subfilmovi 0–1 i 2–3 su potpuno ekvivalentni pa je dovoljno ispitati samo jedan od njih. Zbog toga ćemo ispitati samo subfilmove 0–1 i 1–2.

Za subfilm 0–1 vrednosti koeficijenata L su:

$$L_{11} = 2,01347;\ L_{21} = 2,02689;$$
$$L_{12} = 4,25651;\ L_{22} = 6,54585 . \qquad (44)$$

To znači da je korekcioni član u (42) – treći član na desnoj strani te jednačine:

$$\delta|D| = 4\frac{(M_{f0})^2}{\hbar}\Delta \cdot \frac{2\sigma^2 B_0}{\Theta}\,e^{-\frac{\Delta}{\Theta}} \qquad (45)$$

za $n_z = 0$. Za $n_z = 1$ ova korekcija je:

$$\delta|D| = -4\frac{(M_{f0})^2}{\hbar}\Delta \cdot \frac{2\sigma^2 B_0}{\Theta}\,e^{-\frac{\Delta}{\Theta}}. \qquad (46)$$

Zapaža se da u subfilmu 0–1 koeficijent difuzije zavisi od prostornog indeksa n_z, kojim se numerišu slojevi.

Za subfilm 1–2 koeficijenti L su dati sa:

$$\begin{aligned} L_{11} &= -0{,}07075; \quad L_{21} = 0{,}08599; \\ L_{12} &= 0{,}09624; \quad L_{22} = 0{,}06963. \end{aligned} \qquad (47)$$

Kada se ove vrednosti uvrste u izraz za koeficijent difuzije dobija se da su obe korekcije $\delta|D|$ i za $n_z = 1$ i za $n_z = 2$ jednake nuli. Ovaj rezultat je razumljiv pošto se slojevi 1 i 2 nalaze u istim poljima sila dipol-dipolne interakcije.

V. Zaključak

Rezimirajući izvršene analize možemo navesti sledeće dve činjenice.

1. U tankom molekulskom filmu broj eksitona je manji od broja molekula u filmu za $2 \cdot 10^{16}$.

2. U graničnim slojevima četvoroslojnog filma (0–1 i 2–3) eksitoni imaju različite koeficijente difuzije. U centralnom sloju četvoroslojnog filma (1–2) eksitoni u oba sloja imaju isti koeficijent difuzije. Ovaj rezultat je fizički prihvatljiv s obzirom na činjenicu da se slojevi $n_z = 0$ i $n_z = 3$ nalaze u asimetričnim poljima sila dipol-dipolne interakcije, dok je polje ovih sila simetrično za molekule koji se nalaze u unutrašnjosti filma.

Zahvalnica

Literatura

[1] Tošić B.S*., Statistička fizika*, Novi Sad – Vojvodina, Srbija: IF PMF, 1978.

[2] U.F. Kozmidis-Luburić, B.S. Tošić, *Optička pobuđenja u materijalnim sredinama*, monografija, Novi Sad – Vojvodina, Srbija: Univerzitet u Novom Sadu, 2000.

[3] M. Prutton, *Inroduction to Surface Physics*, Oxford, UK: Oxford Sci. Publ., 1995.

[4] S. Davison S., M. Steslicka, *Basic Theory of Surface States*, Oxford, UK: Clarendon Press, 1996.

[5] V.D. Sajfert, J.P. Šetrajčić, B.S. Tošić, R.P. Đajić," Excitonic Diffusion in Thin Molecular Films", *Czechoslovak J.Phys.* vol. 54, no. 9, pp. 975-988, 2004.

[6] N.I. Ostapenko, V.I. Sugakov, M.T. Shpak, *Spectroscopy of Defects in Organic Crystals*, Dordrecht, Nederlands: Kluwer Academic Publ., 1993.

[7] N.D. Zhevandrov, *Optics Anisotropy and Migration of Energy in Organic crystals*, Moscow, SSSR: Nauka, 1987.

[8] M. Knupfer, T. Schwieger, J. Fink, K. Leo, M. Hoffmann, "Excitons in quasi-one-dimensional organic crystals", *Phys. Rev.*B, vol. 66, no. 3, pp. 035208, 2002.

[9] I.Vragović, R. Scholz, M. Schreiber, "Model Calculation of the Optical Properties of 3,4,9,10-Perylene-Tetracarboxylic-Dianhydride (PTCDA) Thin Films", *Europhys.Lett.* vol. 57, No. 2, pp. 288-294, 2002.

[10] J.P. Šetrajčić, D.Lj. Mirjanić, V.D. Sajfert, B.S. Tošić, "Perturbation Method in the Analysis of Thin Deformed Films and the Possible Applications", *Physica* A, vol. 190, pp. 363-374, 1992.

[11] B.S. Tošić, V.D. Sajfert, J.P. Šetrajčić, D. Popov, D. Ćirić, *Primena diferencnog računa u analizi nanostruktura*, Novi Sad – Vojvodina, Srbija: Vojvođanska akademija nauka i umetnosti, 2005.

[12] B.S. Tošić, J.P. Šetrajčić i S.K. Jaćimovski, *Metodi teorijske fizike*, Zemun – Beograd, Srbija: Kriminalističko-policijska akademija, 2018.

[13] V.D. Sajfert and J.P. Šetrajčić, "Application of Green's Functions and Difference Equations in Theoretical Analyses of Nanostructures", in: *Monograph Series on the Foundations of Natural Science and Technology*, Vol. 15: *Topics in Nanoscience*, Part I: *Basic Views, Complex Nanosystems: Typical Results and Future*, Ed. Schomers W., Ch. 7, pp. 311-412, Singapore, Singapore: World Scientific, 2022.

[14] V.M Agranovich, R. Loudon, *Surface Excitations*, Amsterdam, Nederlands:North Holland,, 1985.

[15] S.V. Tyablikov, *Methods in the Quantum Theory in Magnetism*, New York, USA: Plenum Press, 1967.

[16] N.N. Bogolubov, *Collected Works*, Kiev, SSSR: Naukova Dumka, 1971..

[17] A.S. Davydov, *Theory of Molecular Excitons*, Moscow, SSSR: Nauka, 1978.

[18] R. Knox, *Theory of Excitons*, Moscow, SSSR: Mir, 1968.

[19] R.P. Agarwal, *Difference Equations and Inequalities: Theory, Methods and Applications*, New York, USA: Marcel Dekker, 2000.

[20] S. Goldberg, *Introduction to Difference Equations*, New York, USA: Dover, 1986..

Abstract

The diffusion of Frenkel excitons in a thin molecular film was analyzed. The diffusion coefficient is one of the kinetic characteristics of the material and therefore the analysis of exciton diffusion can be treated as a contribution to better knowledge of diffusion processes in molecular crystals. The diffusion tensor was calculated from the general theory of Green's functions, and the calculation was tested for the example of a molecular film with 4 parallel layers. It is shown that the diffusion coefficients are the same for the inner layers, which is a consequence of the symmetry of the force field due to the dipole-dipole interaction.

Diffusion of optical excitations in thin molecular films

Jovan P. Šetrajčić and Siniša M. Vučenović

Indukovanje stanja sličnih topološkim kod dvoslojnih fosforenskih traka primenom normalnog električnog polja

Vladimir V. Arsoski, Milan Ž. Tadić

Apstrakt—Metoda jake veze je korišćena za analizu elektronske strukture nanotraka od dvoslojnog crnog fosfora u prisustvu električnog polja. Kod traka sa foteljastim ivicama nisu prisutna ivična stanja, pa postoji veliki direktan procep u odsustvu spoljašnjeg polja. Primena električnog polja normalno na površinu trake dovodi do smanjenja procepa. Za određenu kritičnu vrednost amplitude električnog polja procep se skoro u potpunosti zatvara i u centru procepa dolazi do pojave oštrog antiukrštanja stanja najniže energije iz provodne zone i stanja najviše energije iz valentne zone. Ovo ponašanje je karakteristično za konvencionalne topološke izolatore kod kojih do inverzije zonske strukture dolazi usled jake spin-orbitne interakcije koja nije uključena u naš model. Ustanovljeno je da kod nanotraka male debljine postoji jako sprezanje stanja u provodnoj i valentnoj zoni usled anizotropije iako su elektroni i šupljine potisnuti na suprotne površine trake električnim poljem. Povećanje normalnog električnog polja iznad kritične vrednosti dovodi do inverzije i viših stanja iz provodne i valentne zone što je praćeno karakterističnim antiukrštanjima.

Ključne reči—Metoda jake veze; fosforen; topološki izolatori; normalno električno polje.

I. UVOD

Proizvodnja tankih slojeva poluprovodničkih materijala pokrenula je novu eru razvoja elektronskih komponenti koja je započela uspešnim izdvajanjem nekoliko monoslojeva tankog filma grafita iz masivnog kristala [1]. Velika popularnost monosloja grafita, koji je poznat pod imenom grafen [2], dovela je do porasta interesovanja za takozvane dvodimenzione (2D) materijale. Prva teorijska istraživanja su ukazala da smanjena dimenzionalnost u jednom pravcu dovodi do manifestacije specifičnih elektronskih osobina kod tankoslojnih materijala u odnosu na masivne materijale od kojih su dobijeni [3], što ih je učinilo atraktivnim za potencijalne primene u elektronici. Za razliku od tankih slojeva grafita kod kojih energetski procep praktično ne postoji, tanki slojevi crnog fosfora se odlikuju velikom vrednošću energetskog procepa koja je nekoliko puta veća od vrednosti u masivnom uzorku što ga, zajedno sa velikom pokretljivošću šupljina, čini odličnim kandidatom za izradu

Vladimir Arsoski – Elektrotehnički fakultet, Univerzitet u Beogradu, Bulevar kralja Aleksandra 73, 11020 Beograd, Srbija (e-mail: vladimir.arsoski@etf.bg.ac.rs), (https://orcid.org/0000-0002-9326-7809)

Milan Tadić – Elektrotehnički fakultet, Univerzitet u Beogradu, Bulevar kralja Aleksandra 73, 11020 Beograd, Srbija (e-mail: tadic@etf.bg.ac.rs), (https://orcid.org/0000-0002-9408-7957)

pMOS tranzistora [4,5]. Istraživanja predviđaju da izražena anizotropija strukture crnog fosfora može dovesti do intenzivne manifestacije interesantnih efekata kod tankih slojeva materijala, takozvanog fosforena, kao rezultat anizotropije optičkih, električnih, mehaničkih i termalnih svojstava [6]. U cilju zaštite od spoljašnjih uticaja slojevi fosforena se umeću između monoslojeva heksagonalnog bor-nitrida, što u određenoj meri modifikuje njegova elektronska, električna, transportna i optička svojstva [7].

U cilju primene u realnim napravama fosforen se obično izrađuje u formi nanotraka [4]. Kao i svi 2D materijali sa heksagonalnom rešetkom, trake fosforena se mogu fabrikovati tako da imaju karakteristične regularne cik-cak ili foteljaste ivice, koje se razlikuju po elektronskoj strukturi i transportnim svojstvima [8]. Kod traka sa cik-cak ivicama postoje ivična stanja čija je energija u blizini centra procepa i ponašaju se kao metalne, dok trake sa regularnim foteljastim ivicama nemaju stanja u procepu i ponašaju se kao izolatorske. Bez obzira na tip ivica traka, njihove elektronske i transportne osobine se mogu podešavati primenom električnog polja gde u okolini kritične vrednosti polja primenjenog normalno na ravan trake dolazi do karakterističnih prelaza izolator-metal [8].

Ab initio proračuni elektronske strukture višeslojnog fosforena predviđaju da primena naprezanja može dovesti do formiranja Dirakovih konusa [9], što je inherentna karakteristika elektronske strukture topoloških izolatora. U formi masivnog materijala topološki izolatori poseduju energetski procep, dok u materijalu konačnih dimenzija dolazi do pojave karakterističnih stanja lokalizovanih po ivicama ili površinama strukture koja u inverznom prostoru, u vidu Dirakovog konusa, zatvaraju procep i invarijantna su u odnosu na inverziju u vremenu [10]. U ovom radu biće prikazano da se slična svojstva elektronske strukture mogu indukovati u dvoslojnom fosforenu primenom normalnog električnog polja.

II. TEORIJSKI MODEL

Za analizu elektronske strukture nanotraka korišćen je metod jake veze, gde je hamiltonijan dat sa

$$H = \sum_{i \neq j} t_{i,j} c_i^\dagger c_j + \sum_i e\mathbf{K_i}\mathbf{r_i}. \tag{1}$$

Ovde je $t_{i,j}$ energija skoka između i-tog i j-tog atoma, $c_i^\dagger \left(c_j \right)$ je operator kreacije (anihilacije) elektrona u $i(j)$-tom atomskom stanju, $\mathbf{K_i}$ je vektor spoljašnjeg električnog polja na mestu i-tog atoma, $\mathbf{r_i}$ je vektor položaja i-tog atoma, a e je elementarno naelektrisanje. Referentna tačka za izračunavanje dodatnog potencijala u prisustvu električnog polja je postavljena u koordinatni početak i poklapa se sa centrom nanotrake. Korišćeno je 10 parametara za skokove u okviru jednog monosloja, dok su sa 5 parametara opisani skokovi između monoslojeva. Izabrani skup parametara daje verodostojne rezultate za razmatranu višeslojnu strukturu [11]. Rastojanja između atoma, koja figurišu kroz članove zavisne od položaja atoma, su preuzeta iz reference [8]. Širina trake je određena brojem dimera duž poprečnog preseka trake, dok jediničnu ćeliju sačinjava minimalan skup atoma čijim se periodičnim ponavljanjem reprodukuje nanotraka beskonačne dužine. Za implementaciju trake nominalno beskonačne dužine korišćeni su periodični granični uslovi. Dijagonalizacijom matrice hamiltonijana (1) dobija se skup svojstvenih vrednosti i svojstvenih vektora koji opisuje elektronsku strukturu razmatranog sistema.
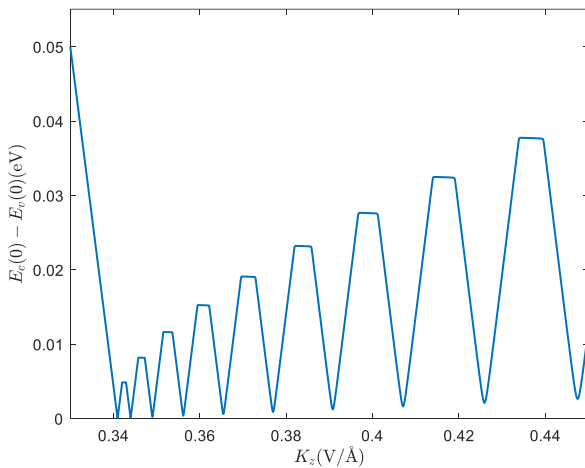

Sl. 1. Razlika svojstvenih vrednosti stanja najniže energije u provodnoj zoni i stanja najviše energije u valentnoj zoni u $\mathbf{k}$=0 u funkciji amplitude normalnog električnog polja K_z.

III. REZULTATI I DISKUSIJA

Analizirane su trake sa regularnim foteljastim ivicama debljine dva monosloja fosforena, pri čemu je broj dimera u jednom monosloju duž poprečnog preseka N_d =61 što približno odgovara širini trake od 10 nm. Referentna tačka za potencijal je tačka na sredini između slojeva na polovini širine trake. Osa x je usmerena duž trake, osa y je paralelna ravni monoslojeva duž poprečnog preseka trake, dok je z osa normalna na ravan strukture.

Najpre je analiziran uticaj električnog polja primenjenog normalno na površinu trake na razliku energija stanja na dnu provodne zone i stanja na vrhu valentne zone u tački $k = 0$. U

određenom opsegu amplituda električnog polja ova razlika odgovara širini energetskog procepa koji je direktan. Povećanje amplitude električnog polja dovodi do smanjenja procepa i za određene kritične vrednosti se pojavljuju minimumi, što je prikazano na Sl.1. Može se uočiti da lokalni minimumi procepa imaju veću vrednost što je amplituda kritičnog polja veća.
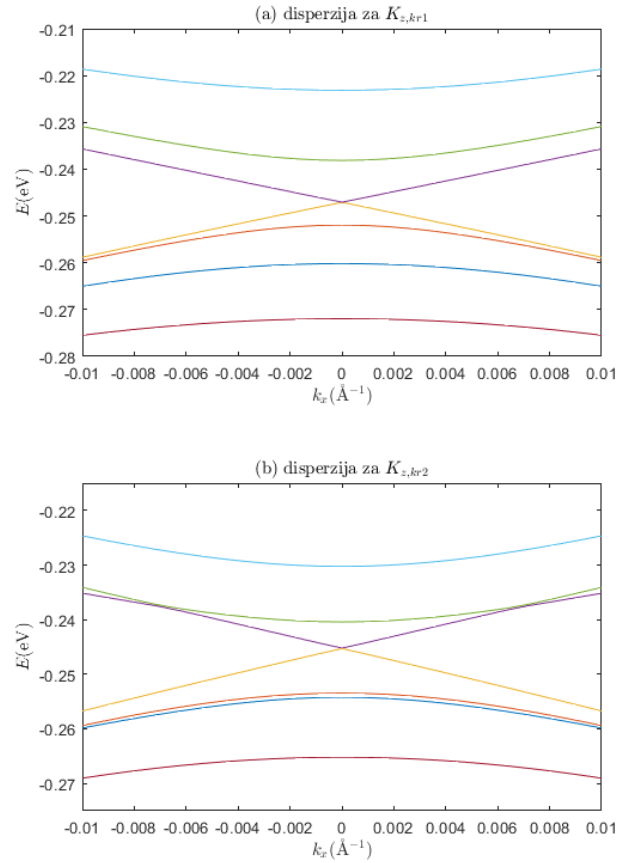
Sl. 2. Prikaz zavisnosti svojstvenih energija u okolini centra zone u funkciji talasnog vektora k_x, usmerenog duž trake, za kritičnu vrednost amplitude električnog polja za koju energetski procep ima minimalnu vrednost: (a) najniža kritična vrednost polja $K_{z,kr1}$ = 0.3409635 V/Å; (b) prvi sledeći (lokalni) minimum $K_{z,kr2}$ = 0.3439790398 V/Å.

Disperzije u okolini centra zone za najnižu kritičnu vrednost polja $K_{z,kr1}$ = 0.3409635 V/Å kada procep ima minimalnu širinu $E_{g1,min}$ = 22.96310 µeV i za prvu sledeću vrednost $K_{z,kr2}$ = 0.3439791 V/Å kada je vrednost procepa $E_{g2,min}$ = 92.49116 µeV su prikazane na Sl.2 (a) i (b), redom. U tački k =0 dolazi do antiukrštanja stanja energija najbližih energetskom procepu, takozvanih najnižih stanja u provodnoj i valentnoj zoni. Ukoliko se kao referentan raspored usvoji raspored stanja na disperziji kada polje nije primenjeno, pri prvoj kritičnoj vrednosti polja dolazi do antiukrštanja najnižih stanja u provodnoj i valentnoj zoni za $K_{z,kr1}$. Za vrednost polja $K_{z,kr2}$ dolazi do antiukrštanja drugog stanja iz provodne i drugog iz valentne zone pri čemu se tačka antiukrštanja prvog stanja iz provodne i valentne zone pomera iz centra zone

većim vrednostima $|k|$, što se lako može uočiti sa Sl.2 (b) (tačka antiukrštanja je za $|k| \cong 0.007 \overset{o}{A}^{-1}$). Ovaj trend se nastavlja sve do amplitude polja $K_{z,kr10} = 0.447989$ V/Å, koja odgovara desetom (krajnjem desnom) lokalnom minimumu na Sl.1, kada procep postaje indirektan. Tada materijal prelazi iz izolatorskog u polumetalno stanje.
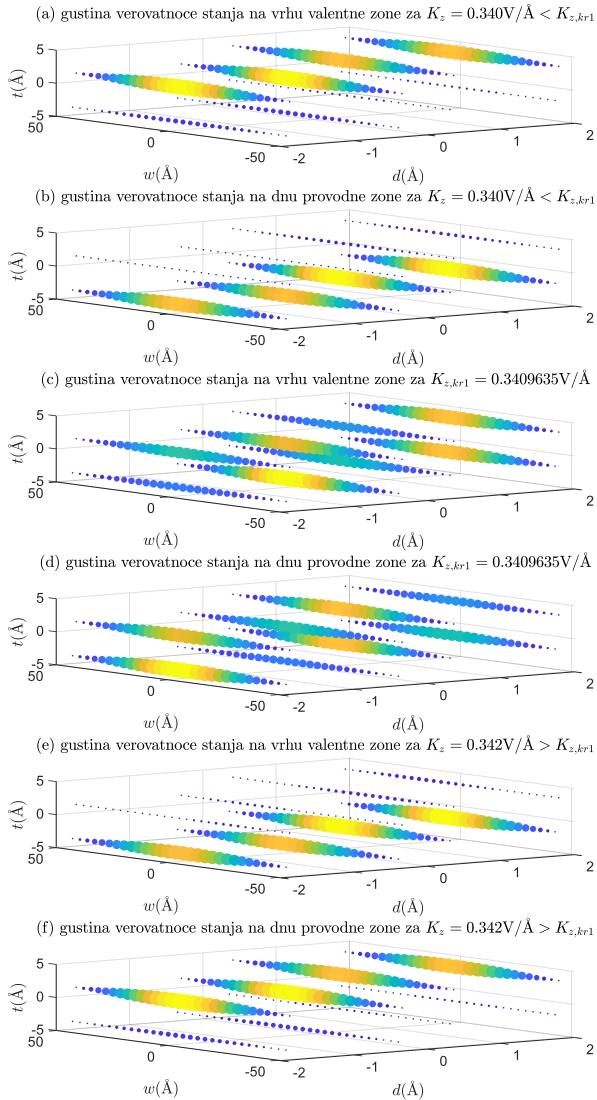
Sl. 3. Prikaz gustine verovatnoće stanja: (a) na vrhu valentne zone za polje K_z = 0.340 V/Å < $K_{z,kr1}$; (b) na dnu provodne zone za polje K_z = 0.340 V/Å < $K_{z,kr1}$; (c) na vrhu valentne zone za polje $K_{z,kr1}$ = 0.3409635 V/Å; (d) na dnu provodne zone za polje $K_{z,kr1}$ = 0.3409653 V/Å; (e) na vrhu valentne zone za polje K_z = 0.342 V/Å > $K_{z,kr1}$; (f) na dnu provodne zone za polje K_z = 0.342 V/Å > $K_{z,kr1}$; Na slici osa w je postavljena po širini trake, d po dužini, dok je t normalno na površinu trake.

Da bi ustanovili koliko je ova struktura slična topološkim izolatorima, izračunate su gustine verovatnoća stanja na dnu provodne i vrhu valentne zone za amplitude električnog polja u okolini prve kritične vrednosti, što je prikazano na Sl.3. Za vrednosti polja koje su manje od $K_{z,kr1}$ stanja u valentnoj zoni su pretežno lokalizovana na gornjoj površini trake, dok su stanja u provodnoj na donjoj, što se može uočiti na Sl. 3 (a) i (b), redom. Električno polje je normalno na površinu trake i usmereno vertikalno naviše (u smeru t ose) tako da potiskuje šupljine na gornju površinu, dok su elektroni potisnuti na donju. Za kritičnu vrednost električnog polja lokalizacija stanja u valentnoj i provodnoj zoni je slična, pri čemu su stanja u različitim zonama lokalizovana na različitim podrešetkama strukture, što je prikazano na Sl. 3 (c) i (d). Ovo je posledica izrazite anizotropije dvoslojnog fosforena i posebno male debljine strukture zbog čega je sprezanje stanja u valentnoj i provodnoj zoni jako čak i pri velikim amplitudama električnog polja koje teži da razdvoji elektrone i šupljine. U slučaju kada je amplituda polja veća od kritične vrednosti, uočava se da su stanja na vrhu valentne zone lokalizovana na donjoj površi, dok su stanja na dnu provodne zone lokalizovana na gornjoj površi (videti Sl.3 (e) i (f)) što je obrnuto od onoga što smo imali na Sl.3 (a) i (b) kada je amplituda polja bila manja od kritične. Ovo je indikacija da je u oblasti antiukrštanja došlo do inverzije zonske strukture, što je ponašanje slično onome koje se sreće kod topoloških izolatora. Inverzija zonske strukture počinje u centru zone i širi se ka ivicama zone sa porastom amplitude električnog polja. Za stanja kod kojih nije došlo do inverzije lokalizacija je takva da su stanja u valentnoj zoni pretežno na atomima na gornjoj površi strukture, dok su stanja u provodnoj zoni dominantno lokalizovana na donjoj, što odgovara efektu koji električno polje ima na šupljine i elektrone.

IV. ZAKLJUČAK

U radu je teorijski razmatrana elektronska struktura dvoslojnih traka od fosforena sa foteljastim ivicama. Utvrđeno je da primenom normalnog električnog polja dolazi do antiukrštanja stanja iz provodne i valentne zone, što je praćeno zonskom inverzijom. Nađene su kritične vrednosti polja za koja je procep između zona minimalan. Za veće kritične vrednosti polja, procep je veći. Za razmatrane kritične vrednosti je nađeno da je u centru zone lokalizacija stanja u različitim zonama energija najbližih ivici procepa bila slična, ali na različitim podrešetkama. Ovo je posledica anizotropije i male debljine strukture. Indukovani efekti su slični onima koji se sreću kod topoloških izolatora. U daljem istraživanju bi trebalo utvrditi kako magnetsko polje u ravni utiče na disperziju, što bi dalo dodatne rezultate koji bi ukazali na topološke efekte.

LITERATURA

[1] K. S. Novoselov, A. K. Geim, S. V. Morozov, D. Jiang, Y. Zhang, S. V. Dubonos, I. V. Grigorieva, and A. A. Firsov, "Electric field effect in atomically thin carbon films," *Science*, vol. 306, pp. *666-669*, Oct. 2004.

[2] A. K. Geim, K. S. Novoselov, "The rise of graphene," *Nat. Mater*, vol. *6*, no. *3*, pp. *183-191*, Feb. 2007.

[3] B. Partoens, F. M. Peeters, "From graphene to graphite: Electronic structure around the K point," *Phys. Rev. B*, vol. *74*, pp. *075404 1-11*, Avg. 2006.

[4] H. Liu, A. T. Neal, Z. Zhu, Z. Luo, X. Xu, D. Tománek, P. D. Ye, "Phosphorene: An Unexplored 2D Semiconductor with a High Hole Mobility", *ACS Nano*, vol. *8*, no. *4*, pp. *4033-4041*, Mar. 2014.

[5] W. Lu, H. Nan, J. Hong, Y. Chen, C. Zhu, Z. Liang, X. Ma, Z. Ni, C. Jin, *Nano Res*, Vol. *7*, pp. *853-859*, May 2014.

[6] Y. Aierken, D. Çakir, C. Sevik, F. M. Peeters, "Thermal properties of black and blue phosphorenes from a first-principles quasiharmonic approach," *Phys. Rev. B*, vol. *92*, no. *8*, pp. *081408 1-5*, Avg. 2015.

[7] T. Hu and J. Hong, Anisotropic Effective Mass, "Optical Property, and Enhanced Band Gap in BN/Phosphorene/BN Heterostructures," *ACS Appl. Mater. Interfaces*, vol. 7, no. *42*, pp. *23489-23495*, Oct. 2015.

[8] V. V. Arsoski, M. M. Grujić, N. A. Čukarić, M. Ž. Tadić, F. M. Peeters, "Normal and skewed phosphorene nanoribbons in combined magnetic and electric fields", *Phys. Rev. B*, vol. *96*, no. *12*, pp. *125434 1-11*, vol. 25, no. 12, Sep. 2017.

[9] R. Fei, V. Tran, L. Yang, "Topologically protected Dirac cones in compressed bulk black phosphorus", *Phys. Rev. B*, vol. *91*, no. *19*, pp. *195319 1-5*, May 2015.

[10] X-L. Qi, S-C. Zhang, "Topological insulators and superconductors", *Rev. Mod. Phys*, vol. *83*, no. *4*, pp. *1057-1110*, Dec. 2011.

[11] A. N. Rudenko, S. Yuan, and M. I. Katsnelson, "Toward a realistic description of multilayer black phosphorus: From GW approximation to large-scale tight-binding simulations," *Phys. Rev. B*, vol. *92*, no. *8*, pp. *085419 1-9*, July 2015; Videti Erratum: A. N. Rudenko, S. Yuan, and M. I. Katsnelson, *Phys. Rev. B*, vol. *93*, no. *19*, pp. *199906*, May 2016.

ABSTRACT

Tight-binding method is employed for electronic structure analysis in bilayer black phosphorous nanoribbons in presence of electric field. Due to the absence of edge states, there is a large gap in arm-chair nanoribbons in absence of an external field. An application of an electric field perpendicular to the ribbon surface decreases the gap width. At the critical value of the electric field, the gap is almost completely closed due to sharp anti-crossing between the lowest energy conduction band state and the highest energy valence band state. This behavior is characteristic in conventional topological insulators where an inversion of the zone structure is due to strong spin-orbit interaction that is not accounted for in our model. It is found that in thin nanoribbons there is a strong coupling between conduction and valence band states due to anisotropy despite the electrons are holes being pushed to the opposite sides of the slab by an external electric field. Increase of the perpendicular electric field above critical value results in an inversion of higher conduction and valence band states that manifests in characteristic anti-crossings.

Inducing the Topological-like States in Bilayer Phosphorene Nanoribbons by Perpendicular Electric Field

Vladimir V. Arsoski, Milan Ž. Tadić

Elektronska svojstva grafenskih nanotraka sa periodičnim defektima

Jovana Vlahović, Vladimir V. Arsoski, Milan Ž. Tadić, Milorad Milošević

Apstrakt—Već više od decenije materijali izrađeni od jednog ili više monoslojeva kristala su u žiži interesovanja zbog boljih elektronskih i transportnih svojstava u odnosu na masivni materijal od kojeg su sačinjeni. Kao posebno interesantan za primenu izdvojio se grafen, koji je prvi dobijen u formi tankog sloja. Određeni broj primena zahteva da u materijalu postoji dovoljno veliki energetski procep, što kod grafena nije slučaj. Razvijene tehnike kontrole procepa nisu dale značajnije rezultate kod ovog materijala. U ovom radu je predložena mogućnost podešavanja procepa grafenskih nanotraka uvođenjem periodičnih defekata u nanostrukturu. Razmotren je uticaj defekta tipa jednog upražnjenog mesta (vakancije) u kristalnoj rešetki koji se periodično ponavlja duž trake. Pokazano je da periodični defekti mogu imati značajan uticaj na razliku energija dna provodne i vrha valentne zone u nanotrakama sa foteljastim ivicama, a samim tim i na elektronske i transportne osobine grafenskih nanotraka. Prisustvo periodičnog defekta rezultuje pojavom specifičnih stanja vezanih za defekt, što se ogleda u pojavi ravne zone unutar procepa na disperzionoj relaciji.

Ključne reči—2D materijali; grafen; metod jake veze; energetski procep; defektna stanja; ravne zone.

I. Uvod

Već više decenija elektronske naprave zasnovane na silicijumu dominiraju u izradi elektronskih naprava. Trendovi minijaturizacije elektronskih naprava doveli su silicijum do granice kada kvantnomehanički efekti, koji dominiraju pri malim dimenzijama strukture, bitno utiču na funkcionisanje naprave. Kao alternativa su se pojavili materijali izrađeni od jednog ili više monoslojeva poluprovodničkog krustala, poznati kao dvodimenzioni (2D) materijali, koji usled malih dimenzija pokazuju poboljšana elektronska, transportna, električna, termička i optička svojstva u odnosu na masivne materijale od kojih su dobijeni. Kao posebno interesantan materijal, zbog velike potencijalne primene, izdvaja se monosloj grafita poznat kao grafen [1]. Uspešna fabrikacija ovog materijala pokrenula je eru razvoja post-silicijumske elektronike koja obećava veliki napredak u domenu

Jovana Vlahović – Faculty of Sciences, University of Antwerp, Groenenborgerlaan 171 2020 Antwerpen, Belgium, (e-mail: jovana.vlahovic@uantwerpen.be).

Vladimir Arsoski – Elektrotehnički fakultet, Univerzitet u Beogradu, Bulevar Kralja Aleksandra 73, 11020 Beograd, Srbija (e-mail: vladimir.arsoski@etf.bg.ac.rs).

Milan Tadić – Elektrotehnički fakultet, Univerzitet u Beogradu, Bulevar Kralja Aleksandra 73, 11020 Beograd, Srbija (e-mail: tadic@etf.bg.ac.rs).

Milorad Milošević – Faculty of Sciences, University of Antwerp, Groenenborgerlaan 171 2020 Antwerpen, Belgium, (e-mail: milorad.milosevic@uantwerpen.be).

elektronskih naprava [2]. Prvobitna fabrikacija grafena zasnivala se na metodi mehaničke eksfolijacije pomoću dvostruko-lepljive trake [3]. Ovako dobijeni uzorci su imali mnogo defekata, bili su relativno malih dimenzija i obično su se sastojali od više monoslojeva grafita, te metoda nije bila reproduktivna. Usledile su tehnike eksfolijacije u tečnoj fazi organskih rastvarača, jonskih tečnosti, rastvora surfaktanata i mnogih rastvarača koji su imali sličan površinski napon kao i grafen [4]. Vremenom se kao dominantna metoda izdvojila sonifikacija [5]. Ultrazvuk se prostire kroz tečnu fazu do grafena gde dovodi do naizmenične promene pritiska, što uzrokuje sabijanje i razvlačenje veza između slojeva atoma. Prilikom razdvajanja monoslojeva u međuprostoru se stvaraju mikromehurići, koji postepeno narastaju i pucaju pri dostizanju kritične veličine, što dovodi do generacije snažnih udarnih talasa. Dalje se centrifugiranjem mogu razdvojiti supernatant i dobijeni grafenski proizvod. Iako zahteva veliku količinu energije i ima malu efikasnost, ova metoda se koristi jer se njome uspešno mogu proizvesti monoslojevi [6]. Kao efikasna metoda za dobijanje grafenskih nanotraka pokazala se tehnika zasecanja i razvijanja ugljeničnih nanotuba. Veličina dobijenih traka zavisi od dijametra i dužine nanotube, dok tip ivica određuje pravac zasecanja nanotrake [7]. Kao efikasna metoda za formiranje slojeva grafena velike površine i sa malo defekata pokazala se tehnika heteroepitaksije, gde se narastanje vrši na supstratu koji ima sličnu kristalnu strukturu kao i grafen [8]. Posebno interesantan supstrat je silicijum karbid (SiC) na kojem je kontrolisanim postupkom moguće narasti jedan monosloj ukoliko se narastanje vrši na površini orijentacije (0001) [9]. Fabrikovane površine grafena se dalje mogu obrađivati radi postizanja željene morfologije.

Kao glavni nedostatak grafena kod primene u tranzistorima navodi se zanemarljiva vrednost energetskog procepa koja otežava njegovu primenu u tranzistorima sa efektom polja. Procep od nekoliko desetina meV može se dobiti oblikovanjem grafena u formu traka malih dimenzija [10] ili slaganjem više slojeva grafena (stekovanjem) na različite načine [11], što nije sasvim dovoljno za veliki broj savremenih primena.

Poznato je da proizvoljno mala periodična perturbacija masivnog dielektričnog materijala dovodi do pojave zabranjenog opsega učestanosti za prostiranje svetlosti u materijalu, što odgovara nastanku fotonskog procepa [12]. Periodične perturbacije imaju sličan efekat i na elektronsku strukturu poluprovodnika. Pokazano je da se specifičnim periodičnim uvijanjem grafena može neznatno otvoriti energetski procep [13]. Ideja je da se pomoću periodičnih

defekata formiranih u grafenu kontroliše veličina energetskog procepa.

Inherentan tip defekta u grafenu predstavljaju upražnjena mesta u rešetki, takozvane vakancije, koje imaju slučajan raspored u strukturi. Površinska koncentracija ovih defekata zavisi od primenjenih tehnika fabrikacije, a najmanja je kod novijih tehnike fabrikacije [7-9]. Utvrđeno je da defekti ovog tipa u izvesnoj meri utiču na elektronska i magnetska svojstva grafenskih nanotraka [14, 15]. Primenom tehnike koja koristi visokoenergetske jone ili elektrone moguće je precizno ukloniti pojedine atome iz rešetke, što otvara mogućnost za preciznu kontrolu položaja defekata [16], a samim tim i kontrolu veličine procepa u strukturama od grafena.

II. IMPLEMENTACIJA MODELA

Modelovanje elektronske strukture grafenskih nanotraka zasnovan je na metodi jake veze. Teorijske osnove razmatranog modela mogu se naći u [17]. Za implementaciju modela je korišćena biblioteka PyBinding 0.9.5 [18] koja je napravljena u programskom jeziku Python. U radu je korišćena aproksimacija koja razmatra skokove samo na najbliže susede. Svi parametri koji figurišu u modelu su preuzeti iz [19].

U zavisnosti od pravca zasecanja sloja grafena, nanotrake mogu imati različite ivice, ali se najčešće razmatraju trake sa cik-cak i foteljastim ivicama [20]. U ovom radu su analizirane trake sa foteljastim ivicama pošto, za razliku od traka sa cik-cak ivicama, kod njih ne postoje ivična stanja. Razmatrane su isključivo trake sa periodičnim defektima u vidu jedne vakancije, pri čemu se u prvoj aproksimaciji usvaja da nije došlo do ismene položaja atoma u okolini upražnjenog mesta u rešetki [21]. Kada nedostaje više susednih ugljenikovih atoma u sloju grafena može doći do građenja novih veza i međusobnog vezivanja nesusednih atoma [22].
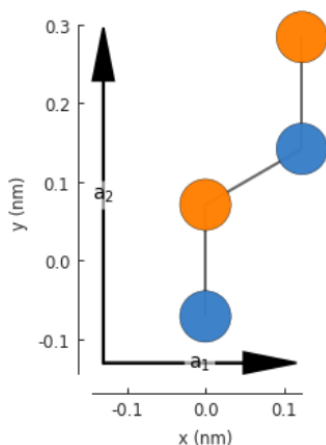

Sl. 1. Izgled elementarne ćelije čijim se ponavljanjem u prostoru reprodukuje traka sa foteljastim ivicama proizvoljne širine [17,18].

III. REZULTATI I DISKUSIJA

Pri analizi nanotraka korišćena je elementarna ćelija

prikazana na Sl.1. Atomi različite boje pripadaju različitim podrešetkama. Periodičnim ponavljanjem elementarne ćelije u pravcu vektora $\mathbf{a}_1$ može se reprodukovati nanotraka sa foteljastim ivicama proizvoljne širine. Minimalna širina trake odgovara dužini vektora $\mathbf{a}_2$. Uvođenje periodičnih graničnih uslova u ovom pravcu ekvivalentno je formiranju trake nominalno beskonačne dužine. Usvojeno je da je minimalno rastojanje defekata $w_{\min}=|\mathbf{a}_2|$. Analiziran je slučaj gde se defekti mogu periodično ponavljati duž trake u pravcu vektora $\mathbf{a}_2$ tako da im je međusobno rastojanje $w = mw_{\min}$, gde je m prirodan broj. Rastojanje defekata w ujedno predstavlja dužinu elementarne ćelije koja gradi traku beskonačne dužine.
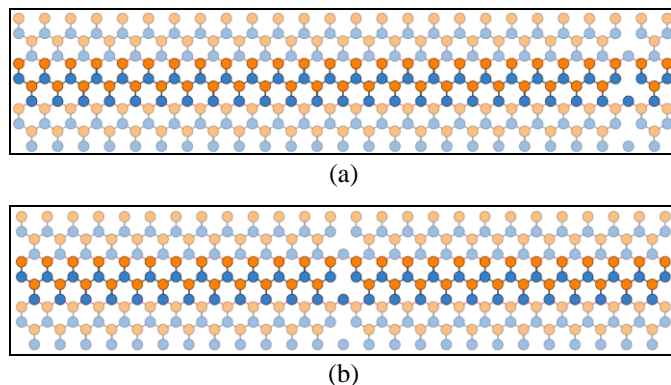
Sl. 2. Jedinična ćelija nanotrake kod koje je rastojanje vakancija $d_{\min}$ za položaj defekta: (a) najbliže ivici trake, (b) na sredini trake [17].

Analizirane su trake sa foteljastim ivicama širine 6.149 nm. U slučaju najmanjeg rastojanja između defekata duž trake, jediničnu ćeliju nanotrake sačinjava 50 C-C dimera i jedan ugljenikov atom. U slučaju trake bez defekta broj dimera bi bio 51. U nedavnim istraživanjima je ustanovljeno da grafenske nanotrake, čija se elementrarna ćelija sastoji od $3N$ nizova dimera, gde je N prirodan broj, mogu da imaju veće energetske procepe i bolje optička svojstva nego trake čije elementrarne ćelije broje $3N+1$ i $3N+2$ dimera [23,24]. Nanotrake kod kojih su defekti periodično raspoređeni na rastojanju w sastoje se od $51 \cdot w$ dimera umanjeno za jedan ugljenikov atom, te približno zadovoljavaju navedeni uslov.

Najpre su analizirane trake kod kojih je rastojanje defekata $d_{\min}$. Položaj vakancije je pomeran po širini trake i menjan je od položaja najbližeg ivici trake (videti Sl. 2(a)) do položaja na sredini trake (videti Sl. 2(b)). Ustanovljeno je da se razlika energija dna provodne i vrha valentne zone povećavala od vrednosti 0.206 eV za slučaj kada je defekt lociran najbliže ivici trake, do vrednosti 0.395 eV za slučaj centralnog defekta, što je veće od vrednosti koja se dobija za traku iste širine bez vakancija [17]. Disperzione relacije za traku sa ivičnim i centralnim defektom su prikazane na Sl. 3(a) i (b), redom. Na obe disperzije se može uočiti pojava ravnih zona u centru energetskog procepa. Ova stanja su slična ivičnim stanjima koja se pojavljuju u nanotrakama sa cik-cak ivicama [17].

(a)

(b)
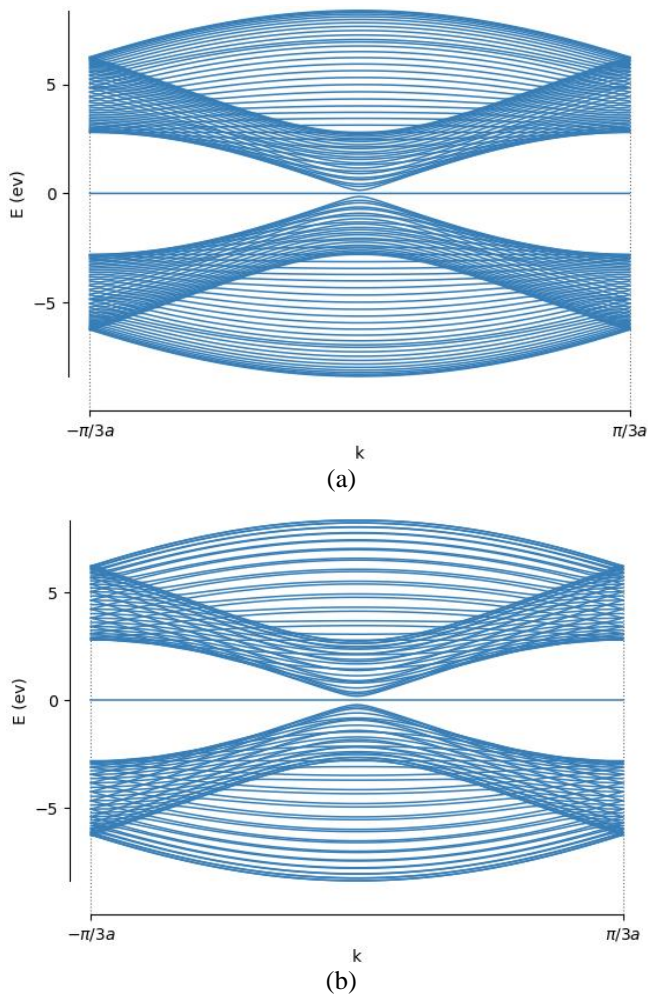
Sl. 3. Disperzione relacije za nanotrake kod kojih je rastojanje vakancija d_{min} za položaj defekta: (a) najbliže ivici trake, (b) na sredini trake [17].

U cilju boljeg uvida u prirodu ravnih zona ispitana je prostorna lokalizacija stanja. Lokalna gustina stanja u centru zone za slučaj trake sa vakancijom na sredini je grafički prikazana na Sl. 4. Uočava se da postoji dominantna lokalizacija na atomima duž linije defekta i njima najbližim susedima, što je slično lokalizaciji koja postoji duž ivica cik-cak nanotraka.
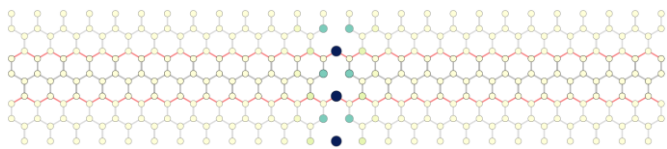
Sl. 4. Lokalna gustina stanja u k=0 u traci sa vakancijom na sredini trake [16]. Granice jedinične ćelije trake su markirane crvenom bojom. Veći poluprečnik kružnice i tamnija boja odgovara jačoj lokalizaciji na markiranoj poziciji u rešetki.

Kako bi razmotrili uticaj periode ponavljanja defekta na elektronsku strukturu, razmotrili smo slučaj nanotrake sa jednom vakancijom na sredini trake i međusobnim rastojanjem defekata koje iznosi $3d_{min}$. Na Sl. 5.(a) i (b) su date skica kristalne strukture i disperzija za ove nanotrake, redom. Disperzija izgleda slično onoj za traku sa manjim

međusobnim rastojanjem vakancija, pri čemu je broj stanja veći zbog većeg broja atoma koji čine jediničnu ćeliju. Razlika energija stanja na dnu provodne i vrhu valentne zone iznosi 0.3952 eV, što se neznatno razlikuje od vrednosti koju smo imali kada je prostorna perioda ponavljanja defekta tri puta manja.

(a)

(b)
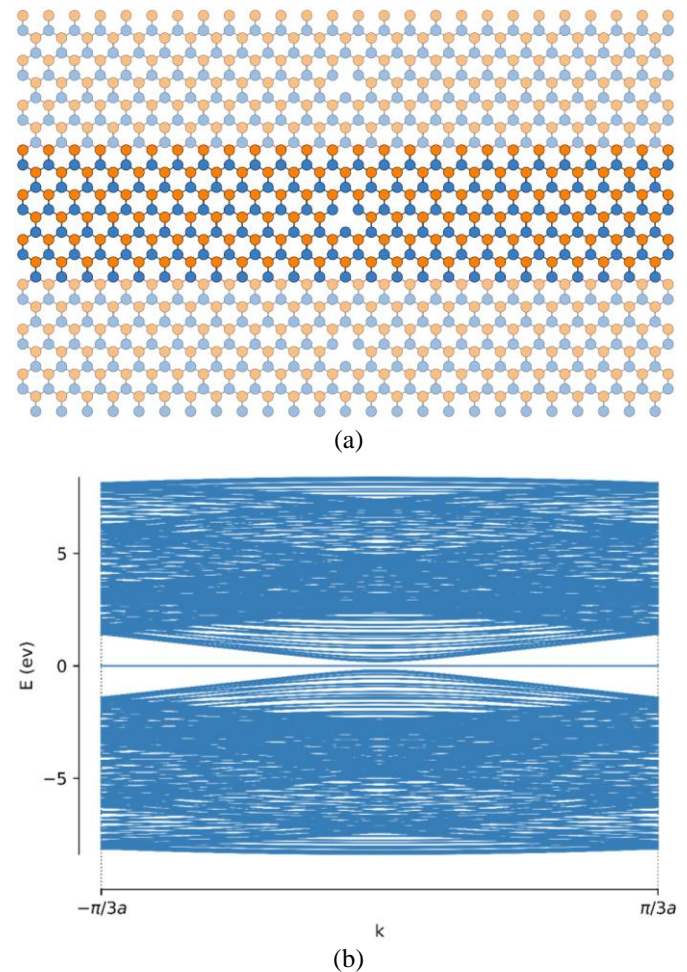
Sl. 5. Prikaz (a) jedinične ćelije i (b) disperzione relacije u nanotraci kod koje je rastojanje vakancija $3d_{min}$, a položaj defekta na sredini trake [17].

IV. Zaključak

U radu je sprovedena teorijska analiza mogućnosti inženjeringa energetskog procepa u grafenskim nanotrakama sa foteljastim ivicama. Analizirane su nanotrake nominalno beskonačne dužine u kojima postoje defekti tipa upražnjenog mesta u rešetki. Ustanovljeno je da položaj defekta u odnosu na ivicu trake bitno utiče na razliku energija stanja na dnu provodne i vrhu valentne zone. Sa druge strane, izmena prostorne periode ponavljanja defekta duž trake nije imala značajnijeg uticaja na procep. Na disperzionoj relaciji je uočeno da uvođenje defekta dovodi do pojave ravnih zona unutar procepa koje karakterišu stanja dominantno lokalizovana duž linije defekta. Interesantno bi bilo razmotriti slučajeve defekata koji nastaju kada se ugljenikov atom zameni drugim atomom, slučaj više vakancija unutar jedinične

ćelije trake, kao i slučaj nasumičnog rasporeda defekata u traci konačnih dimenzija što je posledica nesavršenosti tehnika za fabrikaciju.

LITERATURA

[1] A. K. Geim, K. S. Novoselov, "The rise of graphene," *Nat. Mater*, vol. *6*, no. *3*, pp. *183-191*, Feb. 2007.

[2] X. Du, I. Skachko, A. Barker, E.Y. Andrei, "Approaching ballistic transport in suspended graphene", *Nat. Nanotechnol*, vol. *3*, pp. *491-495*, July 2008.

[3] K. S. Novoselov, A. K. Geim, S. V. Morozov, D. Jiang, Y. Zhang, S. V. Dubonos, I. V. Grigorieva, and A. A. Firsov, *Science*, vol. *306*, pp. *666-669*, Oct. 2004.

[4] J.N. Coleman, M. Lotya, A. O'neill, S.D. Bergin, P.J. King, U. Khan, K. Young, A. Gaucher, S. De, R.J. Smith, I. V Shvets, S.K. Arora, G. Stanton, H.-Y. Kim, K. Lee, G.T. Kim, G.S. Duesberg, T. Hallam, J.J. Boland, J.J. Wang, J.F. Donegan, J.C. Grunlan, G. Moriarty, A. Shmeliov, R.J. Nicholls, J.M. Perkins, E.M. Grieveson, K. Theuwissen, D.W. Mccomb, P.D. Nellist, V. Nicolosi, "Two-Dimensional Nanosheets Produced by Liquid Exfoliation of Layered Materials," *Science*, vol. *331*, no. *3017*, pp. *568-571*, Feb. 2011.

[5] Y. Hernandez, V. Nicolosi, M. Lotya, F.M. Blighe, Z. Sun, S. De, I.T. McGovern, B. Holland, M. Byrne, Y.K. Gun'ko, J.J. Boland, P. Niraj, G. Duesberg, S. Krishnamurthy, R. Goodhue, J. Hutchison, V. Scardaci, A.C. Ferrari, J.N. Coleman, "High-yield production of graphene by liquid-phase exfoliation of graphite," *Nat. Nanotechnol*, vol. *3*, pp. *563-568*, Avg. 2008.

[6] Y. Xu, H. Cao, Y. Xue, B. Li, W. Cai, "Liquid-phase exfoliation of graphene: An overview on exfoliation media, techniques, and challenges," *Nanomaterials*, vol. *8*, no. *11*, pp. *942 1-32*, Oct. 2018.

[7] Z. Yan, Z. Peng, G. Casillas, J. Lin, C. Xiang, H. Zhou, Y. Yang, G. Ruan, A.R.O. Raji, E.L.G. Samuel, R.H. Hauge, M.J. Yacaman, J.M. Tour, "Rebar graphene," *ACS Nano*, vol. *8*, no. *5*, pp. *5061-5068*, Apr. 2014.

[8] A. Adetayo, D. Runsewe, "Synthesis and Fabrication of Graphene and Graphene Oxide: A Review," *Open J. Compos. Mater*, vol. *9*, no. *2*, pp. *207-229*, Apr. 2019.

[9] J. Robinson, X. Weng, K. Trumbull, R. Cavalero, M. Wetherington, E. Frantz, M. LaBella, Z. Hughes, M. Fanton, D. Snyder, "Nucleation of epitaxial graphene on SiC(0001)," *ACS Nano*, vol. *4*, no. *1*, pp. *153-158*, Dec. 2009.

[10] M.Y. Han, B. Özyilmaz, Y. Zhang, P. Kim, "Energy band-gap engineering of graphene nanoribbons," *Phys. Rev. Lett*, vol. *98*, no. 20, pp. *1-4*, May 2007.

[11] J. Jia, E. V. Gorbar, V. P. Gusynin, "Gap generation in ABC-stacked multilayer graphene: Screening versus band flattening," *Phys. Rev. B*, vol. *88*, no. *20*, pp. *205428 1-8*, Nov. 2013.

[12] John D. Joannopoulos, Steven G. Johnson, Joshua N. Winn, and Robert D. Meade, Photonic Crystals: Molding the Flow of Light, second ed. New Jersy, USA, Princeton University Press, 2008.

[13] WenzeXieZhongyaoLi, "Energy band gaps in periodic bent graphene," Solid State Commun, vol. *225*, pp. *22-26*, Jan. 2016.

[14] M. Topsakal, E. Aktürk, H. Sevinçli, S. Ciraci, "First-principles approach to monitoring the band gap and magnetic state of a graphene nanoribbon via its vacancies," *Phys. Rev. B*, vol. *78*, no. *23*, pp. *235435 1-6*, Dec. 2008.

[15] K. Rallis, P. Dimitrakis, I. G. Karafyllidis, A. Rubio, G. C. Sirakoulis, "Electronic Properties of Graphene Nanoribbons With Defects," *IEEE Transactions on Nanotechnology*, vol. *20*, pp. *151-160*, Jan. 2021.

[16] K. Nordlund, J. Keinonen, T. Mattila, "Formation of ion irradiation induced small-scale defects on graphite surfaces," *Phys. Rev. Lett*, vol. *77*, no. *4*, pp. *699-702*, July 1996.

[17] J. Vlahović, "Analiza elektronskih i transportnih svojstava grafenskih nanotraka sa defektima," Master rad, Elektrotehnički fakultet, Univerzitet u Beogradu, Beograd, Srbija, 2021.

[18] D. Moldovan, M. Anđelković, F. Peeters, pybinding v0.9.5: a Python package for tight-binding calculations, 2020.

[19] M.L. Cohen, S.G. Louie, Fundamentals of Condensed Matter Physics, Cambridge, United Kingdom, Cambridge University Press, 2016.

[20] Y. Yano, N. Mitoma, H. Ito, K. Itami, "A Quest for Structurally Uniform Graphene Nanoribbons: Synthesis, Properties, and Applications," *J. Org. Chem*, vol. *85*, no. *1*, pp. *4-33*, Jan. 2020.

[21] G. Xie, Y. Shen, X. Wei, L. Yang, H. Xiao, J. Zhong, G. Zhang, "A bond-order theory on the phonon scattering by vacancies in two-dimensional materials," *Sci. Rep*, vol. *4*, pp. *5085 1-6*, May 2014.

[22] N. Jing, Q. Xue, C. Ling, M. Shan, T. Zhang, X. Zhou, Z. Jiao, "Effect of defects on Young's modulus of graphene sheets: A molecular dynamics simulation," *RSC Adv*, vol. *2*, no. *24*, pp. *9124-9129*, Sep. 2012.

[23] H.C. Chung, M.H. Lee, C.P. Chang, M.F. Lin, "Exploration of edge-dependent optical selection rules for graphene nanoribbons," *Opt. Express*, vol. *19*, no. *23*, pp. *23350-23363*, Nov. 2011.

[24] Y.W. Son, M.L. Cohen, S.G. Louie, "Energy gaps in graphene nanoribbons," *Phys. Rev. Lett*, vol. *97*, no. *21*, pp. *216803 1-4*, Nov. 2006.

ABSTRACT

For more than a decade, materials that consist of one or more monolayers of crystal have been explored because of their superior electronic and transport properties in comparison to their bulk counterparts. An especially interesting material is graphene which was the first manufactured twodimensional material. For many practical applications relatively large energy gap is a necessary. But it is not the case in graphene. Various techniques were developed to tune the gap, but they are almost not employed in current electronic technology. In this paper, we introduce a method for bandgap tunning by inserting periodic defects in a graphene nanostructure. We analyze the influence of a single vacancy defect that periodically repeats along the nanoribbon. It is shown that periodic defects might have a significant influence on the energy difference between states at the bottom of the conduction band and the top of the valence band in nanoribbons with armchair edges. It, in turn, affects the electronic and transport properties of graphene nanoribbons. Moreover, the presence of a periodic defect results in the appearance of specific defect states with the flat band dispersion.

Electronic Properties of Graphene Nanoribbons with Periodic Defects

Jovana Vlahović, Vladimir V. Arsoski, Milan Ž. Tadić, Milorad Milošević